INSTITUTO TECNOLÓGICO
Y DE ESTUDIOS SUPERIORES DE OCCIDENTE

Reconocimiento de validez oficial de estudios de nivel superior según acuerdo secretarial 15018, publicado en el Diario Oficial de la Federación el 29 de noviembre de 1976.

Departamento de Electrónica, Sistemas e Informática

DOCTORADO EN CIENCIAS DE LA INGENIERÍA

DISEÑO MULTIFÍSICO DE CIRCUITOS DE ALTA FRECUENCIA MEDIANTE MODELADO POLINOMIAL EXPLOTANDO EL TEOREMA MULTINOMIAL

Tesis que para obtener el grado de

DOCTOR EN CIENCIAS DE LA INGENIERÍA

presenta: José Luis Chávez Hurtado

Director de tesis: Dr. José Ernesto Rayas Sánchez

Co-director de tesis: Dr. Zabdiel Brito Brito

Tlaquepaque, Jalisco. Diciembre de 2017

DOCTOR EN CIENCIAS DE LA INGENIERÍA (2017) ITESO, Tlaquepaque, Jal., México

TÍTULO: **Diseño multifísico de circuitos de alta frecuencia mediante modelado polinomial explotando el teorema multinomial**

AUTOR: José Luis Chávez Hurtado
Ingeniero en Electrónica (ITESO, México)
Maestro en Diseño Electrónico (ITESO, México)
Maestro en Negocios y Estudios Económicos (Universidad de Guadalajara, México)

DIRECTOR DE TESIS: José Ernesto Rayas Sánchez
Profesor Numerario del Departamento de Electrónica, Sistemas e Informática, ITESO
Ingeniero en Electrónica (ITESO, México)
Maestro en Sistemas Electrónicos (ITESM Campus Monterrey, México)
Doctor en Ingeniería Eléctrica (Universidad McMaster, Canadá)
Senior, IEEE

NÚMERO DE PÁGINAS: xxvi, 90

ITESO – The Jesuit University of Guadalajara

Department of Electronics, Systems, and Informatics

DOCTORAL PROGRAM IN ENGINEERING SCIENCES

MULTIPHYSICS DESIGN OF HIGH FREQUENCY CIRCUITS BY POLYNOMIAL SURROGATE MODELING EXPLOITING THE MULTINOMIAL THEOREM

Thesis to obtain the degree of

DOCTOR IN ENGINEERING SCIENCES

Presents: José Luis Chávez-Hurtado

Thesis Director: Dr. José Ernesto Rayas-Sánchez

Thesis Co-director: Dr. Zabdiel Brito-Brito

Tlaquepaque, Jalisco, Mexico
December 2017

PHD IN ENGINEERING SCIENCES (2017) ITESO, Tlaquepaque, Jal., Mexico

TITLE: **Multiphysics Design of High Frequency Circuits by Polynomial Surrogate Modeling exploiting the Multinomial Theorem**

AUTHOR: José Luis Chávez-Hurtado
Bachelor's degree in electronics engineering (ITESO, Mexico)
Master's degree in electrical engineering (ITESO, Mexico)
Master's degree in business and economics (University of Guadalajara, Mexico)

THESIS DIRECTOR: José Ernesto Rayas-Sánchez
Department of Electronics, Systems, and Informatics, ITESO-The Jesuit University of Guadalajara
Bachelor's degree in electronics engineering (ITESO, Mexico)
Master's degree in electrical engineering (ITESM, Mexico)
Ph.D. degree in electrical engineering (McMaster University, Canada)
Senior, IEEE

NUMBER OF PAGES: xxvi, 90

A Dios

A mi familia

A mis compañeros y amigos

Resumen

Una sola simulación electromagnética, de una estructura de alta frecuencia, usualmente requiere desde algunos minutos hasta algunas horas cuando se emplea un modelo electromagnético muy preciso, lo cual hace prohibitivo el uso de algoritmos de optimización directa para lograr las especificaciones de diseño. Una primera alternativa para solucionar este problema consiste en el desarrollo y uso de modelos sustitutos. Distintas técnicas de modelado se han aplicado al modelo de estructuras de alta frecuencia, tales como la metodología superficie de respuesta, máquinas de vectores de soporte, redes neuronales artificiales y Kriging. En esta tesis doctoral, se estudia y explota el uso de funciones polinomiales, en conjunto con el teorema multinomial, para el modelado y optimización de estructuras de alta frecuencia en el dominio de la frecuencia. La metodología propuesta, basada en polinomios, también es empleada para el desarrollo de modelos sustitutos multifísicos de estructuras de alta frecuencia sujetas a estrés térmico y mecánico debido a cambios en la temperatura del circuito. Una segunda alternativa para reducir el tiempo requerido para optimizar estructuras de alta frecuencia consiste en la utilización de técnicas de mapeo espacial. El mapeo espacial requiere al menos dos modelos del circuito a ser diseñado: un modelo fino, el cual es muy preciso pero computacionalmente muy costoso, y un modelo burdo, el cual es impreciso pero computacionalmente económico. El objetivo del mapeo espacial es minimizar la desviación inherente que existe entre la respuesta del modelo fino y burdo, encontrando la relación matemática entre los espacios de diseño del modelo fino y burdo. Una forma popular de aplicar esta técnica, conocida como mapeo espacial agresivo, explota el algoritmo de Broyden para encontrar dicha relación matemática. En esta tesis doctoral, se explota el uso de funciones polinomiales para aproximar linealmente la relación entre los modelos burdo y fino, en vez de emplear el algoritmo de Broyden, mostrando un desempeño muy competitivo. Los resultados generales mostrados en esta tesis doctoral, demuestran, mediante varios ejemplos sintéticos y realísticos, la capacidad de las funciones polinomiales para modelar y optimizar adecuadamente estructuras de alta frecuencia en el dominio de la frecuencia, teniendo la ventaja de emplear una formulación mucho más sencilla que aquellas utilizadas por técnicas avanzadas de modelado.

Summary

A single electromagnetic (EM) simulation of a high-frequency structure typically takes from several minutes to hours when using a very accurate EM model, making prohibitive the use of direct optimization algorithms to achieve the desired specifications. A first approach to overcome this problem consists of developing and using surrogate models. Several modeling techniques have been applied for modeling high frequency structures, such as response surface methodology, support vector machines, artificial neural networks, and Kriging. In this doctoral dissertation, the use of polynomial functions and the multinomial theorem is studied and exploited for modeling and optimizing high frequency structures in the frequency domain. The proposed polynomial-based methodology is also used to develop multiphysical surrogate models of high frequency structures subject to thermal and mechanical stress due to changes in the circuit temperature. A second approach to reduce the time spent in optimizing high frequency structures is by using space mapping (SM) techniques. Space mapping requires at least two models of the circuit to be designed: a fine model, which is very accurate but computationally expensive, and a coarse model, which is inaccurate but computationally cheap. The purpose of SM is to minimize the inherent deviation between the fine and the coarse model responses by finding the mathematical relationship between the fine and the coarse model design spaces. A very popular approach, known as aggressive space mapping, exploits the Broyden algorithm to find this mathematical relationship. In this doctoral dissertation, polynomial functions are also exploited to linearly approximate the relationship between the fine and coarse model designs, instead of using the Broyden algorithm, showing a very competitive performance. The overall results presented in this thesis dissertation, demonstrated by many examples, considering both realistic and synthetic test cases, demonstrate the capability of polynomial functions to properly model and optimize high frequency structures in the frequency domain, with the main advantage of employing a much simpler formulation than those used by other advanced surrogate modeling techniques.

Acknowledgements

The author wishes to express his sincere appreciation to Dr. José Ernesto Rayas-Sánchez, Professor of the Department of Electronics, Systems, and Informatics at ITESO, and director of research in the Computer-Aided Engineering of Circuits and Systems (CAECAS) group at ITESO, for his encouragement, expert guidance, and keen supervision as doctoral thesis director throughout the course of this work. The author offers his gratitude to Dr. Zabdiel Brito-Brito, for his support as doctoral thesis co-director during the development of this work. He also thanks Dr. José Raúl Loo-Yau, Dr. Omar Humberto Longoria-Gándara, and Dr. Esteban Martínez-Guerrero, members of the Ph.D. Thesis Committee, for their interest, assessment, and suggestions.

The author has greatly benefited from working with COMSOL Multiphysics developed by COMSOL Inc., Sonnet EM developed by Sonnet Software Inc., and MATLAB developed by The MathWorks Inc. The author is particularly grateful to Dr. James C. Rautio, President of Sonnet Software Inc., for making Sonnet EM available for this work.

It is the author's pleasure to acknowledge fruitful collaboration and stimulating discussions with his colleagues of CAECAS research group at ITESO – The Jesuit University of Guadalajara: Francisco Rangel-Patiño, Rafael del-Rey-Acuña, Felipe de Jesús Leal-Romo, Andrés Viveros-Watcher, Jacqueline Sánchez-Mesa, and Jorge Dávalos-Guzmán.

The author gratefully acknowledge the financial assistance through a scholarship granted by the *Consejo Nacional de Ciencia y Tecnología* (CONACYT), Mexican Government, as well as the financial support provided by Intel Corp. during the initial years of my doctoral studies, through a CAECAS research project funded by Intel Mexico.

Finally, special thanks are due to my family, for their understanding, patience, and continuous loving support.

Contenido

Contents

List of Figures

List of Tables

Introduction

In the high frequency circuits arena we can find two very common modeling methodologies: the equivalent circuit approach and the physical device modeling approach. Equivalent circuits modeling methods exhibit two main advantages: they are easy to implement in circuit analysis and design procedures and, maybe more importantly, they are computationally very cheap as compared to physics-based modeling [Hammadi-99]. This second characteristic is very important for optimization procedures, where many circuit simulations are typically required to find an optimal design. However, at higher operation frequencies, equivalent circuit models become increasingly more complex to accurately describe the behavior of the circuit [Hammadi-99]. Additionally, high frequency circuits behavior depends on the physical geometry of the structure that implements the circuit, a characteristic that is difficult to represent in equivalent circuit models. Consequently, in most cases of high-frequency analysis and design, it is necessary to use physics-based models [Hammadi-99], [Vai-99], particularly, full-wave electromagnetic simulators.

Since physics-based models are usually computationally expensive, the use of direct optimization methods is prohibitive. In many practical cases, one electromagnetic (EM) simulation can take from several minutes to hours to be done, especially if the simulation is intended to be highly accurate [Chávez-Hurtado-16c]. An alternative to speed up the optimization process without losing accuracy consists of exploiting surrogate models. Ideally, a surrogate model has to be computationally cheap, smooth, and accurate, in order to be useful to find, in a reasonable time, a set of parameters that allows the original structure to achieve the required design specifications [Barmuta-15].

Surrogate models can be generated by using a set of learning base points from the original high frequency structure implemented in a highly accurate but computationally expensive simulator. These learning base points are usually within a specified region of interest and can be allocated by using Design of Experiments (DoE) [Barmuta-15]. Different approaches can be used to develop functional surrogate models. Some of the most popular for high frequency structures are based on Response Surface Methodologies (RSM), Artificial Neural Networks (ANN), Support Vector Machines (SVM) and Kriging.

In this doctoral dissertation, a methodology based on polynomial functions exploiting the multinomial theorem is studied and adapted to represent the electromagnetic behavior of high frequency structures at each simulated frequency point. This proposal is also extended in its formulation to represent the EM behavior of high frequency structures subject to a multiphysical analysis, where a change in the circuit temperature can cause thermal and mechanical stress on the structure, affecting the original EM response of the high frequency structure.

While surrogate models are relatively easy to implement (we essentially need a set of learning base points to develop the model) they are only valid within the design region of interest. If the optimal design is outside this design, we need a new set of learning base points to ensure the reliability of the surrogate model. This characteristic could highly increase the required number of base points if the optimal design is far from the starting point. An alternative approach to find the optimal design consists of exploiting space mapping techniques.

Space mapping techniques exploit the use of at least two models, a coarse model, which is inaccurate but computationally cheap, and a fine model, which is very accurate but computationally expensive [Bandler-94], [Bandler-95]. The fine model is typically implemented by using a full-wave EM simulator with a very fine resolution discretization and with a detailed geometrical and material properties definition, making it highly accurate but computationally very expensive. On the other hand, the coarse model can be implemented by using a faster EM simulator, by using the same EM simulator but using a coarse discretization for the high frequency structure [Koziel-11], and by removing some features of the structure to speed up the EM simulation [Cervantes-González-15]. The main idea of space mapping is to approximate the inherent deviation between the fine and the coarse model responses by finding the mathematical relationship between the fine and the coarse model design spaces. The most popular space mapping technique is the so-called aggressive space mapping (ASM) [Rayas-Sánchez-16], which exploit the Broyden algorithm to linearly approximate the relationship between the fine and the coarse model designs. In this doctoral dissertation, the use of polynomial functions are also proposed to linearly approximate the relationship between the fine and the coarse models, instead of using the Broyden algorithm.

This doctoral dissertation is organized as follows:

Chapter 1 makes a review of previous polynomial formulations and presents the general formulation for the polynomial-based surrogate modeling technique exploiting the multinomial

theorem. This proposal is exemplified by developing EM-based surrogate models of three high frequency structures: 1) a SIW interconnect with transitions to microstrips, intended for signal transmission from 10 GHz to 40GHz, 2) a package via-stripline interconnect, which starts with a coaxial port in contact with a via pad, whose via connects the top and middle layers, and in the middle layer there is a stripline, and 3) a dual-band planar inverted-F handset antenna intended to operate at bands GSM900 (880-960 MHZ), GSM1900 (1850-1990 MHZ), UMTS2100, and WCDM2100 (1920-2170 MHz). The performance of the proposed modeling approach is compared against four surrogate modeling techniques: RSM, SVM, ANN, and Kriging.

In Chapter 2 are introduced the most important physical parameters to do a multiphysical analysis for high frequency structures. These parameters include elasticity and thermal properties of the materials used in high frequency circuits, such as the thermal expansion coefficient, the specific heat, the thermal conductivity, the Young's modulus, the shear modulus, and the Poisson's ratio. It is also presented the relationship between metallic and dielectric materials conductivity and the circuit temperature. A multiphysical example using COMSOL is presented to illustrate how the physical structure of the circuit is affected when varying the circuit temperature and how it affects the corresponding EM responses.

In Chapter 3 is presented a general formulation for multiphysical surrogate modeling of high frequency structures exploiting polynomial functions. The proposal expands the formulation introduced in Chapter 1 to incorporate the temperature dependence of the design parameters for developing multiphysics surrogate models. It is also presented the training procedure for calculating the weighting factors in two different forms, according to the best-conditioned system. The formulation is exemplified by developing a multiphysics surrogate model for a microstrip line where the corresponding EM responses are affected by the thermo-mechanical stress and changes in its electrical properties, due to variations in the structure temperature.

In Chapter 4 a space mapping approach is presented where polynomial functions are exploited to approximate the relationship between fine and coarse model designs. A very popular approach, known as aggressive space mapping, exploits the Broyden algorithm to find the mathematical relationship between fine and coarse model design spaces. In this chapter, the use of linear polynomials is proposed, instead of using the Broyden algorithm, to find that relationship. The proposal is exemplified by solving three synthetic space mapping problems: 1) a one-section impedance transformer, 2) a two-section impedance transformer, and c) an RLC parallel lumped

resonator.

In the general conclusions, the most relevant remarks about this doctoral dissertation are summarized, discussing the overall results of the proposed polynomial modeling methodology. Additionally, some ideas about possible future research work based on this doctoral dissertation are presented.

Finally, Appendix A shows the reference list of the eleven internal research reports that I wrote during the doctoral studies, and Appendix B shows the list of conference and journal papers published also during my doctoral studies in which I participated as co-author.

1. EM-based Polynomial Surrogate Modeling exploiting the Multinomial Theorem

In some areas of engineering it is computationally expensive to find an optimal design because it implies solving optimization problems involving too many expensive function evaluations [Koziel-14]. Surrogate-based optimization is an effective approach to solve this type of optimization problems.

The basic concept of surrogate-based optimization is that the direct optimization of the computationally expensive model is replaced by an iterative process that involves creating, optimizing, and updating a fast and analytically tractable surrogate model. Because most of the operations are performed on the surrogate model, surrogate-based optimization reduces the computational cost of the optimization process when compared to optimizing the original high-fidelity model directly [Koziel-11].

A surrogate model has to be computationally cheap, preferable smooth and reasonably accurate, so that it can be used to predict the location of high-fidelity model minimizers. Surrogate models can be classified into physical surrogates and functional surrogates. Physical surrogates consist of a low-fidelity physics-based model. This low-fidelity model is a physical representation of the system of interest with relaxed accuracy. It can be implemented, for example, with the same simulator as the one used to implement the high-fidelity model but using a coarse discretization. Functional surrogates are generated using high-fidelity model data obtained through sampling the design space [Koziel-11].

In this chapter, a mathematical formulation to represent EM responses in the frequency domain using polynomial functions is presented. The proposal exploits the multinomial theorem, which is a mathematical formulation that allows us to expand any polynomial function raised to an arbitrary power. The weighting factors can be calculated in closed form using two different approaches: a) by keeping fixed lower-order surrogates or b) by calculating all weighting factors simultaneously at each surrogate model order. This formulation is exemplified by developing surrogate models for three high frequency structures and comparing its performance against four well-stablished surrogate modeling techniques.

1.1. A Brief Introduction to Functional Surrogate Modeling

Different approaches can be used to develop functional surrogate models. Some of the most popular for EM design are based on Response Surface Methodology (RSM), Artificial Neural Networks (ANN), Support Vector Machines (SVM), and Kriging.

RSM generates a surrogate model representing the relationship between the design parameters and the resultant response by a second-order polynomial [Redhe-04], [Zhang-13], [Osborne-97]. The minimum number of function evaluations is equal to the number of unknowns in the polynomial equation [Redhe-04]. Some techniques, such D-optimal design of experiments, require twice that number of function evaluations [Mandic-13].

ANN models can be seen as non-linear data modeling tools capable of representing complex relationships between the input parameters and the EM structure responses [Haykin-99], [Mussetta-09]. A multilayer ANN model can approximate any kind of input-output deterministic relationship by using the correct amount of data and number of hidden neurons for its training [Rayas-Sánchez-04]. Typically, the learning error hypersurface contains many local minima. Global optimization algorithms should be used to train the neural network in order to reach the global minimum of the error surface [Raida-02]. Additionally, the number of learning base points needed to approximate a function grows exponentially with the ratio between dimensionality and the degree of smoothness [Rayas-Sánchez-04]. A particular case of ANNs that does not require an iterative training procedure are the generalized regression neural networks (GRNN) [Mahouti-14]. The number of neurons in the hidden layer of a GRNN is equal to the number of learning samples [Leng-13]. Some advantages of GRNN are fast learning and convergence to the optimal regression surface as the number of samples become very large, and no need of a minimum set of learning points for training the neural network. The GRNN model can be estimated by using even one learning base point, in which case the output of the neuron will be the same regardless the value of the new input vector [Specht-91], [Panda-14]. Examples of ANN surrogate modeling for EM structures can be found in [Raida-02], [Zhang-00], [Li-Na-11].

An alternative to ANN models are the SVM models. SVM modeling solves a complex constrained quadratic optimization problem, allowing the model to find a unique global optimum. The optimization problem is feasible due to the utilization of a kernel function. Some kernels commonly used are linear, polynomial, and radial basis functions. The radial basis function is the

most employed kernel since it creates a nonlinear map, taking the samples into a higher dimensional space with less numerical difficulties to find an optimum solution [Angiulli-07], [Xia-06]. Training of the SVM models is based on the principle of structural risk minimization instead of the empirical risk minimization used by the ANN models. The structural risk minimization principle allows the SVM models to have a good trade-off between the complexity of the model and the generalization capability [Tokan-09], [Ceperic-04]. Since SVM models are based on small sample statistical learning theory, an optimum solution can be found by using a limited number of samples [Xia-06]. Examples of SVM surrogate modeling for EM structures can be found in [Demirel-13], [Tokan-08], [Jacobs-12], [Ren-07].

Kriging is a modeling methodology developed by D. G. Krige in the 1950s to determine true ore bodies based on samples [Van Beers-05]. The prediction of a Kriging model depends on the distance between the input location to be predicted and the input locations already observed. The weights are chosen to minimize the prediction variance using the Best Linear Unbiased Estimator (BLUE) of the output value for a given input [Van Beers-05]. Implementation of RSM and ANN models usually employs classic design of experiments, where extreme scenarios are commonly simulated such as the corners of the corresponding design region. However, Kriging methodology is based on space-filling experiments, usually implemented by using the Latin Hypercube Design (LHD) [Van Beers-05], [Zhang-08]. Methodologically speaking, a Kriging model aims at covering the whole experimental area, consequently, it can be seen as a global metamodel [Van Beers-04]. If there are not enough function evaluations of the EM structure, the Kriging estimated correlation function tends to be noisy and the predictions become inaccurate. As the number of function evaluations increases, the Kriging predictions accuracy also increases [Van Beers-05]. Different Kriging techniques have been developed, such as simple Kriging, ordinary Kriging, universal Kriging, Taylor Kriging, and dynamic Kriging [Xia-14]. Examples of Kriging surrogate modeling of EM structures can be found in [Couckuyt-11], [Koziel-09]

In this doctoral dissertation, the proposed methodology represents the EM model response at each simulated frequency point by using polynomial functions based on the multinomial theorem. Since the surrogate model is implemented by using a simple mathematical formulation, the global minimum can be found in closed form for the weighting factors calculation. A similar approach to develop EM surrogate models based on polynomials is proposed in [Rayas-Sánchez-15b]; however, the approach presented in this chapter differs in three aspects: the surrogate model

formulation, the calculation of weighting factors, and the surrogate order determination. For the surrogate model formulation, [Rayas-Sánchez-15b] implements the *N*th order surrogate model by using an element-wise power operator, which creates some redundant terms, while the new formulation exploits the multinomial theorem, which allow us to expand a polynomial (input parameters) raised to any power including all cross terms and no redundant terms. For the weighting factors calculation, the approach in [Rayas-Sánchez-15b] calculates simultaneously all weighting factors available for each surrogate model order. In contrast, the proposed approach automatically calculates the weighting factors by assuming that lower-order surrogates are fixed or by calculating all weighting factors simultaneously, and the selection between both manners is based on the conditional number of the system matrix. Finally, the proposed methodology in this chapter allows the surrogate model order to be different for each simulated frequency point, while in [Rayas-Sánchez-15a] and [Rayas-Sánchez-15b] the same surrogate model order is used for all simulated frequency points.

1.2. Surrogate Modeling using Polynomial Functions

The computationally expensive high-fidelity model can be approximated around a reference design point $\boldsymbol{x}^{(0)}$ by a computational cheap polynomial surrogate model. The quadratic form of a scalar surrogate model can be placed in the form $a + \boldsymbol{b}^T(\boldsymbol{x} - \boldsymbol{x}^{(0)}) + ½(\boldsymbol{x} - \boldsymbol{x}^{(0)})^T \boldsymbol{B}(\boldsymbol{x} - \boldsymbol{x}^{(0)})$, where scalar $a \in \Re$, vector $\boldsymbol{b} \in \Re^n$, and symmetric matrix $\boldsymbol{B} \in \Re^{n\times n}$ are the unknown parameters of the surrogate model, and $\boldsymbol{x} \in \Re^n$ is the vector containing the design variables. The total number of the polynomial unknowns is $½(n + 1)(n + 2)$ [Koziel-13], [Koziel-14].

Let $\boldsymbol{R}_f \in \Re^p$ denote a fine model response sampled at p independent-variable points. The fine model can be treated as a multidimensional vector function, $\boldsymbol{R}_f(\boldsymbol{x}) : X_f \rightarrow \Re^p$ whose domain is $X_f \subseteq \Re^n$. The main purpose is to develop a surrogate model whose responses are very close to the fine model responses within a region of interest $X_s \subseteq X_f$, around the reference design $\boldsymbol{x}^{(0)}$. To train the surrogate model, L learning points within X_s are used. These points are denoted as $\boldsymbol{x}^{(1)}$, $\boldsymbol{x}^{(2)}$, … , $\boldsymbol{x}^{(L)}$.

1.2.1 Review of a Previous Polynomial Surrogate Modeling Formulation

A polynomial surrogate modeling proposal can be found in [Rayas-Sánchez-10], where the zero-order, first-order and second-order surrogate model are defined as follows.

The zero-order model is defined as the fine model response at the reference design,

$$\boldsymbol{R}_s^{(0)}(\boldsymbol{x}) = \boldsymbol{R}_f(\boldsymbol{x}^{(0)}) \text{ for all } \boldsymbol{x} \in X_s \tag{1-1}$$

The first-order surrogate model at the k-th simulated frequency point is defined in [Rayas-Sánchez-10] as

$$R_{sk}^{(1)}(\boldsymbol{x}) = R_{sk}^{(0)}(\boldsymbol{x}) + \boldsymbol{\Delta x}^T \boldsymbol{w}^{(1)} \tag{1-2}$$

where $\boldsymbol{\Delta x} \in \Re^n$ defines a deviation from a reference base point, $\boldsymbol{\Delta x} = \boldsymbol{x} - \boldsymbol{x}^{(0)}$, and $\boldsymbol{w}^{(1)} \in \Re^n$ contains all the first-order surrogate model weighting factors.

The second-order surrogate model is defined in [Rayas-Sánchez-10] as

$$R_{sk}^{(2)}(\boldsymbol{x}) = R_{sk}^{(1)}(\boldsymbol{x}) + \boldsymbol{\Delta x}^T \boldsymbol{W}^{(2)} \boldsymbol{\Delta x} \tag{1-3}$$

where $\boldsymbol{W}^{(2)} \in \Re^{n \times n}$ contains the second-order surrogate model weighting factors. Notice that formulation used in [Rayas-Sánchez-10] does not assume that $\boldsymbol{W}^{(2)}$ is symmetric. The total number of weighting factors in (1-3) is $n^2 + n$.

Third-order surrogate is defined in [Rayas-Sánchez-10] as

$$R_{sk}^{(3)}(\boldsymbol{x}) = R_{sk}^{(2)}(\boldsymbol{x}) + \boldsymbol{\Delta x}^T \boldsymbol{W}^{(3)} \boldsymbol{\Delta x}^{\wedge 2} \tag{1-4}$$

where operator ^ denotes element-wise power, and $\boldsymbol{W}^{(3)} \in \Re^{n \times n}$ contains the third-order surrogate weighting factors. The total number of weighting factors in (1-4) is $2n^2 + n$.

The weighting factors are obtained simultaneously using L learning base points. The third-order surrogate model response at the j-th learning base point $\boldsymbol{x}^{(j)}$ should match the corresponding fine model response,

$$R_{sk}^{(3)}(\boldsymbol{x}^{(j)}) = R_{sk}^{(2)}(\boldsymbol{x}^{(j)}) + \boldsymbol{\Delta x}^{(j)T} \boldsymbol{W}^{(3)} \boldsymbol{\Delta x}^{(j)\wedge 2} = R_{fk}(\boldsymbol{x}^{(j)}) \tag{1-5}$$

where $\boldsymbol{\Delta x}^{(j)} = \boldsymbol{x}^{(j)} - \boldsymbol{x}^{(0)}$. Applying (1-5) for $j = 1, \ldots, L$, the following system of linear equations is established

$$\boldsymbol{\Delta X w} = \boldsymbol{\Delta R}_k \tag{1-6}$$

where $\boldsymbol{w} \in \Re^{2n^2 + n}$, $\boldsymbol{\Delta X} = [\boldsymbol{\Delta X}^{(1)}\ \boldsymbol{\Delta X}^{(2)}\ \boldsymbol{\Delta X}^{(3)}] \in \Re^{L \times (2n^2 + n)}$,

$$\Delta \boldsymbol{R}_k = \begin{bmatrix} R_{fk}(\boldsymbol{x}^{(1)}) - R_{fk}(\boldsymbol{x}^{(0)}) \\ \vdots \\ R_{fk}(\boldsymbol{x}^{(L)}) - R_{fk}(\boldsymbol{x}^{(0)}) \end{bmatrix} \in \Re^L \tag{1-7}$$

$$\Delta \boldsymbol{X}^{(1)} = \begin{bmatrix} (\boldsymbol{x}^{(1)} - \boldsymbol{x}^{(0)})^{\mathrm{T}} \\ \vdots \\ (\boldsymbol{x}^{(L)} - \boldsymbol{x}^{(0)})^{\mathrm{T}} \end{bmatrix} = \begin{bmatrix} \Delta \boldsymbol{x}^{(1)\mathrm{T}} \\ \vdots \\ \Delta \boldsymbol{x}^{(L)\mathrm{T}} \end{bmatrix} \in \Re^{L \times n} \tag{1-8}$$

$$\Delta \boldsymbol{X}^{(2)} = \begin{bmatrix} \Delta x_1^{(1)} \Delta \boldsymbol{x}^{(1)\mathrm{T}} & \cdots & \Delta x_n^{(1)} \Delta \boldsymbol{x}^{(1)\mathrm{T}} \\ \vdots & \ddots & \vdots \\ \Delta x_1^{(L)} \Delta \boldsymbol{x}^{(L)\mathrm{T}} & \cdots & \Delta x_n^{(L)} \Delta \boldsymbol{x}^{(L)\mathrm{T}} \end{bmatrix} \in \Re^{L \times n^2} \tag{1-9}$$

$$\Delta \boldsymbol{X}^{(3)} = \begin{bmatrix} (\Delta x_1^{(1)})^2 \Delta \boldsymbol{x}^{(1)\mathrm{T}} & \cdots & (\Delta x_n^{(1)})^2 \Delta \boldsymbol{x}^{(1)\mathrm{T}} \\ \vdots & \ddots & \vdots \\ (\Delta x_1^{(L)})^2 \Delta \boldsymbol{x}^{(L)\mathrm{T}} & \cdots & (\Delta x_n^{(L)})^2 \Delta \boldsymbol{x}^{(L)\mathrm{T}} \end{bmatrix} \in \Re^{L \times n^2} \tag{1-10}$$

The surrogate model weighting factors can be found by solving (1-6) for any amount and distribution of learning base points,

$$\boldsymbol{w} = \Delta \boldsymbol{X}^{+} \Delta \boldsymbol{R}_k \text{ for } k = 1 \ \ldots \ p \tag{1-11}$$

where operator $^{+}$ denotes the pseudo-inverse.

1.2.2 New Polynomial Surrogate Modeling Formulation

The proposed surrogate design is based on the multinomial theorem. The multinomial theorem is a generalization of the binomial theorem to more than two variables. The multinomial theorem provides a formula for expanding a polynomial raised to an integer value. The expansion is given by [Encyc. Britannica-15]

$$(x_1 + x_2 + \ldots + x_k)^N = \sum_{N_1, N_2, \ldots, N_k \geq 0} {x_1}^{N_1} {x_2}^{N_2} \ldots {x_k}^{N_k} \tag{1-12}$$

where $N_1 + N_2 + \ldots + N_k = N$.

The zero-order surrogate is defined in the same manner as in (1-1). The first-order surrogate model at the k-th simulated frequency points is defined as

$$R_{sk}^{(1)}(\boldsymbol{x}) = R_{fk}(\boldsymbol{x}^{(0)}) + \boldsymbol{w}_k^{(1)\mathrm{T}} \boldsymbol{q}^{(1)}(\Delta \boldsymbol{x}) \tag{1-13}$$

where $\boldsymbol{w}_k^{(1)} \in \Re^n$ contains all the first-order surrogate model weighting factors and $\boldsymbol{q}^{(1)}(\Delta \boldsymbol{x}) \in \Re^n$

is a function that implements the multinomial theorem defined in (1-12) with respect to $\boldsymbol{\Delta x}$. The scalar elements of $\boldsymbol{q}^{(1)}(\boldsymbol{\Delta x})$ are defined as

$$q^{(1)}(\boldsymbol{\Delta x}) = \Delta x_{\lambda_1} \text{ for } \lambda_1 = 1{:}n \tag{1-14}$$

Notice that (1-14) is equivalent to (1-2).

The second-order surrogate model at the k-th simulated frequency point is defined as

$$R_{sk}^{(2)}(\boldsymbol{x}) = R_{sk}^{(1)}(\boldsymbol{x}) + \boldsymbol{w}_k^{(2)\mathrm{T}}\boldsymbol{q}^{(2)}(\boldsymbol{\Delta x}) \tag{1-15}$$

where $\boldsymbol{w}_k^{(2)} \in \Re^{n(n+1)/2}$ contains the second-order surrogate model weighting factors and $\boldsymbol{q}^{(2)}(\boldsymbol{\Delta x}) \in \Re^{n(n+1)/2}$ is a function that implements the multinomial theorem defined in (1-12) with respect to $\boldsymbol{\Delta x}$. The scalar elements of $\boldsymbol{q}^{(2)}(\boldsymbol{\Delta x})$ are defined as

$$q^{(2)}(\boldsymbol{\Delta x}) = \Delta x_{\lambda_1} \Delta x_{\lambda_2} \text{ for } \lambda_1 = 1{:}n \text{ and } \lambda_2 = \lambda_1{:}n \tag{1-16}$$

The third-order surrogate model at the k-th simulated frequency point is defined as

$$R_{sk}^{(3)}(\boldsymbol{x}) = R_{sk}^{(2)}(\boldsymbol{x}) + \boldsymbol{w}_k^{(3)\mathrm{T}}\boldsymbol{q}^{(3)}(\boldsymbol{\Delta x}) \tag{1-17}$$

where $\boldsymbol{w}_k^{(3)} \in \Re^{n(n+1)(n+2)/6}$ contains the second-order surrogate model weighting factors and $\boldsymbol{q}^{(2)}(\boldsymbol{\Delta x}) \in \Re^{n(n+1)(n+2)/6}$ is a function that implements the multinomial theorem defined in (1-12) with respect to $\boldsymbol{\Delta x}$. The scalar elements of $\boldsymbol{q}^{(3)}(\boldsymbol{\Delta x})$ are defined as

$$q^{(3)}(\boldsymbol{\Delta x}) = \Delta x_{\lambda_1} \Delta x_{\lambda_2} \Delta x_{\lambda_3} \text{ for } \lambda_1 = 1{:}n,\ \lambda_2 = \lambda_1{:}n \text{ and } \lambda_3 = \lambda_2{:}n \tag{1-18}$$

A general expression for an N-order surrogate model at the k-th simulated frequency points can be written as

$$R_{sk}^{(N)}(\boldsymbol{x}) = R_{sk}^{(N-1)}(\boldsymbol{x}) + \boldsymbol{w}_k^{(N)\mathrm{T}}\boldsymbol{q}^{(N)}(\boldsymbol{\Delta x}) \tag{1-19}$$

where $\boldsymbol{q}^{(N)}(\boldsymbol{\Delta x}) \in \Re^{(N+n-1)!/(n-1)!(N)!}$ is a function that implements the multinomial theorem defined in (1-12) to $\boldsymbol{\Delta x}$, and $\boldsymbol{w}_k^{(N)} \in \Re^{(N+n-1)!/(n-1)!(N)!}$ contains the N-order surrogate model weighting factors.

1.3. Training the Polynomial-based Surrogate Model

"Training" the surrogate model formulated in Sub-section 1.2.2 is done by calculating in closed form the corresponding weighting factors.

The size of the training region X_s is defined by a vector $\boldsymbol{\tau} \in \Re^n$ containing the relative deviation for each design variable with respect to $\boldsymbol{x}^{(0)}$. To train the surrogate model, L learning

base points within X_s are used, denoted as $\boldsymbol{x}^{(1)}, \boldsymbol{x}^{(2)}, \ldots, \boldsymbol{x}^{(L)}$. To measure the generalization error of the surrogate model, T testing base points are used. The surrogate model weighting factors can be calculated a) by assuming that the lower-order surrogates are already calculated or, b) by calculating all the weighting factors simultaneously at each surrogate model order.

1.3.1 Weighting Factors Calculation with Lower-order Surrogates Fixed

For the first-order surrogate model, the response at the j-th learning base point $\boldsymbol{x}^{(j)}$ and k-th frequency point should match the corresponding fine model response,

$$R_{sk}^{(1)}(\boldsymbol{x}^{(j)}) = R_{sk}^{(0)}(\boldsymbol{x}^{(j)}) + \boldsymbol{w}_k^{(1)\mathrm{T}}\boldsymbol{q}^{(1)}(\boldsymbol{\Delta x}^{(j)}) = R_{fk}(\boldsymbol{x}^{(j)}) \tag{1-20}$$

where $\boldsymbol{\Delta x}^{(j)} = \boldsymbol{x}^{(j)} - \boldsymbol{x}^{(0)}$. Applying (1-20) for $j = 1, \ldots, L$, the surrogate model weighting factors can be calculated by solving for $\boldsymbol{w}_k^{(1)}$ the following system of linear equations

$$\boldsymbol{Q}^{(1)}\boldsymbol{w}_k^{(1)} = \boldsymbol{\Delta R}_k^{(1)} \text{ for } k = 1 \ldots p \tag{1-21}$$

where $\boldsymbol{Q}^{(1)} \in \Re^{L\times n}$ and $\boldsymbol{\Delta R}_k^{(1)} \in \Re^{L}$ are defined as

$$\boldsymbol{Q}^{(1)} = \begin{bmatrix} \boldsymbol{q}^{(1)}(\boldsymbol{\Delta x}^{(1)})^{\mathrm{T}} \\ \boldsymbol{q}^{(1)}(\boldsymbol{\Delta x}^{(2)})^{\mathrm{T}} \\ \vdots \\ \boldsymbol{q}^{(1)}(\boldsymbol{\Delta x}^{(L)})^{\mathrm{T}} \end{bmatrix} \tag{1-22}$$

$$\boldsymbol{\Delta R}_k^{(1)} = \begin{bmatrix} R_{fk}(\boldsymbol{x}^{(1)}) - R_{sk}^{(0)}(\boldsymbol{x}^{(1)}) \\ \vdots \\ R_{fk}(\boldsymbol{x}^{(L)}) - R_{sk}^{(0)}(\boldsymbol{x}^{(L)}) \end{bmatrix} \tag{1-23}$$

For the second-order surrogate model, the response should match the corresponding fine model response at the j-th learning base point,

$$R_{sk}^{(2)}(\boldsymbol{x}^{(j)}) = R_{sk}^{(1)}(\boldsymbol{x}^{(j)}) + \boldsymbol{w}_k^{(2)\mathrm{T}}\boldsymbol{q}^{(2)}(\boldsymbol{\Delta x}^{(j)}) = R_{fk}(\boldsymbol{x}^{(j)}) \tag{1-24}$$

Notice that it is assumed that lower-order surrogates are already calculated, hence, the weighting factors for $R_{sk}^{(1)}$ in (1-24) are taken from (1-21). Hence, the second-order surrogate weighting factors can be calculated by solving for $\boldsymbol{w}_k^{(2)}$ the following system of linear equations

$$\boldsymbol{Q}^{(2)}\boldsymbol{w}_k^{(2)} = \boldsymbol{\Delta R}_k^{(2)} \text{ for } k = 1 \ldots p \tag{1-25}$$

where $\boldsymbol{Q}^{(2)} \in \Re^{L\times n(n+1)/2}$ and $\boldsymbol{\Delta R}_k^{(2)} \in \Re^{L}$ are defined as

$$\boldsymbol{Q}^{(2)} = \begin{bmatrix} \boldsymbol{q}^{(2)}(\boldsymbol{\Delta x}^{(1)})^{\mathrm{T}} \\ \boldsymbol{q}^{(2)}(\boldsymbol{\Delta x}^{(2)})^{\mathrm{T}} \\ \vdots \\ \boldsymbol{q}^{(2)}(\boldsymbol{\Delta x}^{(L)})^{\mathrm{T}} \end{bmatrix} \tag{1-26}$$

$$\boldsymbol{\Delta R}_k^{(2)} = \begin{bmatrix} R_{\mathrm{f}k}(\boldsymbol{x}^{(1)}) - R_{\mathrm{s}k}^{(1)}(\boldsymbol{x}^{(1)}) \\ \vdots \\ R_{\mathrm{f}k}(\boldsymbol{x}^{(L)}) - R_{\mathrm{s}k}^{(1)}(\boldsymbol{x}^{(L)}) \end{bmatrix} \tag{1-27}$$

For the third-order surrogate model, it is aimed to match the fine model response and the corresponding surrogate model response at the j-th learning base point,

$$R_{\mathrm{s}k}^{(3)}(\boldsymbol{x}^{(j)}) = R_{\mathrm{s}k}^{(2)}(\boldsymbol{x}^{(j)}) + \boldsymbol{w}_k^{(3)\mathrm{T}}\boldsymbol{q}^{(3)}(\boldsymbol{\Delta x}^{(j)}) = R_{\mathrm{f}k}(\boldsymbol{x}^{(j)}) \tag{1-28}$$

Assuming that the lower-order surrogates are already calculated, the weighting factors of $R_{\mathrm{s}k}^{(2)}$ in (1-28) are taken from (1-18). The third-order surrogate weighting factors can be calculated by solving for $\boldsymbol{w}_k^{(3)}$ the following system of linear equations

$$\boldsymbol{Q}^{(3)}\boldsymbol{w}_k^{(3)} = \boldsymbol{\Delta R}_k^{(3)} \text{ for } k = 1 \ldots p \tag{1-29}$$

where $\boldsymbol{Q}^{(3)} \in \Re^{L \times n(n+1)(n+2)/6}$ and $\boldsymbol{\Delta R}_k^{(3)} \in \Re^{L}$ are defined as

$$\boldsymbol{Q}^{(3)} = \begin{bmatrix} \boldsymbol{q}^{(3)}(\boldsymbol{\Delta x}^{(1)})^{\mathrm{T}} \\ \boldsymbol{q}^{(3)}(\boldsymbol{\Delta x}^{(2)})^{\mathrm{T}} \\ \vdots \\ \boldsymbol{q}^{(3)}(\boldsymbol{\Delta x}^{(L)})^{\mathrm{T}} \end{bmatrix} \tag{1-30}$$

$$\boldsymbol{\Delta R}_k^{(3)} = \begin{bmatrix} R_{\mathrm{f}k}(\boldsymbol{x}^{(1)}) - R_{\mathrm{s}k}^{(2)}(\boldsymbol{x}^{(1)}) \\ \vdots \\ R_{\mathrm{f}k}(\boldsymbol{x}^{(L)}) - R_{\mathrm{s}k}^{(2)}(\boldsymbol{x}^{(L)}) \end{bmatrix} \tag{1-31}$$

Finally, for the N-th-order surrogate model, the fine model response and the corresponding surrogate model response are matched at the j-th learning base point,

$$R_{\mathrm{s}k}^{(N)}(\boldsymbol{x}^{(j)}) = R_{\mathrm{s}k}^{(N-1)}(\boldsymbol{x}^{(j)}) + \boldsymbol{w}_k^{(N)\mathrm{T}}\boldsymbol{q}^{(N)}(\boldsymbol{\Delta x}^{(j)}) = R_{\mathrm{f}k}(\boldsymbol{x}^{(j)}) \tag{1-32}$$

Assuming that the lower-order surrogates are already calculated, the corresponding N-th-order weighting factors can be calculated by solving for $\boldsymbol{w}_k^{(N)}$ the following system of linear equations

$$\boldsymbol{Q}^{(N)}\boldsymbol{w}_k^{(N)} = \boldsymbol{\Delta R}_k^{(N)} \text{ for } k = 1 \ldots p \tag{1-33}$$

where $\boldsymbol{Q}^{(N)} \in \Re^{(N+n-1)!/(n-1)!(N)!}$ and $\boldsymbol{\Delta R}_k^{(N)} \in \Re^{L}$ are defined as

$$\boldsymbol{Q}^{(N)} = \begin{bmatrix} \boldsymbol{q}^{(N)}(\boldsymbol{\Delta x}^{(1)})^{\mathrm{T}} \\ \boldsymbol{q}^{(N)}(\boldsymbol{\Delta x}^{(2)})^{\mathrm{T}} \\ \vdots \\ \boldsymbol{q}^{(N)}(\boldsymbol{\Delta x}^{(L)})^{\mathrm{T}} \end{bmatrix} \tag{1-34}$$

$$\boldsymbol{\Delta R}_k^{(N)} = \begin{bmatrix} R_{\mathrm{f}k}(\boldsymbol{x}^{(1)}) - R_{\mathrm{s}k}{}^{(N-1)}(\boldsymbol{x}^{(1)}) \\ \vdots \\ R_{\mathrm{f}k}(\boldsymbol{x}^{(L)}) - R_{\mathrm{s}k}{}^{(N-1)}(\boldsymbol{x}^{(L)}) \end{bmatrix} \tag{1-35}$$

1.3.2 Calculating All Weighting Factors at Each Surrogate Model Order

For the first-order surrogate model, the response at the j-th learning base point $\boldsymbol{x}^{(j)}$ and k-th frequency point should match the corresponding fine model response,

$$R_{sk}{}^{(1)}(\boldsymbol{x}^{(j)}) = R_{sk}{}^{(0)}(\boldsymbol{x}^{(j)}) + \boldsymbol{w}_k{}^{(1)\mathrm{T}}\boldsymbol{q}^{(1)}(\boldsymbol{\Delta x}^{(j)}) = R_{fk}(\boldsymbol{x}^{(j)}) \tag{1-36}$$

Applying (1-36) for $j = 1, \ldots, L$, the surrogate model weighting factors can be calculated by solving for $\boldsymbol{W}^{(1)}$ the following system of linear equations

$$\boldsymbol{Q}_{\mathrm{All}}^{(1)}\boldsymbol{W}^{(1)} = \boldsymbol{\Delta R}_k \text{ for } k = 1 \ \ldots \ p \tag{1-37}$$

where $\boldsymbol{Q}_{\mathrm{All}}^{(1)} \in \Re^{L\times n}$, $\boldsymbol{W}^{(1)} \in \Re^{n}$ and $\boldsymbol{\Delta R}_k{}^{(1)} \in \Re^{L}$ are defined as

$$\boldsymbol{Q}_{\mathrm{All}}^{(1)} = [\boldsymbol{Q}^{(1)}] \tag{1-38}$$

$$\boldsymbol{W}^{(1)} = [\boldsymbol{w}_k^{(1)}] \tag{1-39}$$

$$\boldsymbol{\Delta R}_k = \begin{bmatrix} R_{\mathrm{f}k}(\boldsymbol{x}^{(1)}) - R_{\mathrm{f}k}(\boldsymbol{x}^{(0)}) \\ \vdots \\ R_{\mathrm{f}k}(\boldsymbol{x}^{(L)}) - R_{\mathrm{f}k}(\boldsymbol{x}^{(0)}) \end{bmatrix} \tag{1-40}$$

For the second-order surrogate model, the response should match the corresponding fine model response at the j-th learning base point,

$$R_{sk}{}^{(2)}(\boldsymbol{x}^{(j)}) = R_{sk}{}^{(0)}(\boldsymbol{x}^{(j)}) + \boldsymbol{w}_k{}^{(1)\mathrm{T}}\boldsymbol{q}^{(1)}(\boldsymbol{\Delta x}^{(j)}) + \boldsymbol{w}_k{}^{(2)\mathrm{T}}\boldsymbol{q}^{(2)}(\boldsymbol{\Delta x}^{(j)}) = R_{fk}(\boldsymbol{x}^{(j)}) \tag{1-41}$$

Applying (1-41) for $j = 1, \ldots, L$, the surrogate model weighting factors can be calculated by solving for $\boldsymbol{W}^{(2)}$ the following system of linear equations

$$\boldsymbol{Q}_{\mathrm{All}}^{(2)}\boldsymbol{W}^{(2)} = \boldsymbol{\Delta R}_k \text{ for } k = 1 \ \ldots \ p \tag{1-42}$$

where $\boldsymbol{Q}_{\text{All}}^{(2)} \in \Re^{L\times n+(n+1)/2}$ and $\boldsymbol{W}^{(2)} \in \Re^{n+(n+1)/2}$ are defined as

$$\boldsymbol{Q}_{\text{All}}^{(2)} = \left[\boldsymbol{Q}^{(1)} \quad \boldsymbol{Q}^{(2)}\right] \tag{1-43}$$

$$\boldsymbol{W}^{(2)} = \left[\boldsymbol{w}_k^{(1)} \quad \boldsymbol{w}_k^{(2)}\right] \tag{1-44}$$

For the third-order surrogate model, the purpose is to match the fine model response and the corresponding surrogate model response at the j-th learning base point,

$$R_{sk}^{(3)}(\boldsymbol{x}^{(j)}) = R_{sk}^{(0)}(\boldsymbol{x}^{(j)}) + \boldsymbol{w}_k^{(1)\text{T}}\boldsymbol{q}^{(1)}(\boldsymbol{\Delta x}^{(j)}) + \boldsymbol{w}_k^{(2)\text{T}}\boldsymbol{q}^{(2)}(\boldsymbol{\Delta x}^{(j)}) + \boldsymbol{w}_k^{(3)\text{T}}\boldsymbol{q}^{(3)}(\boldsymbol{\Delta x}^{(j)}) = R_{fk}(\boldsymbol{x}^{(j)}) \tag{1-45}$$

Applying (1-45) for $j = 1, \ldots, L$, the surrogate model weighting factors can be calculated by solving for $\boldsymbol{W}^{(3)}$ the following system of linear equations

$$\boldsymbol{Q}_{\text{All}}^{(3)}\,\boldsymbol{W}^{(3)} = \boldsymbol{\Delta R}_k \text{ for } k = 1 \ldots p \tag{1-46}$$

where $\boldsymbol{Q}_{\text{All}}^{(3)} \in \Re^{L\times n+n(n+1)/2+n(n+1)(n+2)/6}$ and $\boldsymbol{W}^{(3)} \in \Re^{n+n(n+1)/2+n(n+1)(n+2)/6}$ are defined as

$$\boldsymbol{Q}_{\text{All}}^{(3)} = \left[\boldsymbol{Q}^{(1)} \quad \boldsymbol{Q}^{(2)} \quad \boldsymbol{Q}^{(3)}\right] \tag{1-47}$$

$$\boldsymbol{W}^{(3)} = \left[\boldsymbol{w}_k^{(1)} \quad \boldsymbol{w}_k^{(2)} \quad \boldsymbol{w}_k^{(3)}\right] \tag{1-48}$$

For the N-th-order surrogate model, the fine model response and the corresponding surrogate model response are matched at the j-th learning base point,

$$R_{sk}^{(N)}(\boldsymbol{x}^{(j)}) = R_{sk}^{(0)}(\boldsymbol{x}^{(j)}) + \boldsymbol{w}_k^{(1)}\boldsymbol{q}^{(1)\text{T}}(\boldsymbol{\Delta x}^{(j)}) + \ldots + \boldsymbol{w}_k^{(N)}\boldsymbol{q}^{(N)\text{T}}(\boldsymbol{\Delta x}^{(j)}) = R_{fk}(\boldsymbol{x}^{(j)}) \tag{1-49}$$

Applying (1-49) for $j = 1, \ldots, L$, the surrogate model weighting factors can be calculated by solving for $\boldsymbol{W}^{(N)}$ the following system of linear equations

$$\boldsymbol{Q}_{\text{All}}^{(N)}\,\boldsymbol{W}^{(N)} = \boldsymbol{\Delta R}_k \text{ for } k = 1 \ldots p \tag{1-50}$$

where $\boldsymbol{Q}_{\text{All}}^{(N)} \in \Re^{L\times C}$, $\boldsymbol{W}^{(N)} \in \Re^{C}$ and C are defined as

$$\boldsymbol{Q}_{\text{All}}^{(N)} = \left[\boldsymbol{Q}^{(1)} \quad \boldsymbol{Q}^{(2)} \quad \cdots \quad \boldsymbol{Q}^{(N)}\right] \tag{1-51}$$

$$\boldsymbol{W}^{(N)} = \left[\boldsymbol{w}_k^{(1)} \quad \boldsymbol{w}_k^{(2)} \quad \cdots \quad \boldsymbol{w}_k^{(N)}\right] \tag{1-52}$$

$$C = \sum_{1}^{N} \frac{(N+n-1)!}{(n-1)!(N)!} \tag{1-53}$$

1.3.3 Solving the System of Linear Equations

To solve (1-33) and (1-50) the Matlab function called mldivide, which operator symbol is represented as "\", is employed. By using this function, Matlab decides which is the best algorithm

to solve the linear equations system based on the shape of the input matrixes.

1.3.4 Selecting How the Weighting Factors are Calculated

Depending on the condition number of the system matrix, weighting factors are calculated by assuming that the lower order surrogates are already available and fixed, or by calculating simultaneously all weighting factors for each surrogate model order. This is realized by comparing the condition number of matrices $\boldsymbol{Q}^{(N)}$ in (1-33) and $\boldsymbol{Q}^{(N)}{}_{\mathrm{ALL}}$ in (1-50). If the condition number of matrix $\boldsymbol{Q}^{(N)}$ is smaller than that one of matrix $\boldsymbol{Q}^{(N)}{}_{\mathrm{ALL}}$, weighting factors are calculated by solving (1-33), otherwise, by solving (1-50). In other words, we solve the best conditioned system of linear equations between (1-33) and (1-40).

1.4. EM-based Surrogate Modeling Examples

For the following examples, the performance of three EM surrogate model designs is compared by using five different surrogate modeling methods: RSM, SVM, Kriging, GRNN, and the polynomial surrogate modeling method proposed in this doctoral dissertation (PSM). Comparison is done based on the maximum absolute error obtained when using the testing base points.

For the learning base point distributions, a star, a box and a uniform distribution are used. A star distribution results in $2n$ base points, a box distribution results in 2^n base points, while a uniform distribution results in K^n base points, where K corresponds to the number of points uniformly distributed for each parameter.

In all cases, the maximum absolute error in the learning set at each frequency point is calculated, denoted as ϵ_{L}, as well as the maximum absolute error in the testing set at each frequency point, denoted as ϵ_{T}. To denote the largest maximum absolute error in the complete frequency sweep we use ϵ_{Lmax} and ϵ_{Tmax}, for the learning and testing sets, respectively.

In all the following examples, the EM simulations are performed on a core i5 CPU with 8 Gb RAM.

1.4.1 SIW Interconnect with Transitions to Microstrips

As a first example, consider the single-layer substrate integrated waveguide (SIW) interconnect with microstrip transitions proposed in [Rayas-Sánchez-15b]. Its geometry is shown in Fig. 1.1. The tapered microstrip transitions are intended to simultaneously perform field conversion and impedance matching of the two dissimilar guiding structures [Ogurtsov-10]. The SIW is embedded in a dielectric layer with height H = 16 mil, and relative dielectric constant ε_r = 3.6. The SIW waveguide length is $L_{SIW} = 4W$ and has an external width W = 379.71 mil. Each via has a diameter d = 18.9 mil and is separated from its neighboring via by a center-to-center spacing $s = 2d$. The required cutoff frequency for the dominant mode is f_{c10} = 10 GHz, for which the SIW width is W_{SIW} = 341.91 mil [Rayas-Sánchez-15b]. The width of the 50-Ω microstrip line is W_p = 34.14 mil and its length is $L_p = 1.5W$. The initial transition uses $L_{tap} = 3W$ and $W_{tap} = (W_{SIW} + W_p)/2$.

The structure is implemented in COMSOL. Our model neglects dielectric and metallic losses by setting $\tan(\delta) = 0$ and by setting all metals as perfect electric conductors (PEC). The simulation bounding box is configured as scattering boundary condition, excepting for the bottom cover which is configured as PEC to act as a ground plane. A meshing scheme by zones as proposed in [Brito-Brito-13] is used, and the bounding box dimensions as proposed in [Chávez-Hurtado-14]. A relatively coarse resolution discretization is implemented. Each frequency sweeps takes around 1 h 20 min.

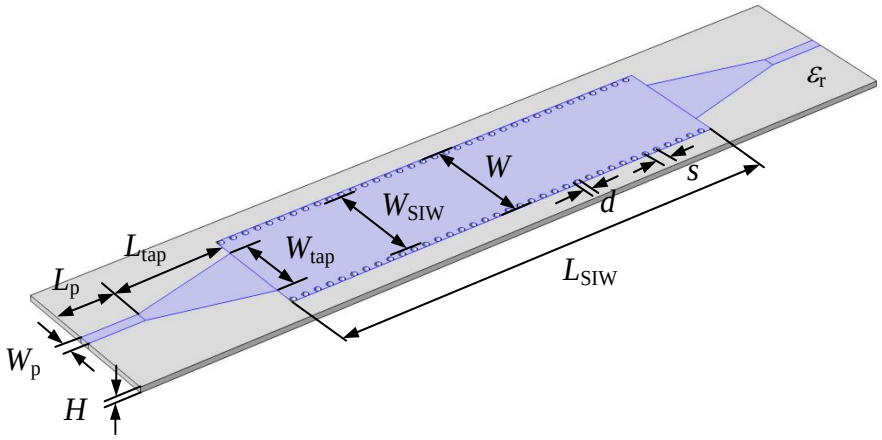

Fig. 1.1 Single-layer substrate integrated waveguide (SIW) interconnect with microstrip transitions. From [Rayas-Sánchez-15a].

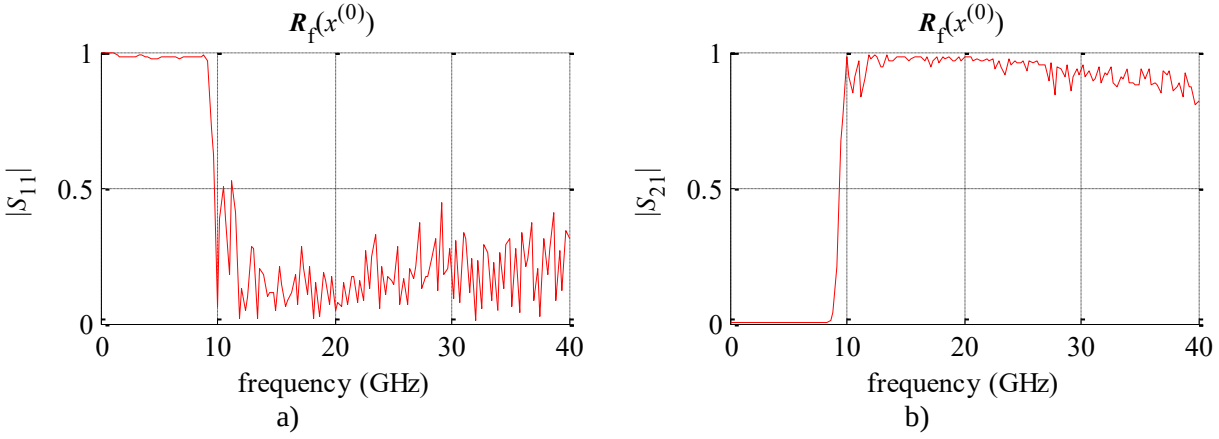

Fig. 1.2 EM responses of the SIW interconnect with microstrip transitions at $\boldsymbol{x}^{(0)}$: a) $|S_{11}|$ and b) $|S_{21}|$.

Transmission in the SIW interconnect can be enhanced by improving the transition [RayasSánchez-15b], for which polynomial surrogate model for $|S_{21}|$ is developed as a function of $\boldsymbol{x} = [W_{tap} \;\; L_{tap}]^T$, using as a reference design $\boldsymbol{x}^{(0)} = [(W_{SIW}+W_p)/2 \;\; 3W_{SIW}]^T$, over a region defined by $\boldsymbol{\tau} = [5\% \;\; 5\%]^T$. EM responses of the SIW interconnect at $\boldsymbol{x}^{(0)}$ are shown in Fig. 1.2.

To train the surrogate models, three different learning base point distributions are used: star, box and a uniform distribution with $K = 5$ (25 learning base points). To test the generalization performance of the implemented surrogate models, a uniform distribution with $K = 4$ (16 testing base points) is used. Maximum absolute errors for all frequency points using RSM, SVM, Kriging, GRNN, and PSM are shown in Table 1.3-1.1. The maximum absolute errors for the three learning base point distributions at each simulated frequency point are illustrated in Fig. 1.4-1.3.

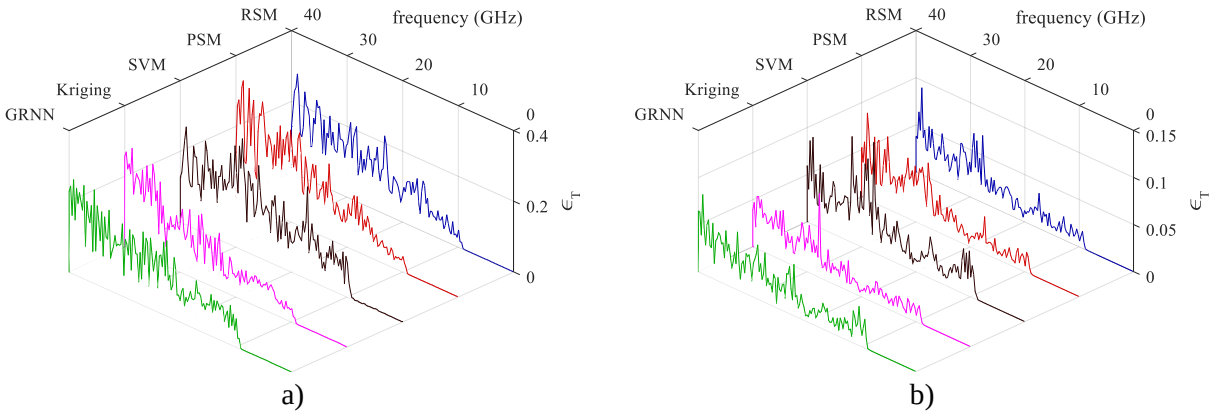

a) b)

Fig. 1.3 Maximum absolute testing error at each simulated frequency point for the SIW interconnect, using a star distribution of learning base points and a uniform distribution of testing base points with $K = 4$: a) for $|S_{11}|$, b) for $|S_{21}|$.

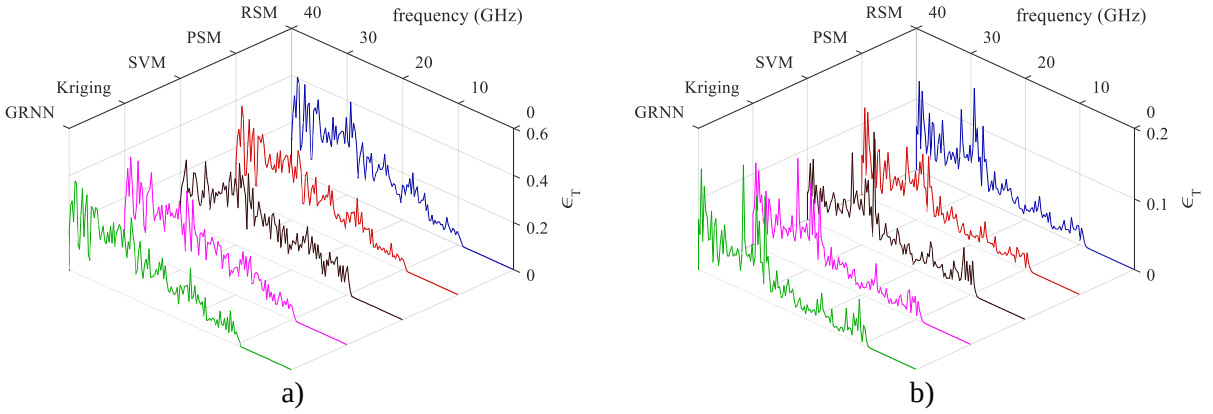

a) b)

Fig. 1.4 Maximum absolute testing error at each simulated frequency point for the SIW interconnect, using a box distribution of learning base points and a uniform distribution of testing base points with $K = 4$: a) for $|S_{11}|$, b) for $|S_{21}|$.

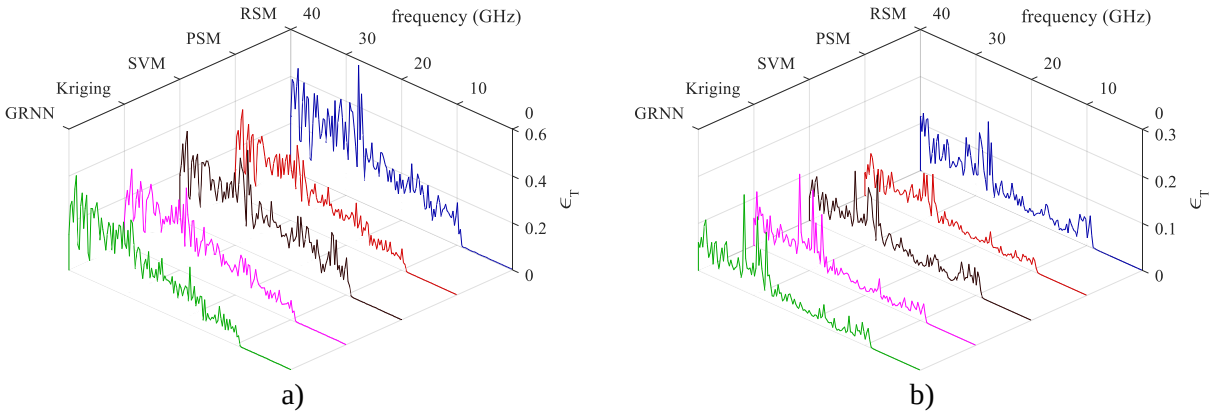

a) b)

Fig. 1.5 Maximum absolute testing error at each simulated frequency point for the SIW interconnect, using a uniform distribution of learning base points with $K = 5$ and a uniform distribution of testing base points with $K = 4$: a) for $|S_{11}|$, b) for $|S_{21}|$.

It can be noted from the corresponding results that PSM has the best performance when

TABLE 1.1. MAXIMUM ABSOLUTE ERROR FOR ALL SIMULATED FREQUENCY POINTS FOR THE SIW INTERCONNECT USING A STAR DISTRIBUTION OF LEARNING BASE POINTS AND A UNIFORM DISTRIBUTION OF TESTING BASE POINTS WITH K = 4

Model	$\|S_{11}\|$		$\|S_{21}\|$	
	ϵ_{Tmax}	ϵ_{Lmax}	ϵ_{Tmax}	ϵ_{Lmax}
RSM	0.57844	4.9183×10^{-14}	0.16921	1.9318×10^{-14}
PSM	0.37909	0.15773	0.11067	0.085665
SVM	0.42733	0.30279	0.16160	0.14324
Kriging	0.36131	0.11158	0.19523	0.12441
GRNN	0.41595	0	0.20462	0

TABLE 1.2. MAXIMUM ABSOLUTE ERROR FOR ALL SIMULATED FREQUENCY POINTS FOR THE SIW INTERCONNECT USING A BOX DISTRIBUTION OF LEARNING BASE POINTS AND A UNIFORM DISTRIBUTION OF TESTING BASE POINTS WITH K = 4

Model	$\|S_{11}\|$		$\|S_{21}\|$	
	ϵ_{Tmax}	ϵ_{Lmax}	ϵ_{Tmax}	ϵ_{Lmax}
RSM	0.40461	4.0856e-14	0.15296	8.4377×10^{-15}
PSM	0.38664	0.11959	0.12502	0.096922
SVM	0.35230	0.26800	0.16686	0.083662
Kriging	0.38300	0.21605	0.15086	0.150860
GRNN	0.38767	0	0.17695	0

TABLE 1.3. MAXIMUM ABSOLUTE ERROR FOR ALL SIMULATED FREQUENCY POINTS FOR THE SIW INTERCONNECT USING A UNIFORM DISTRIBUTION OF LEARNING BASE POINTS WITH K = 5 AND A UNIFORM DISTRIBUTION OF TESTING BASE POINTS WITH K = 4

Model	$\|S_{11}\|$		$\|S_{21}\|$	
	ϵ_{Tmax}	ϵ_{Lmax}	ϵ_{Tmax}	ϵ_{Lmax}
RSM	0.28512	0.26594	0.092123	0.093961
PSM	0.33876	0.28701	0.091595	0.084996
SVM	0.31450	0.37194	0.116660	0.1233
Kriging	0.28822	0.08864	0.088960	0.08896
GRNN	0.26662	5.5016×10^{-08}	0.083849	5.0285×10^{-08}

using a small amount of learning base point (star and box distribution) for $|S_{21}|$, while GRNN performance is the best when using a large amount of learning base points (uniform K = 5).

1.4.2 Package Via-Stripline Interconnect

For a second example, consider the package via-stripline-via interconnect in [Cervantes-González-13]. Its geometry is shown in Fig. 1.6. The structure is implemented on a substrate with a relative dielectric permittivity $\varepsilon_r = 3.34$, a loss tangent $\tan\delta = 0.018$, and a thickness $H_1 = H_2 = 22.5$ μm. The length and width of the stripline are $l_{tr} = 3000$ μm and $W_{tr} = 21$ μm, respectively. Vias, pads and antipads radius are $r_{lv1} = r_{lv2} = 26$ μm, $r_{2p1} = r_{1p1} = r_{2p2} = r_{1p2} = 54$ μm, $r_{1a1} = r_{1a2} =$

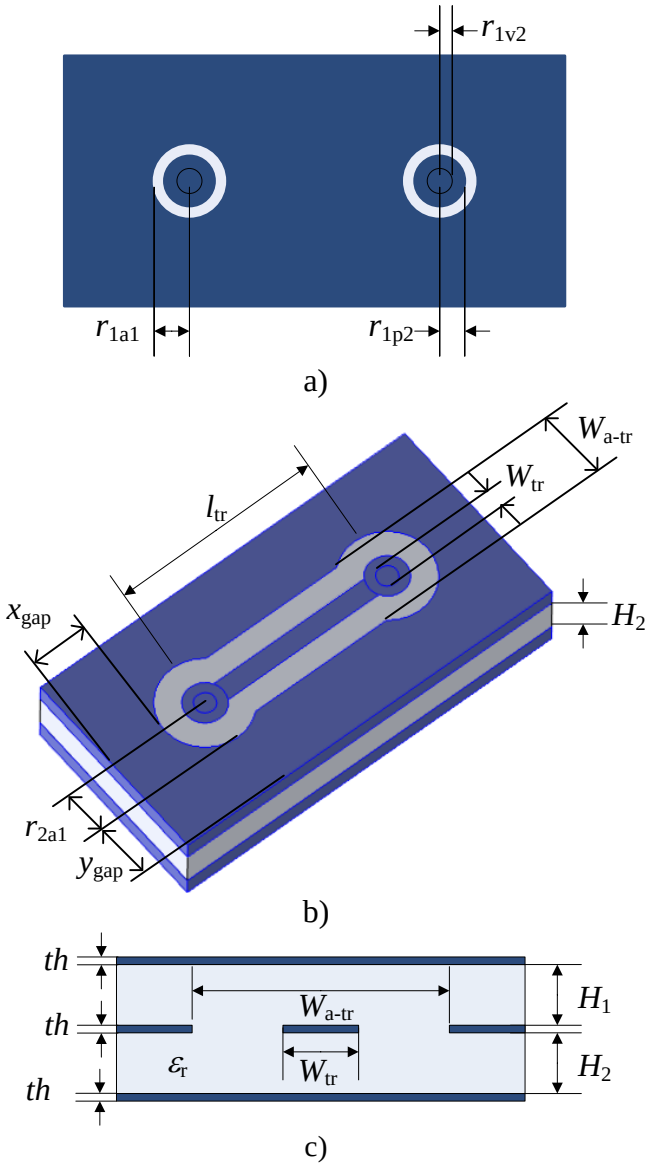

Fig. 1.6 Via-stripline model. A) 2D-Top view (top layer), b) middle layer 3D-model, and c) cross section. From [Cervantes-González-13].

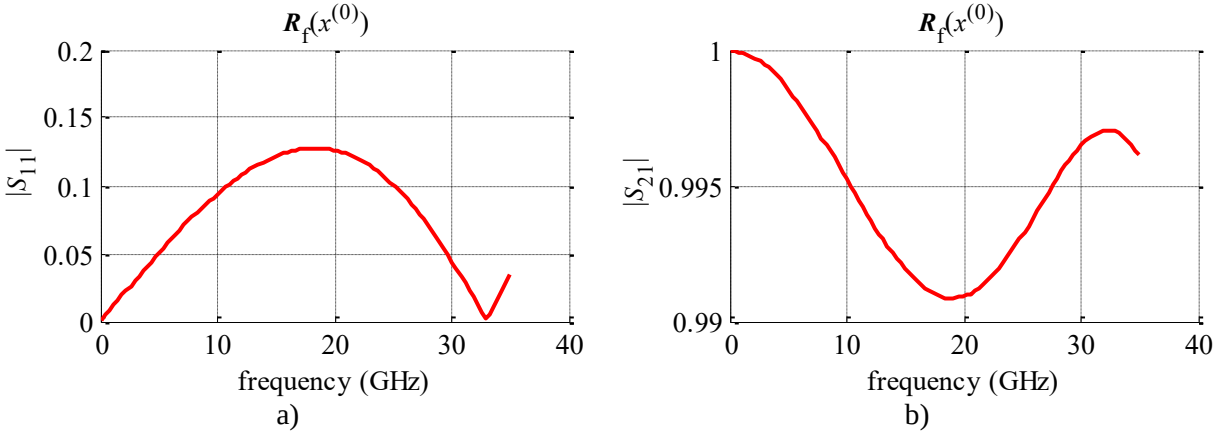

Fig. 1.7 EM response of the via-stripline-via model at $\boldsymbol{x}^{(0)}$: a) $|S_{11}|$ and b) $|S_{21}|$.

104 μm, $r_{2a1} = r_{2a2} = 220$ μm. Distances from the via-stripline-via interconnect to lateral and front walls are $x_{gap} = y_{gap} = 280$ μm, respectively. Metals are defined as perfect electric conductors.

The structure is implemented in COMSOL by using the simulation bounding box dimensions, boundary conditions, and the meshing scheme proposed in [Cervantes-González-13]. A relatively coarse resolution discretization is used, such that each frequency sweeps takes around 1 min 20s.

For developing the surrogate model the anti-pads radius are used as input parameters, with $r_{1a} = r_{1a1} = r_{1a2}$, and $r_{2a} = r_{2a1} = r_{2a2}$. Then, $\boldsymbol{x} = [r_{1a} \quad r_{2a}]^T$. The reference design is defined as $\boldsymbol{x}^{(0)} = [104 \quad 220]^T$ (μm). The design region is delimited by $\boldsymbol{\tau} = [5\% \ 5\%]^T$. EM responses of the via-stripline-via interconnect at $\boldsymbol{x}^{(0)}$ are illustrated in Fig. 1.7.

To train the surrogate model three different learning base points distribution are used: a star, box and uniform distribution with $K = 5$ (25 learning base points). To test their generalization performance of each implemented surrogate model a uniform distribution with $K = 4$ (16 testing base points) is used. Resultant maximum absolute error for the five different surrogate models for all frequency points are reported in Table 1.4-1.6. Maximum absolute errors at each simulated frequency point is illustrated in Fig. 1.8-1.10.

It is seen from the corresponding results that PSM has the best performance when using a small amount of learning base point (star and box cases), while Kriging model has the best generalization performance when using a large amount of learning base points.

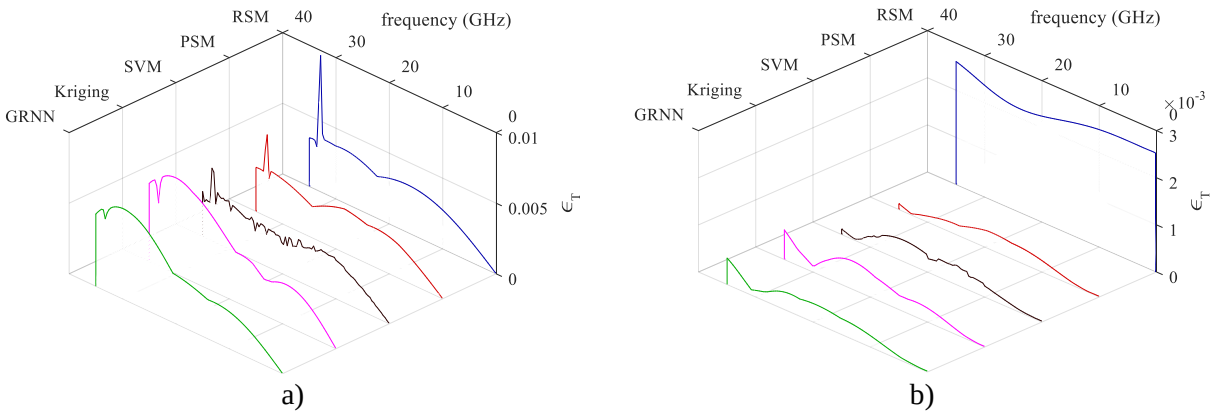

Fig. 1.8 Maximum absolute testing error at each simulated frequency point for the via-stripline-via interconnect, using a star distribution of learning base points and a uniform distribution of testing base points with $K = 4$: a) for $|S_{11}|$, b) for $|S_{21}|$.

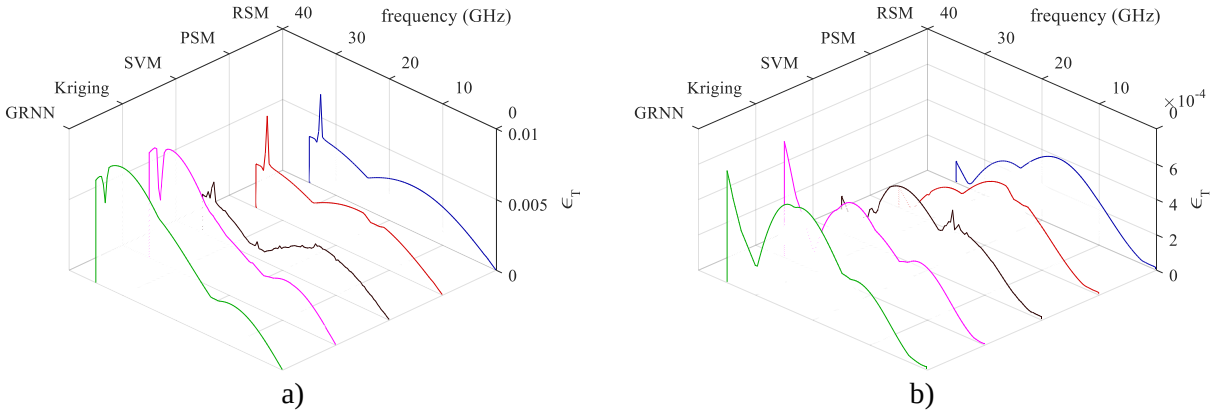

Fig. 1.9 Maximum absolute testing error at each simulated frequency point for the via-stripline-via interconnect, using a box distribution of learning base points and a uniform distribution of testing base points with $K = 4$: a) for $|S_{11}|$, b) for $|S_{21}|$.

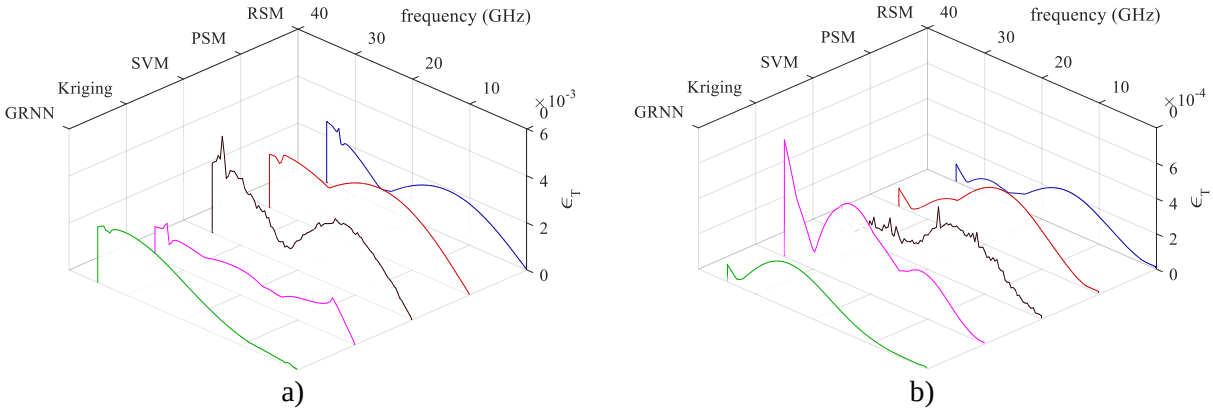

Fig. 1.10 Maximum absolute testing error at each simulated frequency point for the via-stripline-via interconnect, using a uniform distribution of learning base points with $K = 5$ and a uniform distribution of testing base points with $K = 4$: a) for $|S_{11}|$, b) for $|S_{21}|$.

TABLE 1.4. MAXIMUM ABSOLUTE ERROR FOR ALL SIMULATED FREQUENCY POINTS FOR THE PACKAGE VIA-STRIPLINE-VIA INTERCONNECT USING A STAR DISTRIBUTION OF LEARNING BASE POINTS AND A UNIFORM DISTRIBUTION OF TESTING BASE POINTS WITH $K = 4$

Model	$\|S_{11}\|$		$\|S_{21}\|$	
	ϵ_{Tmax}	ϵ_{Lmax}	ϵ_{Tmax}	ϵ_{Lmax}
RSM	0.0096599	1.9845×10^{-15}	0.00260900	1.3323×10^{-15}
PSM	0.0058110	0.0021444	0.00036857	1.399×10^{-05}
SVM	0.0051380	0.0038101	0.00045258	0.00035763
Kriging	0.0067934	0.0025657	0.00062884	0.00059975
GRNN	0.0064009	5.9298×10^{-11}	0.00056085	4.1409×10^{-12}

TABLE 1.5. MAXIMUM ABSOLUTE ERROR FOR ALL SIMULATED FREQUENCY POINTS FOR THE PACKAGE VIA-STRIPLINE-VIA INTERCONNECT USING A BOX DISTRIBUTION OF LEARNING BASE POINTS AND A UNIFORM DISTRIBUTION OF TESTING BASE POINTS WITH $K = 4$

Model	$\|S_{11}\|$		$\|S_{21}\|$	
	ϵ_{Tmax}	ϵ_{Lmax}	ϵ_{Tmax}	ϵ_{Lmax}
RSM	0.0066256	2.0127×10^{-15}	0.00039023	7.7716×10^{-16}
PSM	0.0068661	0.0017732	0.00039023	2.005×10^{-05}
SVM	0.003949	0.0043598	0.00040817	0.00040817
Kriging	0.008344	0.0067654	0.00065689	0.0005975
GRNN	0.0090303	0	0.00063269	0

TABLE 1.6. MAXIMUM ABSOLUTE ERROR FOR ALL SIMULATED FREQUENCY POINTS FOR THE PACKAGE VIA-STRIPLINE-VIA INTERCONNECT USING A UNIFORM DISTRIBUTION OF LEARNING BASE POINTS WITH $K = 5$ AND A UNIFORM DISTRIBUTION OF TESTING BASE POINTS WITH $K = 4$

Model	$\|S_{11}\|$		$\|S_{21}\|$	
	ϵ_{Tmax}	ϵ_{Lmax}	ϵ_{Tmax}	ϵ_{Lmax}
RSM	0.0026026	0.0027952	0.00022200	0.00035162
PSM	0.0028671	0.0039662	0.00034882	0.00048747
SVM	0.0042793	0.0038857	0.00037992	0.00061485
Kriging	0.0016749	0.0016471	0.00066168	0.00063588
GRNN	0.0026336	3.926×10^{-05}	0.00025491	3.001×10^{-06}

1.4.3 Dual-Band Planar Inverted F Antenna with Slotted Ground

As a third example, consider the T-slot PIFA antenna proposed in [Cervantes-González-15]. Its geometry is shown in Fig. 1.11. The T-slot in the patch is the main element of the antenna contributing to the dual-band resonances. The bandwidth is increased by removing two portions of the metallization at the ground plane. The antenna design is intended to operate at the following bands: GSM900 (880-960 MHz), GSM1900 (1850-1990 MHz), UMTS2100 and WCDMA2100 (1920-2170 MHz).

The antenna is designed on a substrate with a relative permittivity $\varepsilon_r = 2.2$, a dielectric loss tangent tan $\delta = 0.009$ and a thickness $H = 3.962$ mm. The initial design parameters values are defined as $W_1 = 3.83$ mm, $W_2 = 8.85$ mm, $W_3 = 11$ mm, $W_4 = 1.54$ mm, $L_1 = 8.10$ mm, $L_2 = 20.34$ mm, $L_p = 24$ mm, $Y_f = 14$ mm, $X_f = 19.16$ mm, $Y_g = 18.9$ mm and, $X_g = 1$ mm.

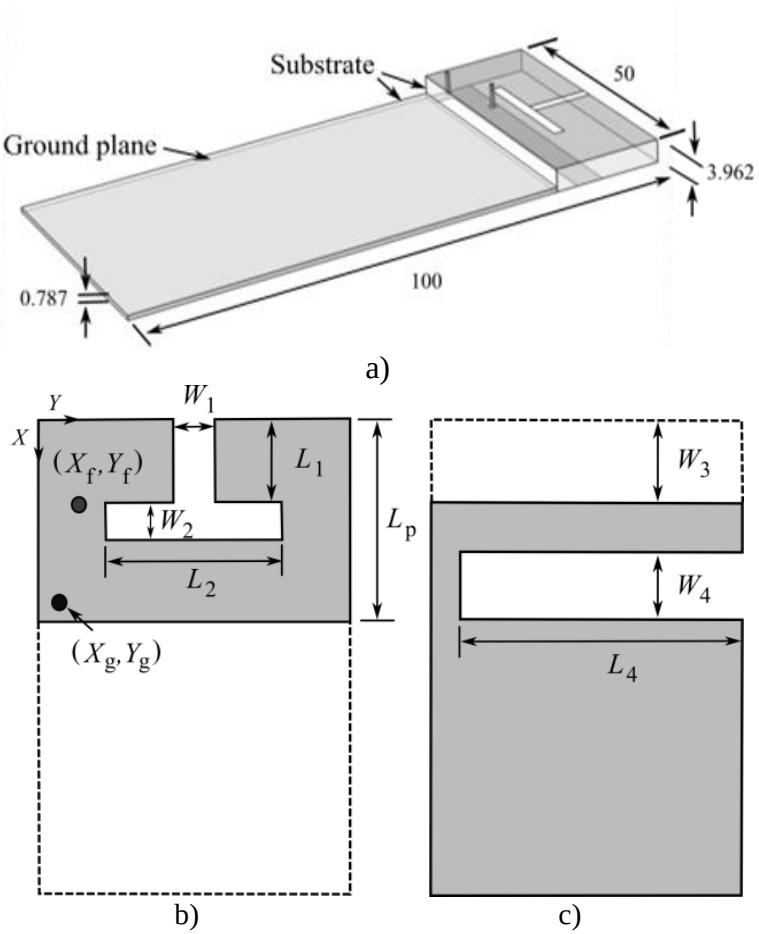

Fig. 1.11 T-slot PIFA antenna a) 3D view, b) top view, c) bottom view. From [Cervantes-González-15].

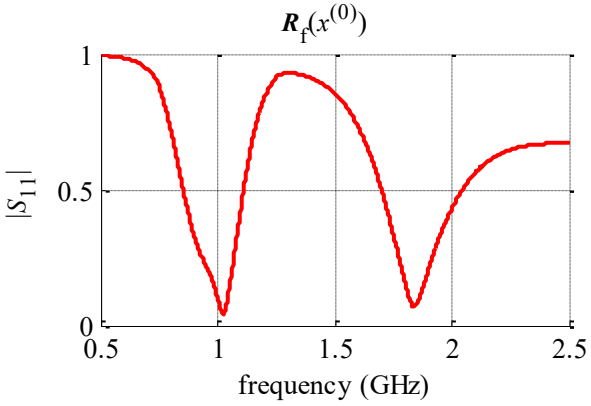

Fig. 1.12 Response of the T-slot PIFA antenna at $\boldsymbol{x}^{(0)}$.

The structure is implemented in COMSOL by using the simulation bounding box dimensions, boundary conditions, and the meshing scheme proposed in [Cervantes-González-15]. All metals are defined as perfect electric conductors. A relatively coarse resolution discretization is used, such that each frequency sweeps takes around 2 min 20 s.

For modeling the antenna response, the input parameters are defined as $\boldsymbol{x} = [W_1 \quad W_2 \quad L_1 \quad L_2]^T$, using as a reference design $\boldsymbol{x}^{(0)} = [3.83 \quad 8.85 \quad 8.10 \quad 20.34]^T$ (mm), over a region delimited by $\boldsymbol{\tau} = [5\% \ 5\% \ 5\% \ 5\%]^T$. EM response of the antenna at $\boldsymbol{x}^{(0)}$ is illustrated in Fig. 1.12.

To train the surrogate models three different learning base point distributions are employed: star, box and uniform distribution with $K = 4$ (256 learning base points). For testing the generalization performance a uniform distribution with $K = 3$ (81 testing base points) is used. Maximum absolute error for all simulated frequency points, by using the five implemented surrogate models, is reported in Table 1.7-1.9. Maximum absolute errors at each simulated frequency points can be shown in Fig. 1.13-1.15.

From the corresponding results, it is seen that PSM has the best generalization performance for the three implemented learning base points distribution. Then, for this case, PSM has the best performance when using a small or even a large amount of learning base points distribution.

1.5. Conclusions

In this chapter, a polynomial surrogate modeling approach based on the multinomial theorem was proposed. Weighting factors can be calculated by assuming that the lower-order

surrogates are already available and fixed, or by calculating all weighting factors simultaneously

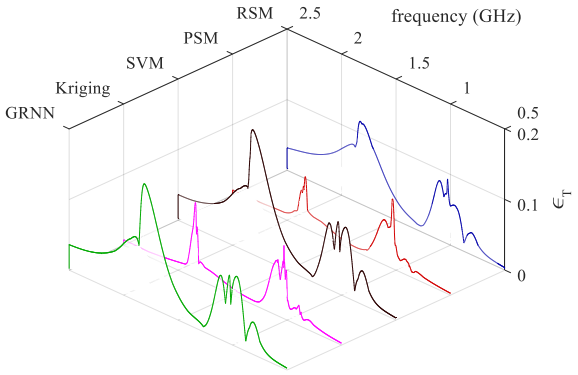

Fig. 1.13 Maximum absolute testing error at each simulated frequency point for the dual-band PIFA antenna, using a star distribution of learning base points and a uniform distribution of testing base points with $K = 3$: a) for $|S_{11}|$, b) for $|S_{21}|$.

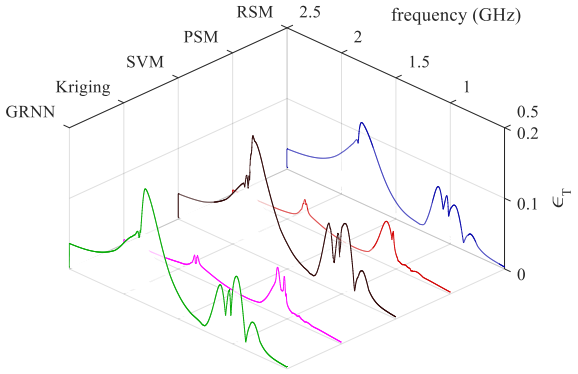

Fig. 1.14 Maximum absolute testing error at each simulated frequency point for the dual-band PIFA antenna, using a box distribution of learning base points and a uniform distribution of testing base points with $K = 3$: a) for $|S_{11}|$, b) for $|S_{21}|$.

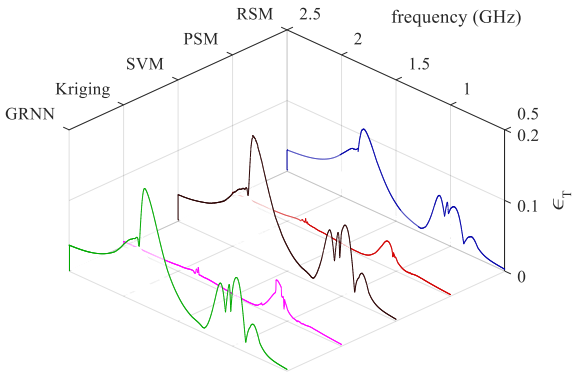

Fig. 1.15 Maximum absolute testing error at each simulated frequency point for the dual-band PIFA antenna, using a uniform distribution of learning base points with $K = 4$ and a uniform distribution of testing base points with $K = 3$: a) for $|S_{11}|$, b) for $|S_{21}|$.

TABLE 1.7. MAXIMUM ABSOLUTE ERROR FOR ALL SIMULATED FREQUENCY POINTS FOR THE DUAL-BAND PIFA ANTENNA USING A STAR DISTRIBUTION OF LEARNING BASE POINTS AND A UNIFORM DISTRIBUTION OF TESTING BASE POINTS WITH K = 3

Model	$\lvert S_{11}\rvert$	
	ϵ_{Tmax}	ϵ_{Lmax}
RSM	0.116770	0.080603
PSM	0.098251	0.054615
SVM	0.176450	0.077729
Kriging	0.106600	0.022197
GRNN	0.170990	0.081205

TABLE 1.8. MAXIMUM ABSOLUTE ERROR FOR ALL SIMULATED FREQUENCY POINTS FOR THE DUAL-BAND PIFA ANTENNA USING A BOX DISTRIBUTION OF LEARNING BASE POINTS AND A UNIFORM DISTRIBUTION OF TESTING BASE POINTS WITH K = 3

Model	$\lvert S_{11}\rvert$	
	ϵ_{Tmax}	ϵ_{Lmax}
RSM	0.114430	0.10788
PSM	0.061406	0.013724
SVM	0.166740	0.16674
Kriging	0.066893	0.013126
GRNN	0.162690	0.16269

TABLE 1.9. MAXIMUM ABSOLUTE ERROR FOR ALL SIMULATED FREQUENCY POINTS FOR THE DUAL-BAND PIFA ANTENNA USING A UNIFORM DISTRIBUTION OF LEARNING BASE POINTS WITH K = 4 AND A UNIFORM DISTRIBUTION OF TESTING BASE POINTS WITH K = 3

Model	$\lvert S_{11}\rvert$	
	ϵ_{Tmax}	ϵ_{Lmax}
RSM	0.109400	0.110720
PSM	0.037066	0.034142
SVM	0.169920	0.169920
Kriging	0.051592	0.031348
GRNN	0.166080	0.166080

for each surrogate model order, depending on the condition number of the system matrix. The

proposed methodology allows the polynomial order to be different at each simulated frequency point based on the generalization performance.

Performance of the proposed methodology is compared against four surrogate modeling approaches: response surface methodology, support vector machines, generalized regression neural networks and Kriging. Final results, based on three implemented EM structures, show that the proposed PSM methodology has the best performance when using a small amount of learning base points (star and box distribution were tested). When using a large amount of learning base points, the performance of the five implemented surrogate models varies depending on the implemented EM structure.

Based on the obtained results, the proposed PSM methodology proves to be suitable for developing EM surrogate models when the amount of learning base points is very limited (e.g. for computationally expensive EM simulations), while it could be suitable in some cases when a large amount of learning base points is available (e.g. for computationally cheap EM simulations).

2. Multiphysical Characterization of Microwave Structures in Frequency Domain

The properties of the materials used to implement high frequency circuits are temperature- and frequency-dependent. This dependency results in more attenuation and/or a frequency shifting in the corresponding EM responses. In addition, an increase in the circuit temperature produces a thermal expansion of the metallic and the dielectric materials of the circuit. The combination of both thermal expansions causes a thermal and mechanical stress in the circuit, which also affects the EM responses of the circuit [Sánchez-Soriano-14].

The impact of circuits' dependence to thermal, mechanical and electromagnetic (EM) variations has been studied in several areas of electronics, including systems on chips (SoC) [Parry-00], power electronics [Li-15], sensors [García-Guzmán-15], and optics [Burford-14]. However, there are almost no published articles studying the performance of planar high frequency circuits under EM-thermo-mechanical variations; only one reference was found [Sánchez-Soriano-14] using IEEE Xplore.

In this chapter, the most important thermo-mechanical properties of materials used in high frequency structures are described. It is also presented how to properly configure COMSOL to simulate the corresponding changes in the EM responses due to these multiphysics variations. The thermo-mechanical effects due to variations in the circuit temperature are exemplified by performing a multiphysical simulation of a microstrip line.

2.1. Thermal and Elasticity Properties of Metallic and Dielectric Materials

2.1.1 Thermal Properties of Metallic and Dielectric Materials

The most common parameters used for describing the thermal properties of materials are the thermal expansion coefficient α, the specific heat c_p, and the thermal conductivity λ. The thermal expansion coefficient is a material property that indicates how much a material expands

TABLE 2.1. THERMAL PROPERTIES OF THE MATERIALS INVOLVED IN THE MICROSTRIP LINE EXAMPLE

Parameter	Units	Material		
		Copper	99.5 % Alumina	Air
Thermal expansion coefficient	1/Kelvins	17×10^{-6}	8×10^{-6}	1.75×10^{-3}
Specific heat	J/gKelvins	0.385	0.900	0.001
Thermal conductivity	W/(mKelvins)	400	27	0.0257

TABLE 2.2. ELASTICITY PROPERTIES OF THE MATERIALS INVOLVED IN THE MICROSTRIP LINE EXAMPLE

Parameter	Units	Material		
		Copper	99.5 % Alumina	Air
Young´s modulus	Pa	110×10^{9}	300×10^{9}	1
Shear modulus	Pa	40×10^{9}	110×10^{9}	-
Poisson´s ratio	-	0.35	0.23	0

upon heating. The specific heat refers to the amount of heat per unit mass required to raise the temperature of a material by one degree Celsius. Finally, the thermal conductivity is defined as the property of a material to conduct heat [Gere-04].

Thermal properties for copper, alumina and air are reported in Table 2.1.

2.1.2 Elasticity Properties of Metal and Dielectric Materials

For describing the elasticity properties of materials, the most common parameters are the Young's modulus *E*, the shear modulus *G*, and the Poisson's ratio *ν*. The Young's modulus defines the relationship between stress and strain in a material. The shear modulus is defined as the ratio of shear stress to the shear strain. The Poisson's ratio measures the material fraction of expansion divided by the fraction of compression [Gere-04].

Elasticity properties for copper, alumina and air are reported in Table 2.2.

2.2. Effects of Temperature on the Electrical Properties of Metallic and Dielectric Materials

2.2.1 Electrical Properties for Dielectric Materials

Following [Auerkari-96], the dielectric substrate has a relationship between temperature and conductivity given by

$$\sigma(T) = \sigma_0 \exp\left(-\frac{U}{k(T - T_0)}\right) \tag{2-1}$$

where U is the activation energy, σ_0 is the electrical conductivity reported at a reference temperature T_0, and k = 8.314 J/molKelvins is the Boltzmann's constant.

For 99.5% alumina, the activation energy is $U = 440\times10^3 \pm 40\times10^3$ J/mol and the electrical conductivity is $\sigma_0 = 10^{-12}$ S/m at T_0 = 293.15 Kelvins [Auerkari-96]. When the circuit is operating near T_0, the electrical conductivity is cero, and it becomes significant when reaching the melting point. For alumina, the melting point is reached at T = 2,345 Kelvins [Furukawa-56].

The loss tangent and the relative permittivity for dielectric materials are weak functions of temperature. Both becomes significant at high temperatures (above 1,275 Kelvins) [Furukawa-56]. For lower temperatures, an average value for loss tangent and relative permittivity are sufficient [Auerkari-96].

2.2.2 Electrical Properties for Metallic Materials

For metals, the relationship between temperature and conductivity can be approximated by using the polynomial function reported in [Cervantes-González-12]. The third-order polynomial used in the EM simulation is defined as

$$\sigma(T) = 10^7 \sum_{k=0}^{3} a_k T^k \tag{2-2}$$

where σ is the metal conductivity given in S/m, T is the temperature in Kelvins and a_k is the k-th coefficient of the polynomial expansion.

For copper, coefficient values are defined as $a_0 = 16.96471$, $a_1 = -0.05724$, $a_2 = 8\times10^{-5}$, and $a_3 = -3.68098\times10^{-8}$. These are valid for a temperature range from 253 Kelvins to 500 Kelvins.

2.3. Effects of the Operating Frequency on the Electrical Properties of Dielectric Materials

Losses in the dielectric material are also dependent of the operating frequency. The loss tangent can be calculated by [Aguilar-Torrentera-11]

$$\tan(\delta) = \frac{\sigma}{\varpi \varepsilon_0 \varepsilon_r} \tag{2-3}$$

where ω is the angular frequency, $\varepsilon_0 = 8.854\times10^{-12}$ F/m is the permittivity of free space, ε_r is the relative permittivity, and σ is the dielectric leakage conductivity. For alumina, the dielectric leakage conductivity was not found, hence, in this doctoral dissertation the losses in the substrate caused by the operating frequency are not considered.

2.4. COMSOL Multiphysics Configuration

To illustrate the configuration process of COMSOL multiphysics, consider the microstrip line shown in Fig. 2.1. The general design parameters are taken from [Chávez-Hurtado-14a] and correspond to L = 10.9 mm, W = 0.7 mm, and H = 0.66 mm. The microstrip line is implemented using alumina as substrate, with $\varepsilon_r = 9$ and $\tan(\delta) = 1\times10^{-4}$.

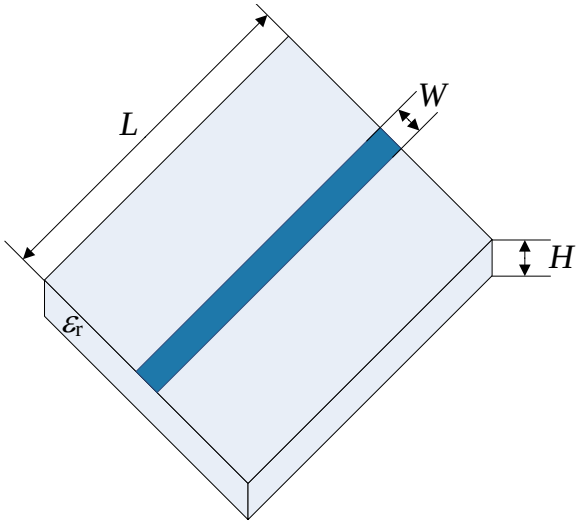

Fig. 2.1 Ideal microstrip line with infinitesimally thin metals in both the main trace and the ground plane (not shown).

2.4.1 COMSOL Simulation Bounding Box

The microstrip line is simulated in COMSOL using a simulation bounding box. Distance from the microstrip line to side walls of such box is defined as x_{gap}. Distance from the microstrip line to front box walls is defined as y_{gap}. Finally, distance from the microstrip line to upper wall is defined as $H_{air.}$ The simulation bounding box dimensions must be properly configured to avoid interferences to the EM responses of the microstrip line. By following the procedure reported in [Chávez-Hurtado-14a], final box dimensions are defined as $x_{gap} = 10W$, $y_{gap} = 10W$, and $H_{air} = 10H$.

Additionally, to measure the EM responses of the microstrip line, two ports must be placed at each extreme of the microstrip line. The length of the ports is defined as L_p = 0.05W. The microstrip line structure, as implemented in COMSOL, is shown in Fig. 2.2.

2.4.2 COMSOL Meshing Scheme

For the meshing scheme, three different meshing regions are defined (see Fig. 2.3). The first meshing size is defined for the microstrip line domain. The second meshing size is defined for the lumped ports domain, while the third meshing size is defined for the rest of the structure

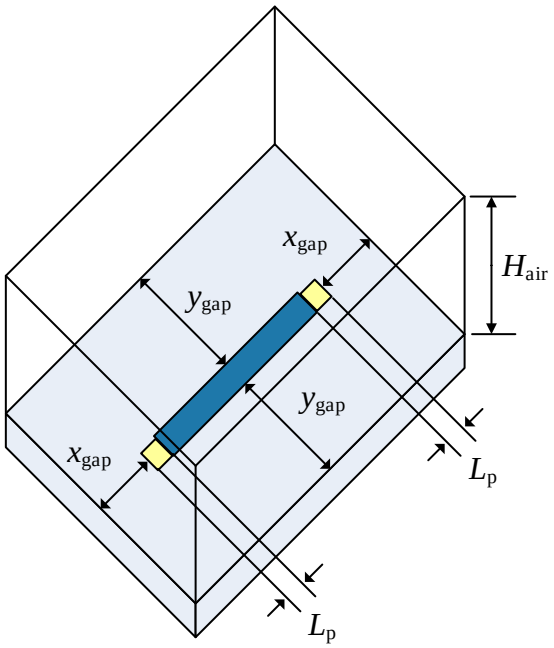

Fig. 2.2 Microstrip line geometry as implemented in COMSOL simulation box.

(substrate and air box domains).

Let the minimum element size in the microstrip line be δ_m. The minimum element size in port is δ_{port}. Similarly, the minimum element size for the rest of the structure is δ_{glob}. The wavelength on air and around the microstrip metallic trace are defined as $\lambda_a = c/f_{max}$ and $\lambda_m = v_p/f_{max}$, respectively, where f_{max} = 10 GHz is the maximum simulated frequency, c = 299792458 m/s is the speed of the light in free-space, $v_p = c/(\varepsilon_{eff})^{½}$ is the propagation velocity, and ε_{eff} = 6.13 is the effective dielectric constant. For computational cost purposes, a coarse mesh discretization is implemented by defining the minimum element size for the microstrip line region as $\delta_{min\text{-}m}$ = min{λ_m/10 sqrt(WH)}, the minimum element size for the port region as $\delta_{min\text{-}port}$ = min{λ_m/10 L_p}, and the minimum element size for the global region as $\delta_{min\text{-}glob}$ = min{λ_a/10 H}. The maximum element sizes are defined as $\delta_{max\text{-}m} = 5\delta_{min\text{-}m}$, $\delta_{max\text{-}port} = 5\delta_{min\text{-}port}$, and $\delta_{max\text{-}glob} = 10\delta_{min\text{-}glob}$. The maximum element growth rate is selected as δ_{GR} = 1.6. The resolution of narrow regions is defined as $RNR = x_{gap}/2W$. The resultant meshing for the microstrip line is illustrated in Fig. 2.4.

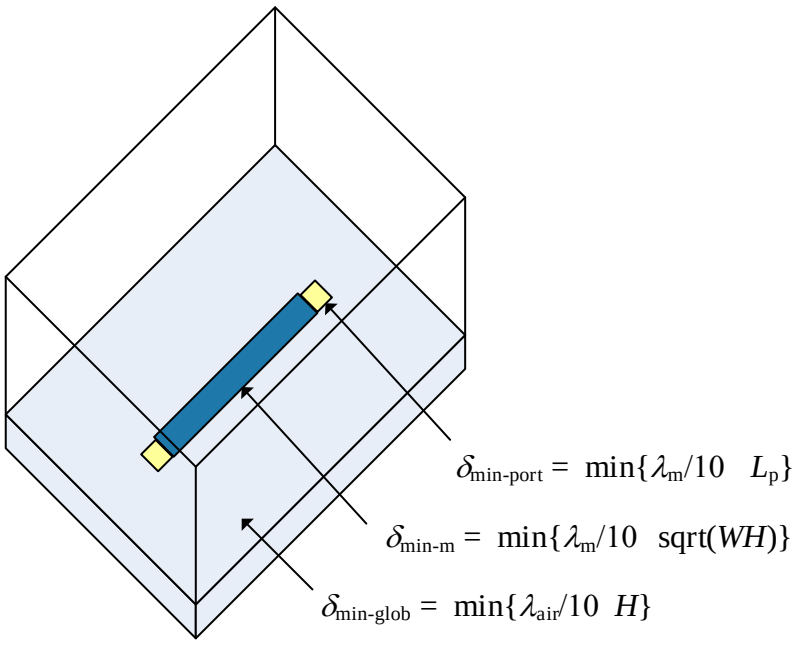

Fig. 2.3 Defined meshing scheme regions for the microstrip line structure implemented in COMSOL.

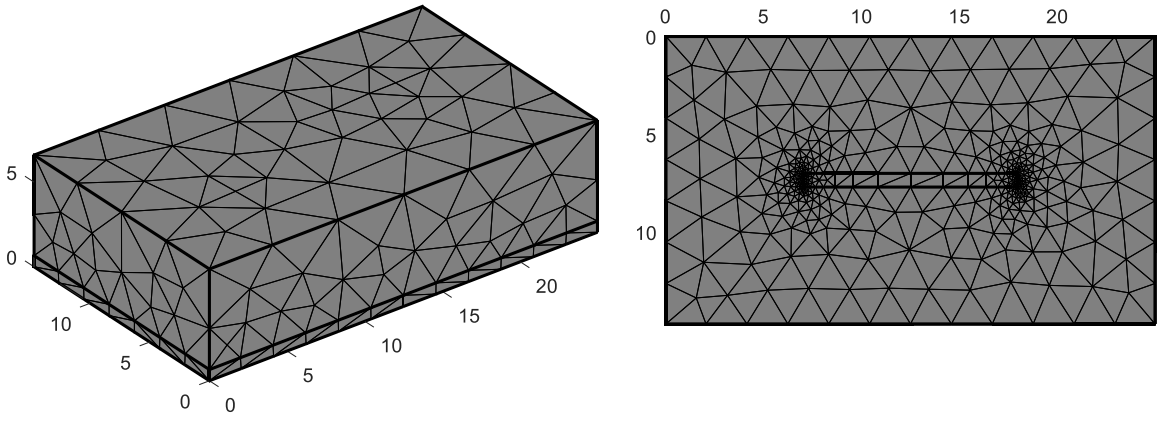

a) b)

Fig. 2.4 Resultant coarse mesh discretization for the microstrip line under study: a) 3D view and b) bottom view.

2.4.3 COMSOL Solid Mechanics and Moving Mesh Studies

In order to implement the multiphysics analysis of the microstrip line, two physics studies in COMSOL must be added. The first study corresponds to solid mechanics. Linear elastic materials are defined for the air domain and the substrate domain. Under the linear elastic material options, the corresponding values for the Young's modulus (E), the Poisson's ration (ν), and the density (ρ) are specified. Additionally, for each linear elastic material the thermal expansion parameter must be added. Inside the thermal expansion option, the coefficient of thermal expansion (α) for air domain and substrate is specified. A fixed constrain parameter must also be added under the solid mechanics study. Under this configuration, the two lumped ports boundaries are selected as reference for the thermo-mechanical analysis.

In addition to the solid mechanics study, the moving mesh study has to be added. Under this study, the prescribed deformation parameter is included and configured as $d_x = u$, $d_y = v$, and $d_z = w$. The values of u, v, and w are taken automatically from the previous solids mechanics study. A screen caption illustrating both physics studies is presented in Fig. 2.5.

2.4.4 COMSOL Study Configuration

Under the study options, two steps must be computed to obtain the corresponding

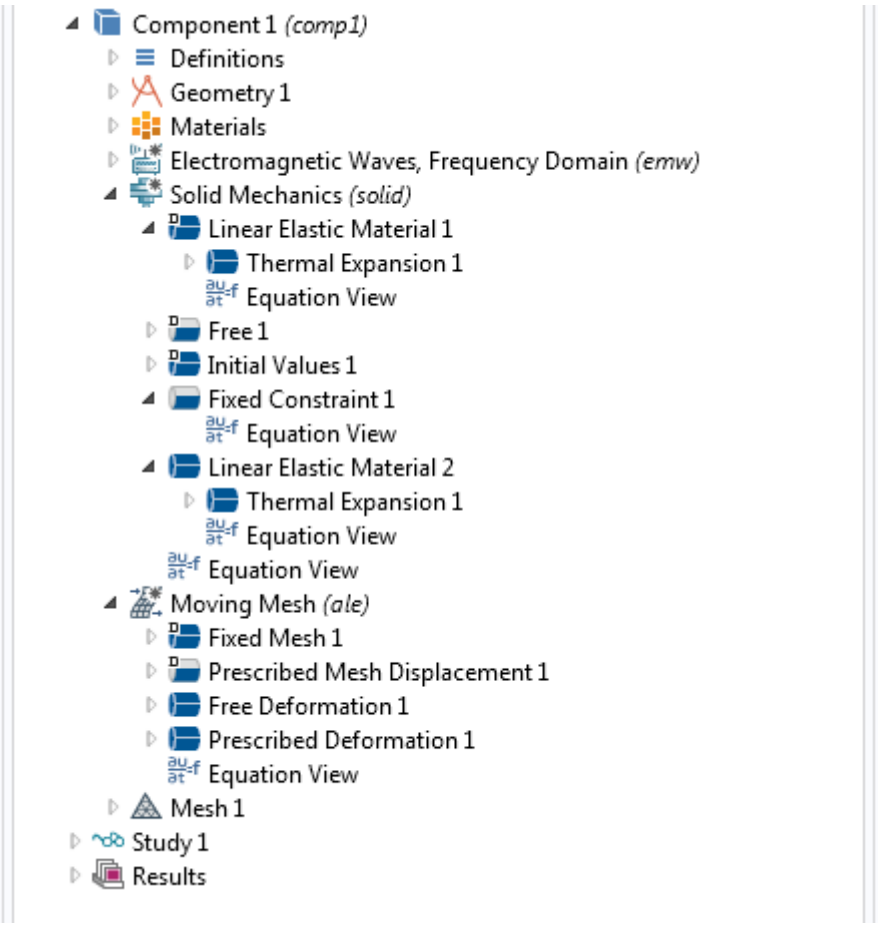

Fig. 2.5 Screen capture for the solid mechanics and moving mesh studies added for the multiphysics analysis of the microstrip line in COMSOL.

multiphysics analysis. The first step is a stationary type and must be solved only for the solid mechanics study. The second step is a frequency domain type and must be solved for both EM and moving mesh studies. Solver configurations option must be set to default solver and then the multiphysics computation of the microstrip line can be started.

2.5. Microstrip Line Multiphysics Results

For the following multiphysics simulation the dielectric and metallic materials are considered as lossless. The microstrip line and the bounding box walls are set to copper with a thickness of 17 μm. COMSOL is configured to generate 1,000 frequency points using AWE. By using a personal computer with core i5 and 8GB RAM, each multiphysics simulation takes approximately 8 min.

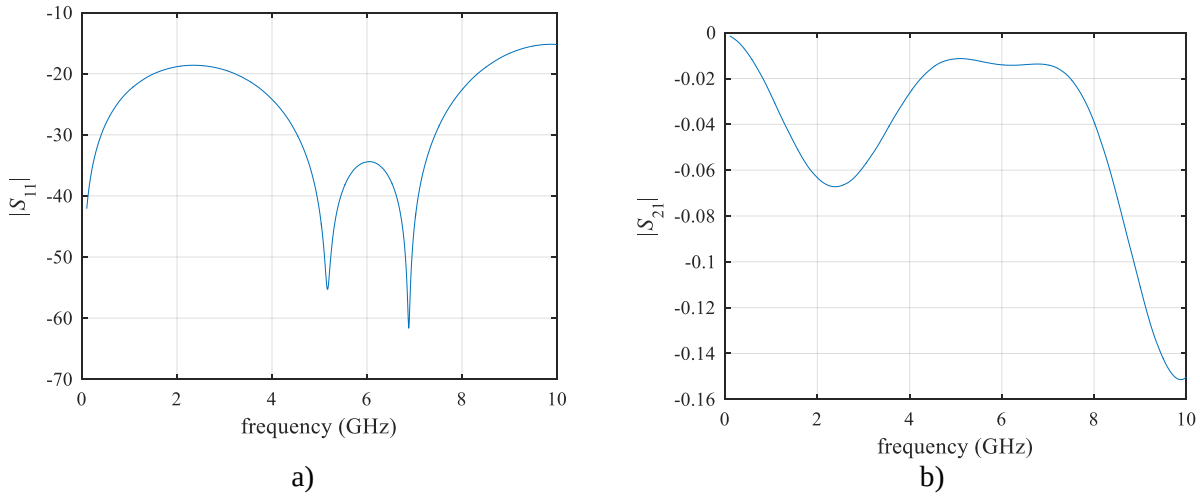

a) b)

Fig. 2.6 EM responses of the microstrip line at room temperature: a) $|S_{11}|$ and b) $|S_{21}|$.

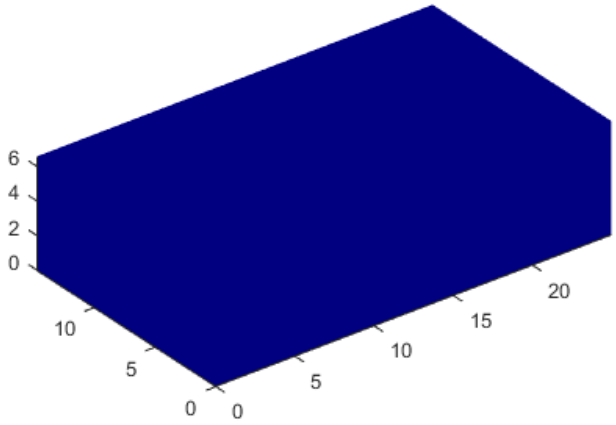

Fig. 2.7 Mechanical deformation of the structure at room temperature. There is no mechanical deformation, as expected.

2.5.1 Microstrip Line Multiphysics Simulation at Room Temperature

At room temperature, the microstrip line structure does not suffer any mechanical stress or deformation. Corresponding EM responses at room temperature (20 °C) are shown in Fig. 2.6. The microstrip line structure at room temperature (without deformation) is shown in Fig. 2.7.

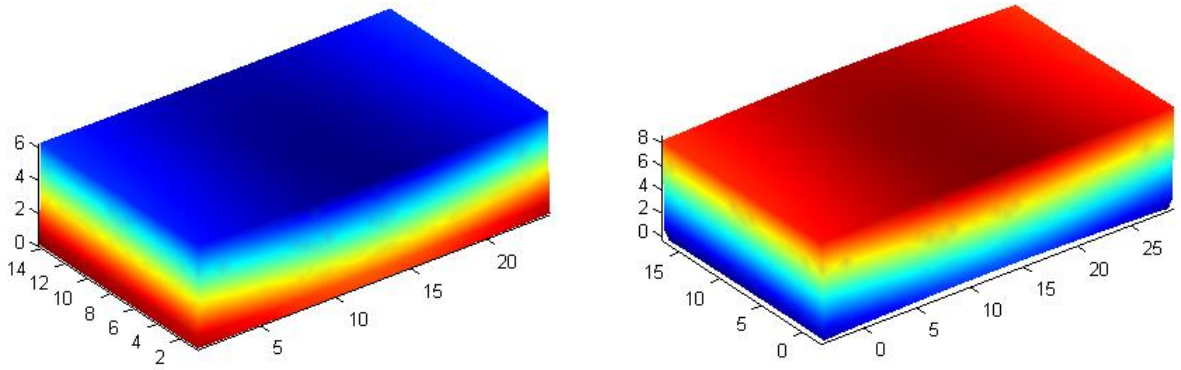

a) b)

Fig. 2.8 Mechanical deformation in mm of the microstrip line when varying the circuit temperature: a) -40 °C and b) 180 °C.

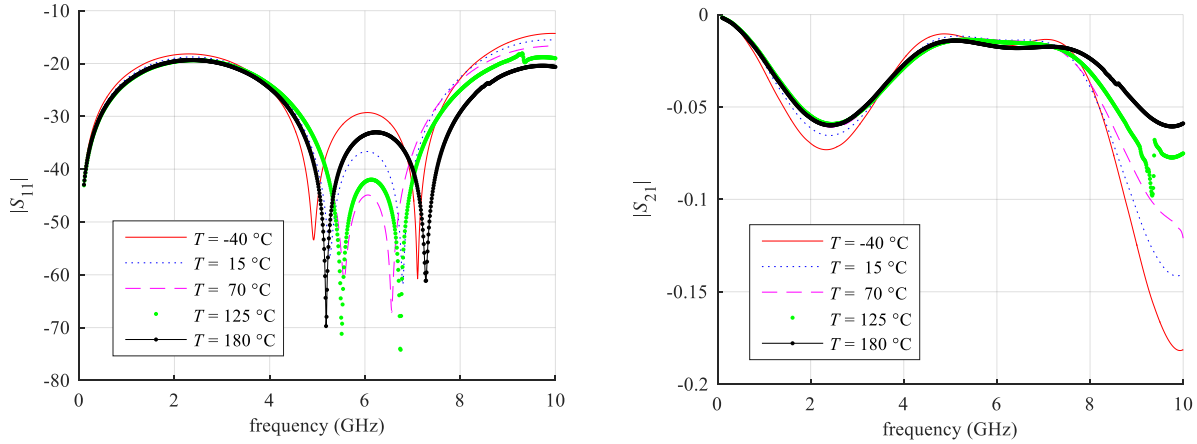

a) b)

Fig. 2.9 EM responses of the microstrip line when varying the circuit temperature from -40 °C to 180 °C: a) $|S_{11}|$ and b) $|S_{21}|$.

2.5.2 Microstrip Line Multiphysics Simulation varying the Temperature

Now the temperature is varied from -40 °C to 180 °C, using steps of 55 °C. The previously defined thermal and elasticity properties for copper, air, and alumina are used. EM responses for the microstrip line when varying the circuit temperature are shown in Fig. 2.9. Examples of the mechanical deformation of the structure when varying the temperature is shown in Fig. 2.8. It is seen that a variation of the circuit temperature within the predefined temperature range causes a change in the EM responses, affecting the magnitude of *S*-parameters and causing a frequency shifting. There is also a slight mechanical deformation of the microwave structure due to the

variations of the circuit temperature.

2.6. Conclusions

In this chapter, a procedure to characterize the multiphysics behavior of a microstrip line and the most common parameters for describing the thermal and elasticity properties of materials were presented. Both set of parameters were used by COMSOL to properly simulate the multiphysics behavior of the microwave structure. As a multiphysics design example, it was presented a microstrip line using copper for metals and 99.5% alumina for the substrate. The circuit temperature was varied form -40 °C to 180 °C. From the corresponding results, it was corroborated that a change in the circuit temperature modifies the EM losses and causes a frequency shift of the EM responses. The microwave structure also suffered a small mechanical deformation.

3. Multiphysics Modeling of Microwave Structures in Frequency Domain using Polynomial-based Surrogate Modeling

In this chapter, the polynomial surrogate modeling methodology (PSM) presented in Chapter 1 is used to develop a surrogate model in the frequency domain for microwave structures subject to variations in the circuit temperature. To simulate the corresponding changes in the EM responses due to multiphysics variations, COMSOL is configured by using the thermal and elasticity properties defined in Chapter 2. The final multiphysics surrogate model uses as inputs the design variables and the circuit temperature to represent the corresponding EM responses in the frequency domain. The proposed methodology is exemplified by developing a multiphysics surrogate model for a microstrip line subject to variations in its circuit temperature.

3.1. Multiphysics Polynomial-based Surrogate Modeling Formulation

Most of the actual design variables (geometrical dimensions, material properties, etc.) are affected by temperature, due to thermal expansion phenomena and conductivity effects. In consequence, the actual design variables, $\boldsymbol{x}_a$, should be expressed as

$$\boldsymbol{x}_a = \boldsymbol{x} + \boldsymbol{x}_T(T) \tag{3-1}$$

where $\boldsymbol{x} \in \Re^n$ contains the nominal design variables and $\boldsymbol{x}_T \in \Re^n$ represents the unidimensional vector function that takes into account the above temperature dependence. This dependence is, in general, an unknown function and extremely difficult to analytically determine.

Let $\boldsymbol{R}_f \in \Re^p$ denote the fine EM model response sampled at p frequency points. It is assumed that $\boldsymbol{R}_f$ depends on the actual design variables $\boldsymbol{x}_a \in \Re^n$ and the circuit temperature $T \in \Re$. The main purpose is to develop a surrogate model $\boldsymbol{R}_s(\boldsymbol{x},T)$ that approximates the fine model responses $\boldsymbol{R}_f(\boldsymbol{x}_a,T)$ around a region of interest for the nominal design variables and the circuit temperature.

3.1.1 Lower Order Surrogates

Taking as a basis the PSM formulation presented in Chapter 1, the zero-order model at the *k*-th simulated frequency point is defined as the fine model response at the reference design,

$$R_{sk}^{(0)}(\boldsymbol{x},T) = R_{fk}(\boldsymbol{x}_a^{(0)},T^{(0)}) \tag{3-2}$$

with $\boldsymbol{x}_a^{(0)} = \boldsymbol{x}^{(0)} + \boldsymbol{x}_T(T^{(0)})$, where $\boldsymbol{x}^{(0)}$ represents the reference nominal design variables and $T^{(0)}$ represents the reference temperature of the circuit.

The first-order surrogate model at the *k*-th simulated frequency point is defined as

$$R_{sk}^{(1)}(\boldsymbol{x},T) = R_{sk}^{(0)}(\boldsymbol{x},T) + \boldsymbol{w}_k^{(1)\mathrm{T}}\boldsymbol{q}^{(1)}(\boldsymbol{\Delta\varphi}) \tag{3-3}$$

where $\boldsymbol{\Delta\varphi} \in \Re^{n+1} = [\boldsymbol{\Delta x}\ \ \Delta T]$, $\boldsymbol{\Delta x}$ represents the distance from a given nominal design point to $\boldsymbol{x}^{(0)}$, ΔT represents the difference from a given temperature to $T^{(0)}$, $\boldsymbol{w}_k^{(1)}$ contains the corresponding surrogate model weighting factors and $\boldsymbol{q}^{(1)} \in \Re^{n+1}$ contains the first-order multinomial terms for $\boldsymbol{\Delta\varphi}$. The scalar elements of $\boldsymbol{q}^{(1)}$ are given by

$$q^{(1)}(\boldsymbol{\Delta\varphi}) = \Delta\varphi_{\lambda_1} \quad \text{for } \lambda_1 = 1{:}n \tag{3-4}$$

Similarly, the second-order surrogate model at the *k*-th simulated frequency point is defined as

$$R_{sk}^{(2)}(\boldsymbol{x},T) = R_{sk}^{(1)}(\boldsymbol{x},T) + \boldsymbol{w}_k^{(2)\mathrm{T}}\boldsymbol{q}^{(2)}(\boldsymbol{\Delta\varphi}) \tag{3-5}$$

where $\boldsymbol{w}_k^{(2)} \in \Re^{(n+1)(n+2)/2}$ contains the second order weighting factors and $\boldsymbol{q}^{(2)}(\boldsymbol{\Delta\varphi}) \in \Re^{(n+1)(n+2)/2}$ contains the second-order multinomial terms for $\boldsymbol{\Delta\varphi}$. The scalar elements of $\boldsymbol{q}^{(2)}$ are given by

$$q^{(2)}(\boldsymbol{\Delta\varphi}) = \Delta\varphi_{\lambda_1}\Delta\varphi_{\lambda_2} \quad \text{for } \lambda_1 = 1{:}n \text{ and } \lambda_2 = \lambda_1{:}n \tag{3-6}$$

3.1.2 *N*th-order Surrogate Model

A general expression for an *N*th-order surrogate model at the *k*-th simulated frequency point can be written as

$$R_{sk}^{(N)}(\boldsymbol{x},T) = R_{sk}^{(N-1)}(\boldsymbol{x},T) + \boldsymbol{w}_k^{(N)\mathrm{T}}\boldsymbol{q}^{(N)}(\boldsymbol{\Delta\varphi}) \tag{3-7}$$

where $\boldsymbol{w}_k^{(N)} \in \Re^{(N+n)!/((n)!(N)!)}$ contains the corresponding weighting factors and $\boldsymbol{q}^{(N)} \in \Re^{(N+n)!/(n)!(N)!}$ contains the *N*th-order multinomial terms for $\boldsymbol{\Delta\varphi}$. The scalar elements of $\boldsymbol{q}^{(N)}$ are given by

$$q^{(N)}(\Delta\varphi) = \Delta\varphi_{\lambda_1}\Delta\varphi_{\lambda_2}\cdots\Delta\varphi_{\lambda_N} \text{ for } \lambda_1 = 1{:}n,\ \lambda_2 = \lambda_1{:}n,\ \ldots,\ \lambda_N = \lambda_{N-1}{:}n \tag{3-8}$$

3.2. Training the Multiphysics Polynomial-based Surrogate Model

The size of the training region is defined by: a) a vector $\boldsymbol{\tau} \in \Re^n$, containing the relative deviation for each design variable with respect to $\boldsymbol{x}^{(0)}$; and b) a temperature range $\Delta T \in \Re$. To train the surrogate model, L learning base points, denoted as $\boldsymbol{\varphi}^{(1)}$, $\boldsymbol{\varphi}^{(2)}$, …, $\boldsymbol{\varphi}^{(L)}$, are used, where $\boldsymbol{\varphi} = [\boldsymbol{x}\ T]^{\mathrm{T}}$. To measure the generalization error of the surrogate model, a set of testing base points within the same modeling region is used.

Following the procedure in Chapter 1, the surrogate model weighting factors are calculated in closed form in two manners: a) by assuming that the lower-order surrogates are already calculated and their weighting factors are fixed, or, b) by calculating all the weighting factors simultaneously for each surrogate model order.

3.2.1 Weighting Factors Calculation with Lower-Order Surrogates Fixed

Our purpose is to develop a surrogate model whose response match the original fine EM model response at the j-th learning base point $\boldsymbol{\varphi}^{(j)}$ for the k-th simulated frequency point,

$$R_{sk}^{(1)}(\boldsymbol{\varphi}) = R_{sk}^{(0)}(\boldsymbol{\varphi}) + \boldsymbol{w}_k^{(1)\mathrm{T}}\boldsymbol{q}^{(1)}(\Delta\boldsymbol{\varphi}^{(j)}) = R_{fk}(\boldsymbol{x}_a^{(j)}, T^{(j)}) \tag{3-9}$$

Applying (3-9) for $j = 1, \ldots, L$, the surrogate model weighting factors can be calculated by solving for $\boldsymbol{w}_k^{(1)}$ the following system of linear equations

$$\boldsymbol{Q}^{(1)}\boldsymbol{w}_k^{(1)} = \Delta\boldsymbol{R}_k^{(1)} \text{ for } k = 1, \ldots, p \tag{3-10}$$

where $\boldsymbol{Q}^{(1)} \in \Re^{L\times(n+1)}$ and $\Delta\boldsymbol{R}_k^{(1)} \in \Re^L$ are defined as

$$\boldsymbol{Q}^{(1)} = \begin{bmatrix} \boldsymbol{q}^{(1)}(\Delta\varphi^{(1)})^{\mathrm{T}} \\ \boldsymbol{q}^{(1)}(\Delta\varphi^{(2)})^{\mathrm{T}} \\ \vdots \\ \boldsymbol{q}^{(1)}(\Delta\varphi^{(L)})^{\mathrm{T}} \end{bmatrix} \tag{3-11}$$

$$\boldsymbol{\Delta R}_k^{(1)} = \begin{bmatrix} R_{fk}(\boldsymbol{\varphi}^{(1)}) - R_{sk}^{(0)}(\boldsymbol{\varphi}^{(1)}) \\ \vdots \\ R_{fk}(\boldsymbol{\varphi}^{(L)}) - R_{sk}^{(0)}(\boldsymbol{\varphi}^{(L)}) \end{bmatrix} \tag{3-12}$$

Now, for the second-order surrogate model, the surrogate model response should match the corresponding fine model response at the j-th learning base point,

$$R_{sk}^{(2)}(\boldsymbol{\varphi}) = R_{sk}^{(1)}(\boldsymbol{\varphi}) + \boldsymbol{w}_k^{(2)\mathrm{T}}\boldsymbol{q}^{(2)}(\boldsymbol{\Delta\varphi}^{(j)}) = R_{fk}(\boldsymbol{x}_a^{(j)}, T^{(j)}) \tag{3-13}$$

Since lower-order surrogates are already calculated and fixed, the second-order weightings factors can be calculated for $j = 1, \ldots, L$ by solving for $\boldsymbol{w}_k^{(2)}$ the following system of linear equations

$$\boldsymbol{Q}^{(2)}\boldsymbol{w}_k^{(2)} = \boldsymbol{\Delta R}_k^{(2)} \text{ for } k = 1, \ldots, p \tag{3-14}$$

where $\boldsymbol{Q}^{(2)} \in \Re^{L\times(n+1)(n+2)/2}$ and $\boldsymbol{\Delta R}_k^{(2)} \in \Re^{L}$ are defined as

$$\boldsymbol{Q}^{(2)} = \begin{bmatrix} \boldsymbol{q}^{(2)}(\boldsymbol{\Delta\varphi}^{(1)})^{\mathrm{T}} \\ \boldsymbol{q}^{(2)}(\boldsymbol{\Delta\varphi}^{(2)})^{\mathrm{T}} \\ \vdots \\ \boldsymbol{q}^{(2)}(\boldsymbol{\Delta\varphi}^{(L)})^{\mathrm{T}} \end{bmatrix} \tag{3-15}$$

$$\boldsymbol{\Delta R}_k^{(2)} = \begin{bmatrix} R_{fk}(\boldsymbol{\varphi}^{(1)}) - R_{sk}^{(1)}(\boldsymbol{\varphi}^{(1)}) \\ \vdots \\ R_{fk}(\boldsymbol{\varphi}^{(L)}) - R_{sk}^{(1)}(\boldsymbol{\varphi}^{(L)}) \end{bmatrix} \tag{3-16}$$

In the same manner, the Nth-order surrogate model response should match the corresponding fine model response at the j-th learning base point,

$$R_{sk}^{(N)}(\boldsymbol{\varphi}) = R_{sk}^{(N-1)}(\boldsymbol{\varphi}) + \boldsymbol{w}_k^{(N)\mathrm{T}}\boldsymbol{q}^{(N)}(\boldsymbol{\Delta\varphi}^{(j)}) = R_{fk}(\boldsymbol{x}_a^{(j)}, T^{(j)}) \tag{3-17}$$

By assuming that the lower-order surrogates are already calculated and fixed, the Nth-order weighting factors can be calculated for $j = 1, \ldots, L$ by solving for $\boldsymbol{w}_k^{(N)}$ the following system of linear equations

$$\boldsymbol{Q}^{(N)}\boldsymbol{w}_k^{(N)} = \boldsymbol{\Delta R}_k^{(N)} \text{ for } k = 1, \ldots, p \tag{3-18}$$

where $\boldsymbol{Q}^{(N)} \in \Re^{(N+n)!/((n)!(N)!)}$ and $\boldsymbol{\Delta R}_k^{(N)} \in \Re^{L}$ are defined as

$$\boldsymbol{Q}^{(N)} = \begin{bmatrix} \boldsymbol{q}^{(N)}(\boldsymbol{\Delta\varphi}^{(1)})^{\mathrm{T}} \\ \boldsymbol{q}^{(N)}(\boldsymbol{\Delta\varphi}^{(2)})^{\mathrm{T}} \\ \vdots \\ \boldsymbol{q}^{(N)}(\boldsymbol{\Delta\varphi}^{(L)})^{\mathrm{T}} \end{bmatrix} \tag{3-19}$$

$$\boldsymbol{\Delta R}_k{}^{(N)} = \begin{bmatrix} R_{fk}(\varphi^{(1)}) - R_{sk}{}^{(N-1)}(\varphi^{(1)}) \\ \vdots \\ R_{fk}(\varphi^{(L)}) - R_{sk}{}^{(N-1)}(\varphi^{(L)}) \end{bmatrix} \tag{3-20}$$

3.2.2 Calculating All Weighting Factors at Each Surrogate Model Order

Now, let us assume that all the weighting factors are calculated simultaneously at each surrogate model order. For the first-order surrogate, the responses of the surrogate model and the fine model are matched at the *j*-th learning base point,

$$R_{sk}{}^{(1)}(\boldsymbol{\varphi}) = R_{sk}{}^{(0)}(\boldsymbol{\varphi}) + \boldsymbol{w}_k{}^{(1)\mathrm{T}}\boldsymbol{q}^{(1)}(\boldsymbol{\Delta\varphi}^{(j)}) = R_{fk}(\boldsymbol{x}_a{}^{(j)}, T^{(j)}) \tag{3-21}$$

Applying (3-21) for $j = 1, \ldots, L$, the weighting factors can be calculated by solving for $\boldsymbol{W}^{(1)}$ the following system of linear equations

$$\boldsymbol{Q}_{All}^{(1)}\boldsymbol{W}^{(1)} = \boldsymbol{\Delta R}_k \text{ for } k = 1 \ldots p \tag{3-22}$$

where $\boldsymbol{Q}_{All}^{(1)} \in \Re^{L\times(n+1)}$, $\boldsymbol{W}^{(1)} \in \Re^{n+1}$ and $\boldsymbol{\Delta R}_k{}^{(1)} \in \Re^{L}$ are defined as

$$\boldsymbol{Q}_{All}^{(1)} = [\boldsymbol{Q}^{(1)}] \tag{3-23}$$

$$\boldsymbol{W}^{(1)} = [\boldsymbol{w}_k^{(1)}] \tag{3-24}$$

$$\boldsymbol{\Delta R}_k = \begin{bmatrix} R_{fk}(\varphi^{(1)}) - R_{fk}(\varphi^{(0)}) \\ \vdots \\ R_{fk}(\varphi^{(L)}) - R_{fk}(\varphi^{(0)}) \end{bmatrix} \tag{3-25}$$

Notice that equations (3-22) and (3-10) are equivalent only for the first-order surrogate model.

Now, for the second-order surrogate model, the responses of the surrogate model and the fine model are matched at the *j*-th learning base point,

$$R_{sk}{}^{(2)}(\boldsymbol{\varphi}) = R_{sk}{}^{(0)}(\boldsymbol{\varphi}) + \boldsymbol{w}_k{}^{(1)\mathrm{T}}\boldsymbol{q}^{(1)}(\boldsymbol{\Delta\varphi}^{(j)}) + \boldsymbol{w}_k{}^{(2)\mathrm{T}}\boldsymbol{q}^{(2)}(\boldsymbol{\Delta\varphi}^{(j)}) = R_{fk}(\boldsymbol{x}_a{}^{(j)}, T^{(j)}) \tag{3-26}$$

Applying (3-26) for $j = 1, \ldots, L$, the weighting factors can be calculated by solving for $\boldsymbol{W}^{(2)}$ the following system of linear equations

$$\boldsymbol{Q}_{All}^{(2)}\boldsymbol{W}^{(2)} = \boldsymbol{\Delta R}_k \text{ for } k = 1 \ldots p \tag{3-27}$$

where $\boldsymbol{Q}_{All}^{(2)} \in \Re^{L\times(n+1)+(n+1)/2}$ and $\boldsymbol{W}^{(2)} \in \Re^{(n+1)+(n+2)/2}$ are defined as

$$\boldsymbol{Q}_{\mathrm{All}}^{(2)} = \left[\boldsymbol{Q}^{(1)} \quad \boldsymbol{Q}^{(2)}\right] \tag{3-28}$$

$$\boldsymbol{W}^{(2)} = \left[\boldsymbol{w}_k^{(1)} \quad \boldsymbol{w}_k^{(2)}\right] \tag{3-29}$$

By following the same procedure, the *N*th-order surrogate model response should match the fine model response at the *j*-th learning base point,

$$R_{sk}^{(2)}(\boldsymbol{\varphi}) = R_{sk}^{(0)}(\boldsymbol{\varphi}) + \boldsymbol{w}_k^{(1)\mathrm{T}}\boldsymbol{q}^{(1)}(\boldsymbol{\Delta\varphi}^{(j)}) + \ldots + \boldsymbol{w}_k^{(N)\mathrm{T}}\boldsymbol{q}^{(N)}(\boldsymbol{\Delta\varphi}^{(j)}) = R_{fk}(\boldsymbol{x}_{\mathrm{a}}^{(j)}, T^{(j)}) \tag{3-30}$$

where $\boldsymbol{Q}_{\mathrm{All}}^{(N)} \in \Re^{L\times C}$, $\boldsymbol{W}^{(N)} \in \Re^{C}$ and C are defined as

$$\boldsymbol{Q}_{\mathrm{All}}^{(N)} = \left[\boldsymbol{Q}^{(1)} \quad \boldsymbol{Q}^{(2)} \quad \cdots \quad \boldsymbol{Q}^{(N)}\right] \tag{3-31}$$

$$\boldsymbol{W}^{(N)} = \left[\boldsymbol{w}_k^{(1)} \quad \boldsymbol{w}_k^{(2)} \quad \cdots \quad \boldsymbol{w}_k^{(N)}\right] \tag{3-32}$$

$$C = \sum_{1}^{N} \frac{(N+n)!}{(n)!(N)!} \tag{3-33}$$

3.2.3 Selecting How the Weighting Factors are Calculated

Weighting factors can be calculated in two different forms. The selection between both of them is done automatically in our algorithm by selecting the matrix with smaller condition number between $\boldsymbol{Q}^{(N)}$ in (3-19) and $\boldsymbol{Q}_{\mathrm{ALL}}{}^{(N)}$ in (3-31). If the condition number of matrix $\boldsymbol{Q}^{(N)}$ is smaller than the condition number of matrix $\boldsymbol{Q}_{\mathrm{ALL}}{}^{(N)}$, weighting factors are calculated by solving (3-18), otherwise, by solving (3-27). This test is inexpensive since no fine model evaluations are required.

3.2.4 Selecting the Order of the Polynomial Function

The order of the polynomial function at each simulated frequency point is increased until generalization (testing) error is deteriorated. This is done automatically by the proposed algorithm by calculating at the current polynomial order the maximum absolute generalization error, denoted with ε_{T}, and comparing it with the previous calculated maximum absolute generalization error, denoted with $\varepsilon_{\mathrm{T}}{}^{\mathrm{old}}$. A representation of the PSM process as implemented in this doctoral

dissertation is illustrated in Fig. 3.1.

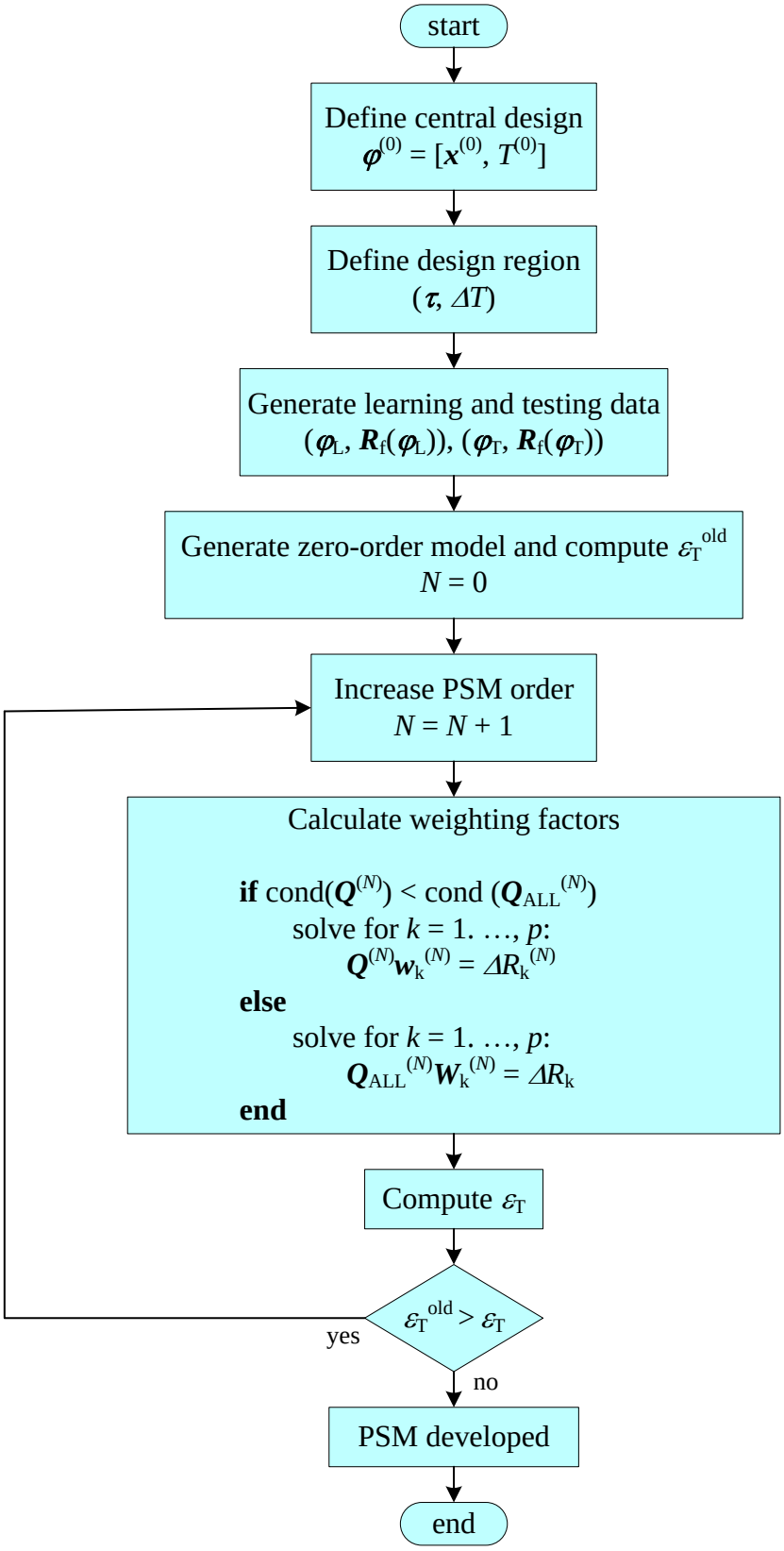

Fig. 3.1 Multiphysics PSM diagram flow.

3.3. Multiphysics Surrogate Modeling of a Microstrip Line

Consider the microstrip line shown in Fig. 2.1. It uses a dielectric substrate whose height is H = 0.66 mm with a relative dielectric constant ε_r = 9 and a dielectric loss tangent tan δ = 0.0025. The metallic trace width is W = 0.7 mm and the length is L = 10.9 mm. The structure is implemented in COMSOL using a simulation bounding box (see Fig. 2.2) with $\boldsymbol{x}_{gap}$ = 0.17 mm, y_{gap} = 9.52 mm, and H_{air} = 10.56 mm. The meshing scheme proposed in [Chávez-Hurtado-16a] as followed. All metallic traces are defined as copper with a thickness t = 0.25 μm.

To develop the multiphysics surrogate model of the microstrip line, design variables are defined as $\boldsymbol{\varphi} = [W \quad T]^T$, by using as a reference design $\boldsymbol{\varphi}^{(0)}$ = [0.7 mm 20 °C], over a region delimited by τ = ±5%, for W, and a temperature range from –20 °C to 180 °C, for T. The EM response of the microstrip line at $\boldsymbol{\varphi}^{(0)}$ is shown in Fig. 2.6. Thermal and elasticity properties of material used in the high frequency structure are taken from Table 2.1-2.2.

To develop the surrogate model, for W, 2 uniform distributed learning base points and 10 uniform distributed testing base points are used. Additionally, 5 uniform distributed temperature points are used within the pre-defined temperature range. Hence, to train and test the multiphysics surrogate model a total number of 10 learning base points and 50 testing base points are used, respectively. EM responses of the microstrip line at the learning and testing base points are shown in Fig. 3.2-3.3.

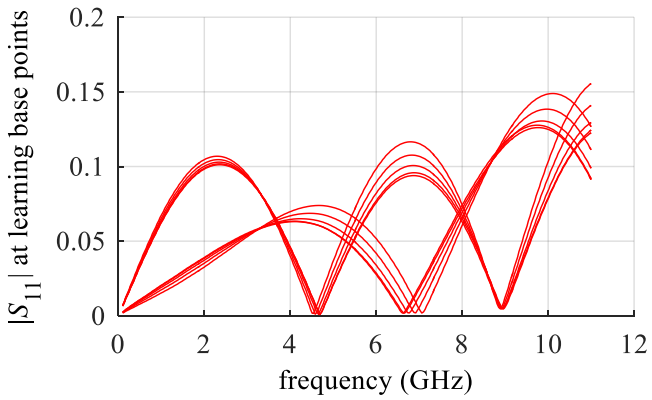

Fig. 3.2 EM response of the microstrip line at learning base points.

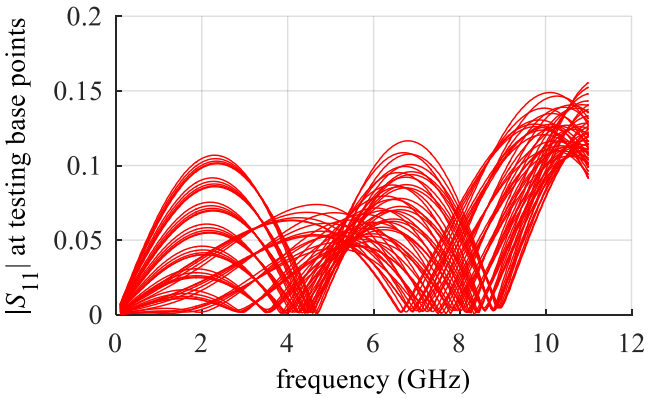

Fig. 3.3 EM responses of the microstrip line at testing base points.

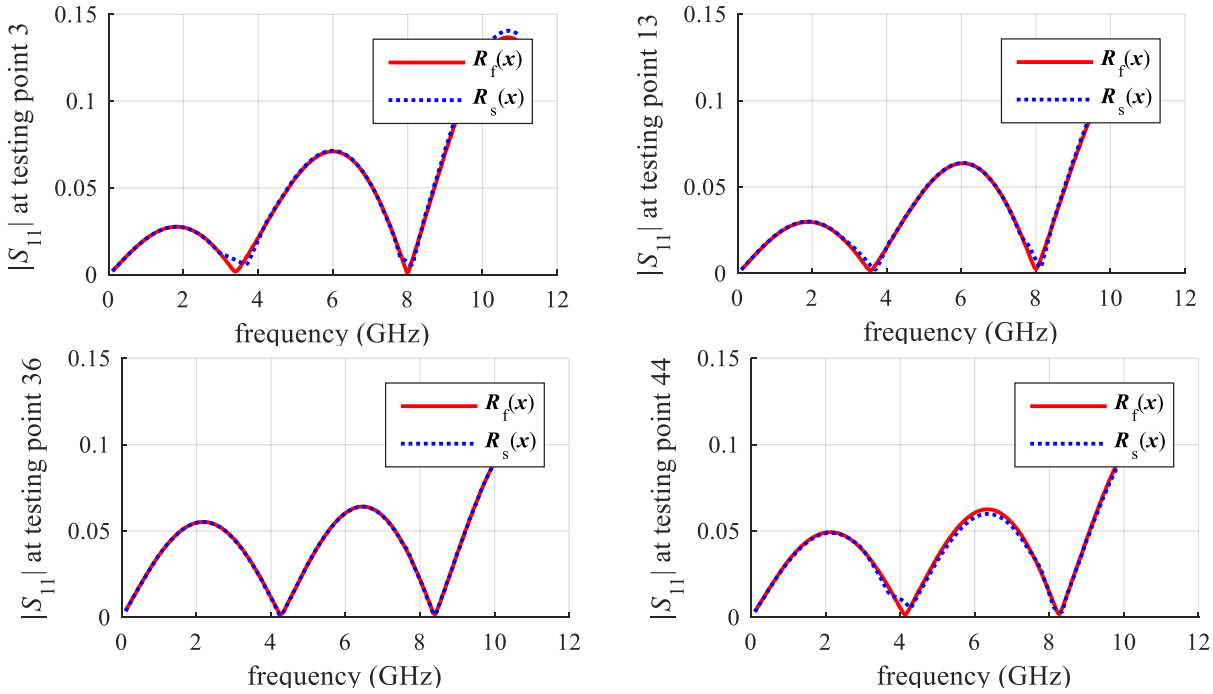

Fig. 3.4 Comparison between EM model and polynomial surrogate model responses at some testing base points, for the microstrip line example.

The performance of the multiphysics surrogate model is measured by calculating the maximum absolute testing error at each frequency point, denoted as ϵ_T, and the largest maximum absolute testing error in the complete frequency sweep, denoted as ϵ_{Tmax}.

Fig. 3.5 illustrates the performance of the surrogate model as well as the order of the polynomial required at each frequency point. The value of ϵ_{Tmax} is 0.017. EM responses of the surrogate model at some testing base points are shown in Fig. 3.4. It is seen that there is a very

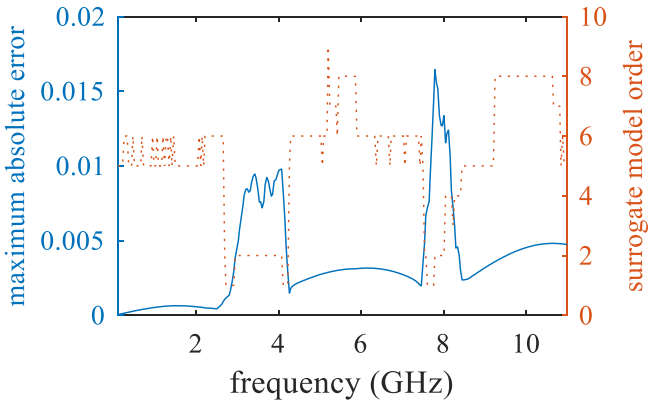

Fig. 3.5 Surrogate model maximum absolute testing error (solid line) and polynomial order (dotted line) at each simulated frequency point, for the microstrip line example.

good match between the fine and the surrogate model responses at the testing base points.

3.4. Conclusions

In this chapter, a polynomial surrogate modeling formulation for high frequency structures subject to multiphysics variations was presented. Corresponding results show a very good match between the actual FEM multi-physical model and the corresponding surrogate model. These results confirm that the PSM methodology is an excellent candidate for multiphysics modeling of high frequency structures.

4. Space Mapping Technique exploiting Polynomial Functions

Space mapping (SM) is a class of surrogate-based optimization techniques [Koziel-13]. It was originally developed to reduce the amount of time required to optimize high frequency structures [Bandler-94], [Bandler-95]. This technique employs at least two models: a fine model, which is very accurate and computationally expensive, and a coarse model, which is inaccurate but computationally very cheap. The purpose of the space mapping technique is to find the mathematical relationship between the fine and coarse model design parameters (input mapping) or fine and coarse model responses (output mapping), such that the mapped coarse model can be exploited to speed up the optimization process without a significant loss in accuracy [Bandler-04].

There are many types of space mapping approaches; the one used in this work for comparison is the so-called aggressive space mapping (ASM). ASM exploits the Broyden method to linearly approximate at each iteration the input mapping between the fine and the coarse models [Rayas-Sánchez-16].

In this chapter, a space mapping design optimization algorithm that exploits a linear approximations method based on first-order polynomial functions is proposed. The linear polynomial functions are used instead of the Broyden formula to linearly approximate the map between the fine and coarse models. Both methodologies are compared by solving three space mapping problems using synthetic models.

4.1. Linear Approximation Method

We aim at iteratively solving a system of equations $\boldsymbol{f}(\boldsymbol{x}) = \boldsymbol{y} = \boldsymbol{0}$, which can be linear or nonlinear, using a starting point $\boldsymbol{x}^{(0)}$ which could lead us to the system solution $\boldsymbol{x}^{*}$. To find a solution or root of the system, it can solved by the Newton method, the Broyden method, or fixed point methods, among others [Deuflhard-11].

Let us suppose that system inputs and outputs are defined as $\boldsymbol{x} \in \Re^{n\times 1}$ and $\boldsymbol{y} \in \Re^{n\times 1}$, respectively. It is assumed that the analytical relationship between $\boldsymbol{y}$ and $\boldsymbol{x}$ is unknown but can be

approximated, at the current iterate, by a first-order polynomial function using linear regression, then

$$\boldsymbol{y} = \boldsymbol{A}\boldsymbol{x} + \boldsymbol{b} \tag{4-1}$$

where $\boldsymbol{A} \in \Re^{n \times n}$ and $\boldsymbol{b} \in \Re^{n \times 1}$.

For a given amount of inputs-outputs pairs available, $N \in \Re$, (4-1) can be used to define the following system of linear equations,

$$\boldsymbol{Y} = \boldsymbol{X}\boldsymbol{w} \tag{4-2}$$

where

$$\boldsymbol{Y} = \begin{bmatrix} \boldsymbol{y}^{(1)\mathrm{T}} \\ \vdots \\ \boldsymbol{y}^{(N)\mathrm{T}} \end{bmatrix} \in \Re^{N \times n}, \boldsymbol{X} = \begin{bmatrix} \boldsymbol{x}^{(1)\mathrm{T}} & 1 \\ \vdots & \vdots \\ \boldsymbol{x}^{(N)\mathrm{T}} & 1 \end{bmatrix} \in \Re^{N \times (n+1)}, \ \boldsymbol{w} = \begin{bmatrix} \boldsymbol{A}^{\mathrm{T}} \\ \boldsymbol{b}^{\mathrm{T}} \end{bmatrix} \in \Re^{(n+1) \times n} \tag{4-3}$$

Now, $\boldsymbol{w}$ can be calculated in closed form by using

$$\boldsymbol{w} = \boldsymbol{X}^{+}\boldsymbol{Y} \tag{4-4}$$

where $\boldsymbol{X}^{+}$ represents the pseudo inverse matrix of $\boldsymbol{X}$.

The first pair of inputs-outputs can be obtained by using a seed value $\boldsymbol{x}^{(0)}$ and its corresponding output $\boldsymbol{y}^{(0)} = \boldsymbol{f}(\boldsymbol{x}^{(0)})$. The second pair can be calculated by perturbing the seed value by an arbitrary amount, e.g. $\boldsymbol{x}^{(0)} = 0.95\boldsymbol{x}^{(0)}$. Then $\boldsymbol{y}^{(1)} = \boldsymbol{f}(\boldsymbol{x}^{(1)})$.

By having two pairs of inputs-outputs, a linear function can be approximated by solving (4-4) for $\boldsymbol{w}$, and using the corresponding results in (4-1). The value of $\boldsymbol{x}$ for the next iteration, $\boldsymbol{x}^{(i+1)}$, can be calculated by using the Newton method [Antia-12], [Parkhurst-06], which exploits the first-order terms of the Taylor series expansion of $\boldsymbol{f}(\boldsymbol{x}^{(i+1)})$ around the point $\boldsymbol{x}^{(i+1)} = \boldsymbol{x}^{(i)} + \varepsilon$:

$$\boldsymbol{f}(\boldsymbol{x}^{(i)} + \varepsilon) \approx \boldsymbol{f}(\boldsymbol{x}^{(i)}) + \boldsymbol{f}'(\boldsymbol{x}^{(i)})\varepsilon \tag{4-5}$$

where $\boldsymbol{f}'$ corresponds to the Jacobian of the vector function $\boldsymbol{f}$, defined as

$$\boldsymbol{J}(\boldsymbol{f}(x)) = \begin{bmatrix} \dfrac{\partial f_1}{\partial x_1} & \cdots & \dfrac{\partial f_1}{\partial x_n} \\ \vdots & \ddots & \vdots \\ \dfrac{\partial f_m}{\partial x_1} & \cdots & \dfrac{\partial f_m}{\partial x_n} \end{bmatrix} \tag{4-6}$$

Since the purpose is to find a root where $\boldsymbol{f}(\boldsymbol{x}^{(i+1)}) = \boldsymbol{f}(\boldsymbol{x}^{(i)} + \varepsilon) = 0$, from (4-5) we obtain

$$\varepsilon = -\boldsymbol{f}'(\boldsymbol{x}^{(i)})^{-1}\boldsymbol{f}(\boldsymbol{x}^{(i)}) \tag{4-7}$$

which can be rewritten as

$$\boldsymbol{x}^{(i+1)} = \boldsymbol{x}^{(i)} - \boldsymbol{f}'(\boldsymbol{x}^{(i)})^{-1}\, \boldsymbol{f}(\boldsymbol{x}^{(i)}) \tag{4-8}$$

Since in our method $\boldsymbol{f}(\boldsymbol{x})$ is represented by a linear function at the current iterate, $\boldsymbol{f}'(\boldsymbol{x})$ can be easily calculated and corresponds to

$$\boldsymbol{f}'(\boldsymbol{x}) = \boldsymbol{A} \tag{4-9}$$

Then, by using (4-9) in (4-8), $\boldsymbol{x}^{(i+1)}$ can be calculated by solving

$$\boldsymbol{x}^{(i+1)} = \boldsymbol{x}^{(i)} - \boldsymbol{A}^{-1}\, \boldsymbol{f}(\boldsymbol{x}^{(i)}) \tag{4-10}$$

The new pair of inputs-outputs is now added to recalculate $\boldsymbol{w}$ by using (4-4). We keep adding pairs until a stopping criteria is reached, such as finding a root, having a relative small change in $\boldsymbol{x}$, having a relative small change in $\boldsymbol{y}$, or reaching a maximum number of iterations i.

4.2. Space Mapping Optimization by using Linear Approximation Method

Let $\boldsymbol{R}_{\mathrm{f}} \in \Re^p$ denote the fine model response sampled at p frequency points. Its n design variables are in $\boldsymbol{x}_{\mathrm{f}} \in \Re^n$. Similarly, let $\boldsymbol{R}_{\mathrm{c}} \in \Re^p$ denote the coarse model response, with design variables in $\boldsymbol{x}_{\mathrm{c}} \in \Re^n$. Evaluating $\boldsymbol{R}_{\mathrm{f}}(\boldsymbol{x}_{\mathrm{f}})$ is accurate but computationally expensive, while evaluating $\boldsymbol{R}_{\mathrm{c}}(\boldsymbol{x}_{\mathrm{c}})$ is inaccurate but computationally cheap.

Since $\boldsymbol{R}_{\mathrm{c}}(\boldsymbol{x}_{\mathrm{c}})$ is fast to evaluate, it is possible to find by classical numerical optimization an optimal coarse model design $\boldsymbol{x}_{\mathrm{c}}^{*}$ that achieves the desired specifications. Then, the purpose of SM-based optimization algorithms is to find a fine model design whose response is as close as possible to the optimal coarse model response. This solution is called the space-mapped solution $\boldsymbol{x}_{\mathrm{f}}^{\mathrm{SM}}$.

In order to find the space-mapped solution, the optimization algorithm solves a system of nonlinear equations, defined as

$$\boldsymbol{f}(\boldsymbol{x}_{\mathrm{f}}) = \boldsymbol{P}(\boldsymbol{x}_{\mathrm{f}}) - \boldsymbol{x}_{\mathrm{c}}^{*} \tag{4-11}$$

where $\boldsymbol{P}(\boldsymbol{x}_{\mathrm{f}})$ corresponds to a process called parameter extraction and consist of finding, for the i-th fine model design, the coarse model design $\boldsymbol{x}_{\mathrm{c}}^{(i)}$ whose response is as close as possible to current fine model response. The parameter extraction is usually done by solving

$$\boldsymbol{P}(\boldsymbol{x}_{\mathrm{f}}^{(i)}) = \arg\min_{\boldsymbol{x}_{\mathrm{c}}} \left\| \boldsymbol{R}_{\mathrm{f}}(\boldsymbol{x}_{\mathrm{f}}^{(i)}) - \boldsymbol{R}_{\mathrm{c}}(\boldsymbol{x}_{\mathrm{c}}) \right\| \tag{4-12}$$

After the parameter extraction is done, an algorithm is used to predict the next iterate in the solution of the system of nonlinear equations defined in (4-1). While aggressive space mapping

exploits the Broyden algorithm to solve (4-1), the linear approximations algorithm is used to linearly approximate, at the current iterate, the relationship between $\boldsymbol{f}(\boldsymbol{x}_f)$ and $\boldsymbol{x}_f$, defined as

$$\boldsymbol{f}(\boldsymbol{x}_f) = \boldsymbol{A}\boldsymbol{x}_f + \boldsymbol{b} \tag{4-13}$$

where $\boldsymbol{A} \in \Re^{n\times n}$ and $\boldsymbol{b} \in \Re^{n}$.

In order to apply the linear approximations method, two pairs of inputs ($\boldsymbol{x}_f$) and outputs ($\boldsymbol{f}(\boldsymbol{x}_f)$) are needed. The first pair corresponds to $\boldsymbol{f}(\boldsymbol{x}_f^{(0)})$ with $\boldsymbol{x}_f^{(0)} = \boldsymbol{x}_c^{*}$. The second pair corresponds to $\boldsymbol{f}(\boldsymbol{x}_f^{(1)})$ with $\boldsymbol{x}_f^{(1)} = \boldsymbol{P}(\boldsymbol{x}_f^{(0)}) - \boldsymbol{x}_c^{*} = \boldsymbol{f}(\boldsymbol{x}_f^{(0)})$. Now, $\boldsymbol{A}$ and $\boldsymbol{b}$ can be calculated by following the procedure in Section 4.1. The next fine model design can be found by solving

$$\boldsymbol{x}_f^{(i+1)} = \boldsymbol{x}_f^{(i)} - \boldsymbol{A}^{-1}\boldsymbol{f}(\boldsymbol{x}_f^{(i)}) \tag{4-14}$$

The new pair of inputs-outputs is now added to the algorithm to recalculate $\boldsymbol{A}$ and $\boldsymbol{b}$. We keep adding pairs until a stopping criteria is reached, such as finding a root, having a relative small change in $\boldsymbol{x}$, having a relative small change in $\boldsymbol{f}(\boldsymbol{x}_f)$, having a relative small difference between the fine model response and the optimum coarse model response, or reaching a maximum number of iterations i_{max}. The final value of $\boldsymbol{x}_f^{(i)}$ corresponds to $\boldsymbol{x}_f^{SM}$.

4.3. Stopping Criteria and Other Settings

As mentioned before, in the following examples two space mapping optimization techniques are compared: one exploiting the linear approximations method and the other one exploiting the Broyden method. For both methodologies, five stopping criteria were specified: 1) a relatively small change in $\boldsymbol{x}_f$, defined by $\|\boldsymbol{x}_f^{(i+1)} - \boldsymbol{x}_f^{(i)}\|_2 \le \epsilon_x (\|\boldsymbol{x}_f^{(i)}\|_2 + \epsilon_x)$, with $\epsilon_x = 1\times10^{-3}$; 2) an acceptable root of the system $\boldsymbol{f}(\boldsymbol{x}_f)$, defined by $\| \boldsymbol{f}(\boldsymbol{x}_f^{(i)})\|_{inf} < \epsilon_f$, with $\epsilon_f = 1\times10^{-3}$; 3) a maximum number of iterations, $i_{max} = 100$; 4) an achievement of the design specifications $u(\boldsymbol{R}(\boldsymbol{x}_f^{(i)}))$, defined by $u(\boldsymbol{R}(\boldsymbol{x}_f^{(i)})) < \epsilon_u$, with $\epsilon_u = -1\times10^{-2}$; and 5) a relative small difference in the fine model response $\boldsymbol{R}_f(\boldsymbol{x}_f)$ with respect to the target response $\boldsymbol{R}_c(\boldsymbol{x}_c^{*})$, defined by $\|\boldsymbol{R}_f(\boldsymbol{x}_f^{(i)}) - \boldsymbol{R}_c(\boldsymbol{x}_c^{*})\|_{inf} < \epsilon_r (\|\boldsymbol{R}_c(\boldsymbol{x}_c^{*})\|_{inf} + \epsilon_r)$, with $\epsilon_r = 0.1$.

The objective function $u(\boldsymbol{R}(\boldsymbol{x}_f))$ is defined as

$$U(\boldsymbol{R}(\boldsymbol{x}_f)) = \max\{\ldots e_k(\boldsymbol{x}_f)\ldots\} \tag{4-15}$$

where a negative value in the k-th error function, $e_k(\boldsymbol{x}_f)$, implies that the corresponding design specifications are satisfied, otherwise some design specification is violated.

The corresponding k-th error function is calculated by

$$e_k(\boldsymbol{x}) = \begin{cases} R_{fk}(\boldsymbol{x}_f) - S^{ub} & \text{for all } k \in I^{ub} \\ S^{lb} - R_{fk}(\boldsymbol{x}_f) & \text{for all } k \in I^{lb} \end{cases} \tag{4-16}$$

where S^{ub} corresponds to the upper bound specification, and S^{lb} corresponds to the lower bound specification, I^{ub} and I^{lb} are subsets of suitable indices.

The termination criteria is represented with the flag EF (exit flag), where EF = –1 indicates that the maximum number of iterations has been reached, EF = 1 indicates that an acceptable root of $\boldsymbol{f}(\boldsymbol{x}_f)$ has been found, EF = 2 indicates that a small relative change in $\boldsymbol{x}_f$ has been achieved, EF = 3 indicates that the design specifications have been achieved, and EF = 4 indicates that the difference between the fine model response and the coarse model response is small enough.

4.4. Test Examples and Results

Results for all the implemented examples are reported in Table 4.1-4.5. In those tables, EF indicates the termination criteria, *i* indicates the number of iterations required, $\boldsymbol{x}_f$ represents the root found (space mapped solution found), and *u* indicates the value of the objective function according to the desired specifications.

For all the examples, seed values correspond to the optimal coarse model design and are initially normalized ($\boldsymbol{x}_f(0) = 1$).

4.4.1 One-section Impedance Transformer

Consider a one-section impedance transformer, whose fine and the coarse models are shown in Fig. 4.1. The reference impedance is $Z_0 = 50\ \Omega$, the load impedance is $R_L = 100\ \Omega$, and the transmission line characteristic impedance is $Z_1 = \text{sqrt}(Z_0 R_L)$ [Pozar-98]. Additionally, for the fine model $C_1 = 0.5$ pF and $C_2 = 0.05$ pF. Transmission line length is defined as L_1. For this example, the design variable corresponds to $x_f = L_1$ (degrees).

Desired design specifications are

$$|S_{11}| \le 0.1 \text{ for } 0.85 \text{ GHz} \le f \le 1.15 \text{ GHz} \tag{4-17}$$

By using direct optimization algorithms or by using basic transmission line theory [Pozar-98], the optimal coarse design is found and corresponds to $x_c^* = L_1 = 90$ (degrees).

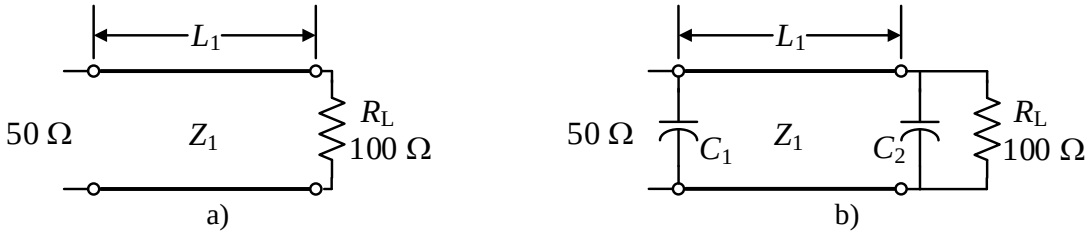

Fig. 4.1 One-section impedance transformer: a) coarse model, b) fine model.

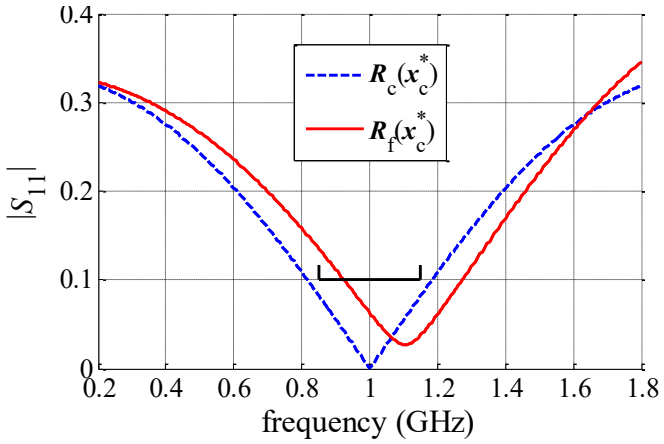

Fig. 4.2 Coarse and fine model response at the optimal coarse model design for the one-section impedance transformer.

TABLE 4.1. PERFORMANCE COMPARISON FOR THE ONE-SECTION IMPEDANCE TRANSFORMER

SM technique	x_f	i	EF	u
Broyden	1.0937	4	1	–0.0070805
Linear approximations	1.0939	4	1	–0.0069193

Using p = 301 frequency points uniformly distributed from 0.2 GHz to 1.8 GHz, the optimal coarse model response and the corresponding fine model response at x_c^* are shown in Fig. 4.2.

According to the results in Table 4.1 (normalized design parameter), both Broyden and linear approximations methods stop after 4 iterations. For both cases, the final design achieves the required design specifications, however, Broyden solution achieves a value for the objective function slightly better than the linear approximations method, with practically a negligible difference. Final responses for both methodologies are illustrated in Fig. 4.3-4.4, showing that final fine model responses are almost the same for both methodologies.

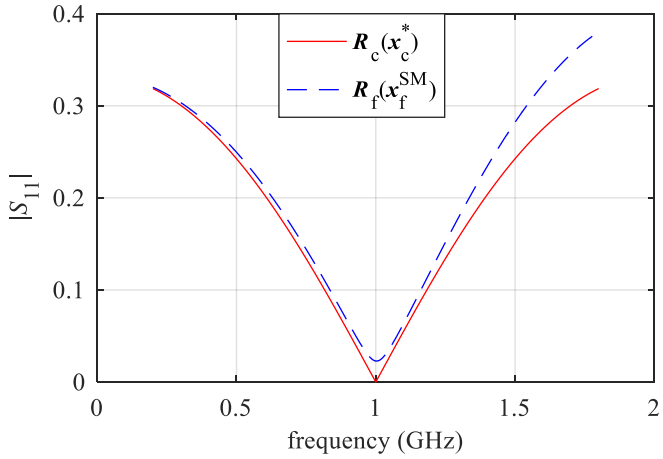

Fig. 4.3 Space mapped response found by using aggressive space mapping for the one-section impedance transformer.

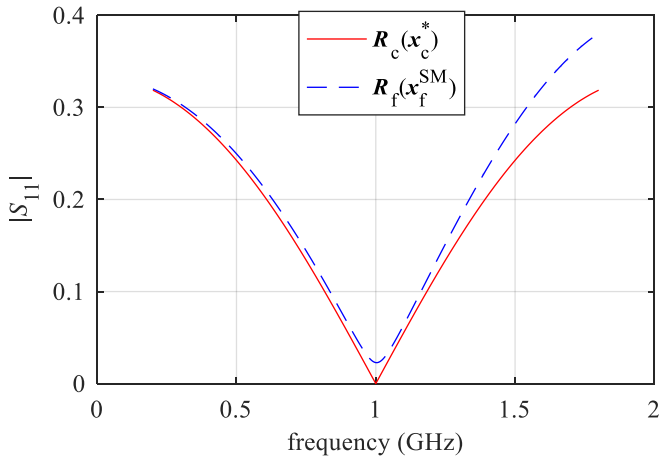

Fig. 4.4 Space mapped response found by using linear approximations space mapping for the one-section impedance transformer.

4.4.2 Two-section Impedance Transformer

Consider a two-section impedance transformer, whose fine and the coarse models are shown in Fig. 4.5 [Rayas-Sánchez-06]. The reference impedance is $Z_0 = 50\ \Omega$, the load impedance is $R_L = 500\ \Omega$, and the transmission line characteristic impedances are $Z_1 = 1.8233Z_0\,\Omega$ and $Z_2 = 5.4845\ Z_0\,\Omega$ [Pozar-98]. Additionally, for the fine model $C_1 = 0.4$ pF, $C_2 = 0.2$ pF, and $C_3 = 0.1$ pF. Transmission line lengths are denoted as L_1 and L_2. For this example, the design variables correspond to $\boldsymbol{x}_f = [L_1 \quad L_2]^T$ (degrees).

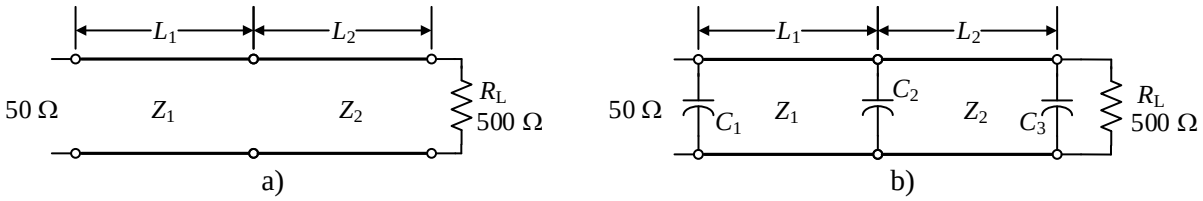

Fig. 4.5 Two-section impedance transformer: a) coarse model, b) fine model.

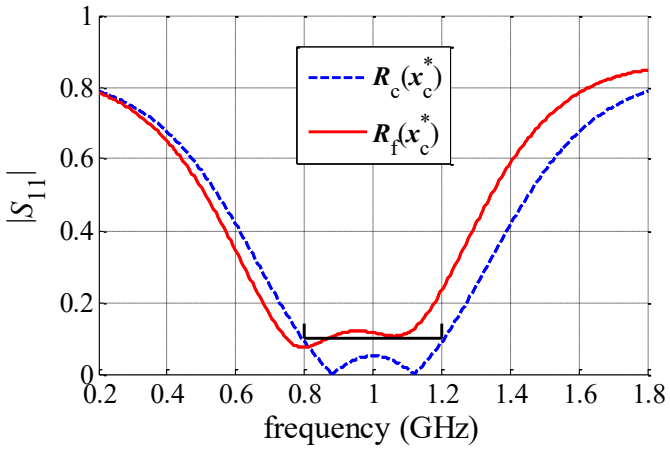

Fig. 4.6 Coarse and fine model response at the optimal coarse model design for the two-section impedance transformer.

TABLE 4.2. PERFORMANCE COMPARISON FOR THE TWO-SECTION IMPEDANCE TRANSFORMER

SM technique	$\boldsymbol{x}_f$	i	EF	u
Broyden	$[0.88540 \quad 0.98338]^T$	7	2	–0.018869
Linear approximations	$[0.87095 \quad 0.99339]^T$	6	3	–0.023085

Desired specifications are

$$|S_{11}| \le 0.1 \text{ for } 0.8 \text{ GHz} \le f \le 1.2 \text{ GHz} \tag{4-18}$$

By using either direct optimization algorithms or basic transmission line theory [Pozar-98], the optimal coarse design is found and corresponds to $\boldsymbol{x}_c^* = [L_1 \quad L_2]^T = [90 \quad 90]^T$ (degrees).

Using $p = 301$ frequency points uniformly distributed from 0.2 GHz to 1.8 GHz, the optimal coarse model response and the corresponding fine model response at x_c^* are shown in Fig. 4.6.

According to the results reported in Table 4.2 (normalized design parameters), linear approximations method stops after 6 iterations while Broyden method stops after 7 iterations. Both methodologies accomplished the desired design specifications, but, for this case, linear

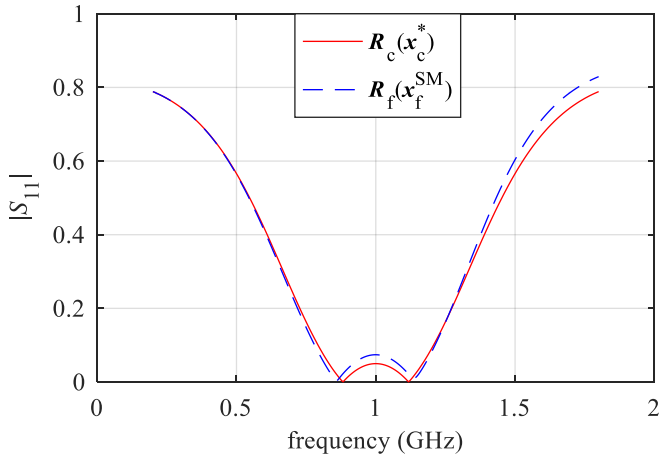

Fig. 4.7 Space mapped response found by using aggressive space mapping for the two-section impedance transformer.

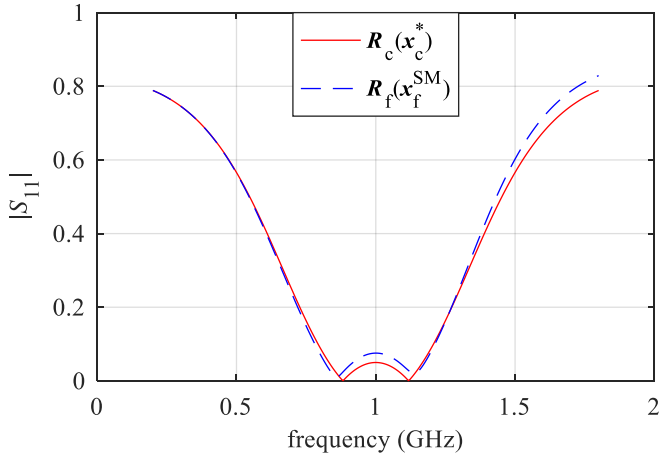

Fig. 4.8 Space mapped response found by using linear approximations space mapping for the two-section impedance transformer.

approximations method achieves a better objective function value and using less iterations than the Broyden method. Final responses obtained for both methodologies are shown in Fig. 4.7-4.8. Again, it is seen that both final fine model responses are almost equivalent.

4.4.3 RLC Parallel Lumped Resonator

Consider a RLC parallel lumped resonator, whose fine and the coarse models are shown in Fig. 4.9 [Rayas-Sánchez-05]. Design parameters are defined as R = 50 Ω, L = 0.2683 nH, and C = 10.4938 pF. Additionally, the fine model includes parasitic elements R_p and L_p. By changing the

a) b)

Fig. 4.9 RLC parallel lumped resonator: a) coarse model, b) fine model.

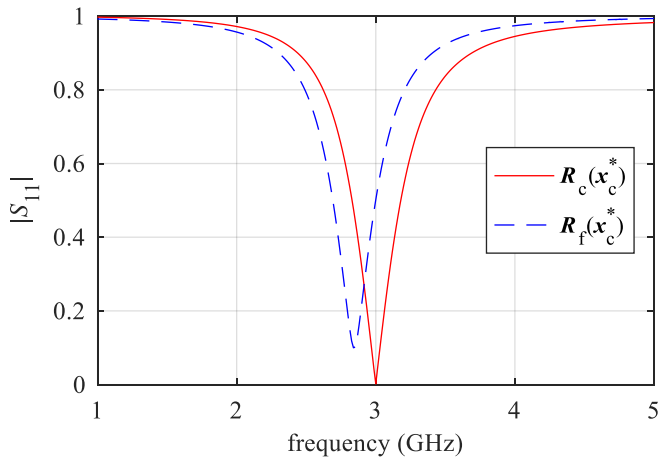

Fig. 4.10 Coarse and fine model response at the optimal coarse model design for the easy case of the RLC parallel lumped resonator.

values of R_p and L_p, the behavior of the fine model circuit response can be modified. An easy case is defined with R_p = 0.1 Ω and L_p = 0.03 nH (fine model with small parasitic effects). A medium case is defined by R_p = 0.4 Ω and L_p = 0.09 nH. Finally, a difficult case is defined with R_p = 0.5 Ω and L_p = 0.13 nH (fine model with strong parasitic effects). Design variables correspond to $\boldsymbol{x}_f = [R\ (\Omega)\quad L\ (\text{nH})\quad C\ (\text{pF})]^T$.

For the three cases, the desired specifications are

$$\begin{aligned} |S_{11}| &> 0.8 \text{ from 1 GHz to 2.5 GHz and from 3.5 GHz to 5 GHz} \\ |S_{11}| &< 0.2 \text{ from 2.95 GHz to 3.05 GHz} \end{aligned} \tag{4-19}$$

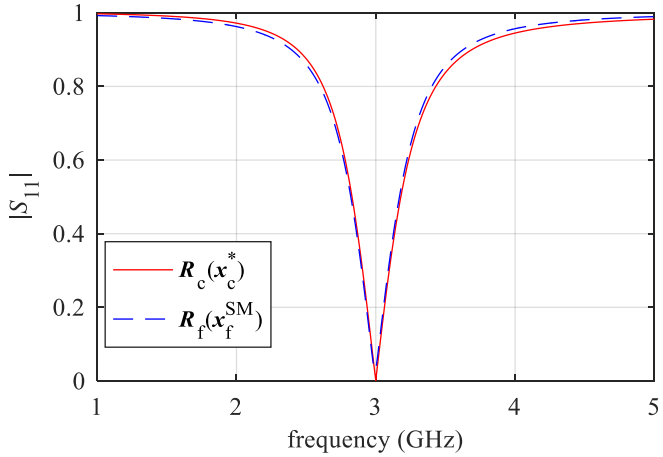

Fig. 4.11 Space mapped response found by using aggressive space mapping for the easy case of the RLC parallel lumped resonator.

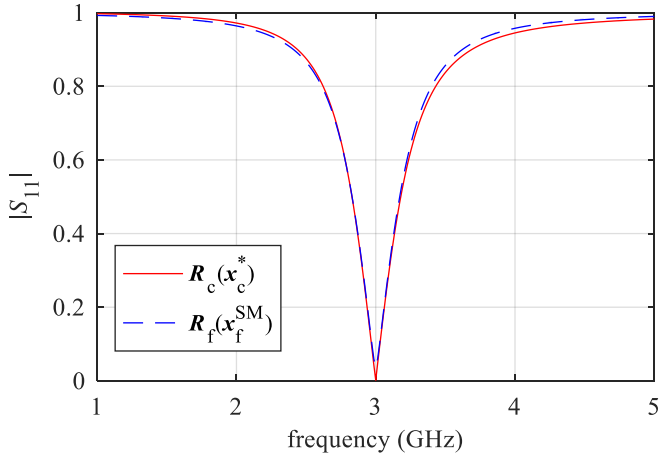

Fig. 4.12 Space mapped response found by using linear approximations space mapping for the easy case of the RLC parallel lumped resonator.

TABLE 4.3. PERFORMANCE COMPARISON FOR THE EASY CASE OF THE RLC PARALLEL LUMPED RESONATOR

SM technique	$\boldsymbol{x}_f$	i	EF	u
Broyden	$[1.1405 \quad 1.0800 \quad 0.8420]^T$	7	3	–0.017047
Linear approximations	$[1.2306 \quad 1.0767 \quad 0.8445]^T$	9	3	–0.010239

By using classical direct optimization algorithms the optimal coarse design is found and corresponds to $\boldsymbol{x}_c^* = [R\ (\Omega) \quad L\ (\text{nH}) \quad C\ (\text{pF})]^T = [50 \quad 0.2683 \quad 10.4938]^T$.

Using $p = 301$ frequency points uniformly distributed from 1 GHz to 5 GHz, the optimal

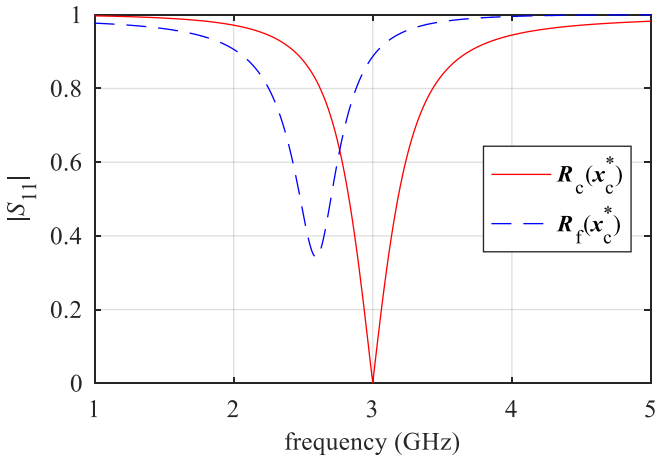

Fig. 4.13 Coarse and fine model response at the optimal coarse model design for the medium case of the RLC parallel lumped resonator.

TABLE 4.4. PERFORMANCE COMPARISON FOR THE MEDIUM CASE OF THE RLC PARALLEL LUMPED RESONATOR

SM technique	$\boldsymbol{x}_f$	i	EF	u
Broyden	$[1.9971 \quad 1.4068 \quad 0.57255]^T$	70	3	–0.01915
Linear approximations	$[7.0765 \quad 1.5205 \quad -0.80637]^T$	100	-1	0.79427

coarse model response and the corresponding fine model response for the easy case at $\boldsymbol{x}_c^*$ are shown in Fig. 4.10.

Final results for the easy case are reported in Table 4.3 (normalized design parameters). Broyden method stops after 7 iterations while linear approximations method stops after 9 iterations. Both of them achieve the design specifications, however, the Broyden method obtained a better objective function value. Final responses for both methodologies are shown in Fig. 4.11-4.12, showing that both fine model responses are almost the same.

For the medium case, initial responses of fine and coarse models at the optimal coarse model design are illustrated in Fig. 4.13, where it is seen a larger misalignment between both responses due to the larger parasitic values (compare versus Fig. 4.10). Final results are reported in Table 4.4. It is seen that linear approximations method did not find a solution for the space mapping problem, while Broyden method found a solution after 70 iterations. Corresponding response for both methods are shown in Fig. 4.14-4.15, showing that fine model response using the Broyden methodology fits very well the optimal coarse model response, while the fine model

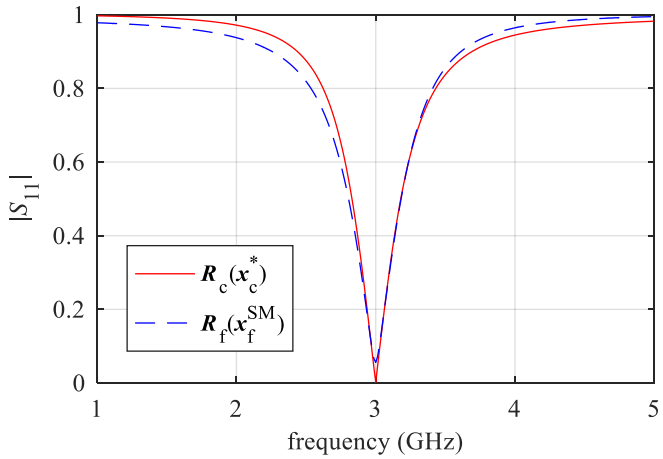

Fig. 4.14 Space mapped response found by using aggressive space mapping for the medium case of the RLC parallel lumped resonator.

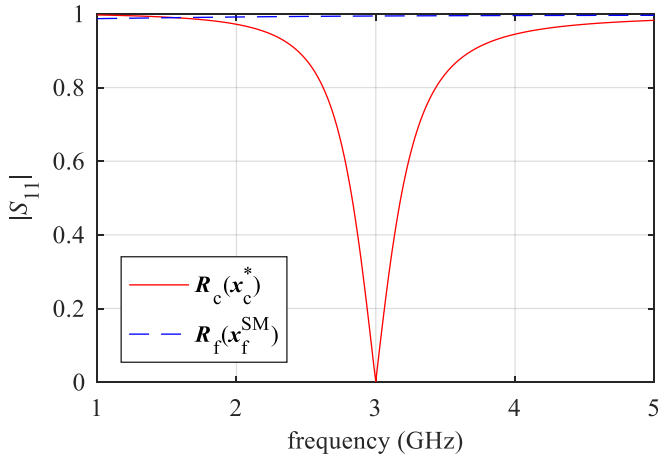

Fig. 4.15 Space mapped response found by using linear approximations space mapping for the medium case of the RLC parallel lumped resonator.

response obtained with the linear approximations methodology is far from the expected target response.

Finally, for the difficult case, initial fine and coarse model responses at the optimal coarse model design are illustrated in Fig. 4.16, showing an even stronger misalignment between both model responses. Corresponding results are reported in Table 4.5. It is seen that both methodologies fail to find a root for this particular space mapping problem. Final responses for both methods are shown in Fig. 4.17-4.18.

For the RLC problem, Broyden method found a solution for the easy and the medium case, while linear approximations method only found a solution for the easy case. This particular problem exhibits a severely non-linear mapping between the corresponding coarse and fine

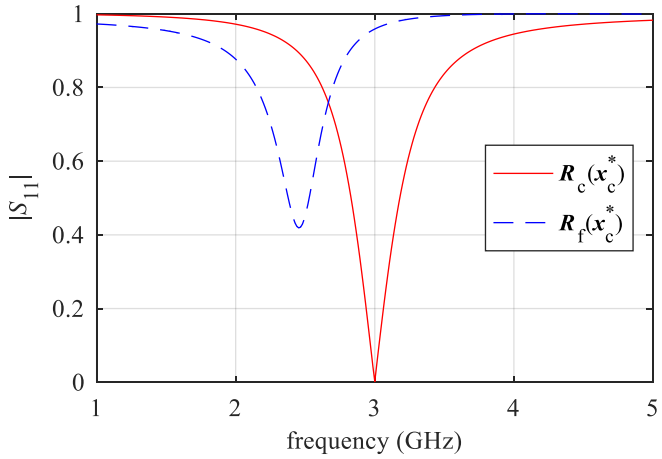

Fig. 4.16 Coarse and fine model response at the optimal coarse model design for the difficult case of the RLC parallel lumped resonator.

TABLE 4.5. PERFORMANCE COMPARISON FOR THE DIFFICULT CASE OF THE RLC PARALLEL LUMPED RESONATOR

SM technique	$\boldsymbol{x}_f$	i	EF	u
Broyden	$[0.03216 \quad -4.7099 \quad -4.7214]^T$	78	2	0.74579
Linear approximations	$[3.0147 \quad -12.542 \quad -11.343]^T$	68	1	0.79758

models, especially for the cases of large parasitic values [Rayas-Sánchez-05].

4.5. Conclusions

In this chapter, a linear approximations method to solve space mapping design optimization problems was presented. The proposed methodology was compared against the aggressive space mapping algorithm, which exploits the Broyden method to linearly approximate the mapping between fine and coarse models. Both methodologies were tested by solving three synthetic problems, the last of them with three different cases: easy, medium, and difficult. Obtained results exhibit a similar performance for both methodologies, having an almost equal final response. In the overall performance, the Broyden methodology successfully converges in 4 of the 5 implemented cases while linear approximations methodology successfully converges in 3 of the 5 implemented cases. Both methods fail when addressing a space mapping problem with a severely

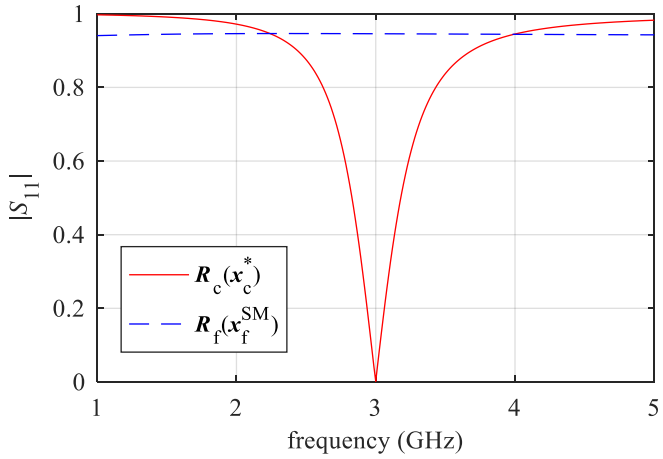

Fig. 4.17 Space mapped response found by using aggressive space mapping for the difficult case of the RLC parallel lumped resonator.

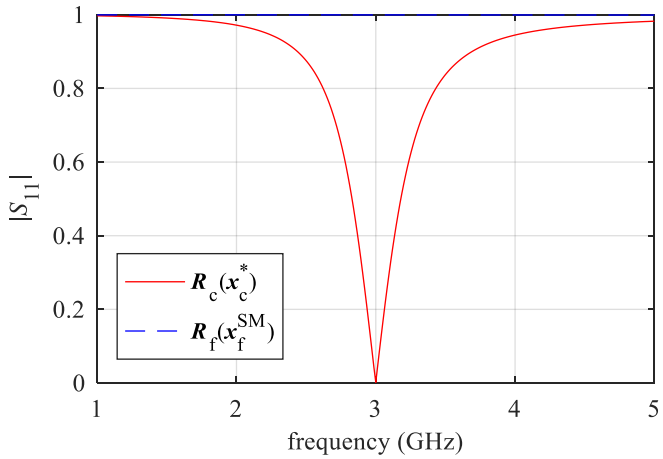

Fig. 4.18 Space mapped response found by using linear approximations space mapping for the difficult case of the RLC parallel lumped resonator.

non-linear mapping between coarse and fine models. A couple of interesting characteristics of the linear approximations methodology lies in its simplicity and the no need of explicit Jacobian approximation. These results show that the proposed methodology based on linear approximations is a suitable alternative to solve space mapping design optimization problems, especially when the mapping between the coarse and fine models is not too complex.

General Conclusions

Different techniques exploiting polynomial functions for modeling and optimizing high frequency structures in the frequency domain were presented in this doctoral dissertation. Such techniques included polynomial-based surrogate modeling and polynomial-based space mapping.

In Chapter 1, it was presented a general formulation for polynomial-based surrogate modeling (PSM) exploiting the multinomial theorem to represent the EM responses of high frequency structures in the frequency domain. The performance of the PSM proposal was compared against four other well-established surrogate modeling techniques: RSM, SVM, GRNN, and Kriging. Corresponding results show a better performance for PSM when the region of interest is small and when using a frugal amount of learning base points.

In Chapter 2, the effects on the EM responses of high frequency structures due to changes in the structure temperature were described. These effects were illustrated by defining the most important electro-thermo-mechanical parameters of high frequency materials. As a fundamental and simple illustration, a microstrip line was implemented in COMSOL, showing how the structure is deformed due to changes in temperature, and demonstrating how this deformation, along with the changes in its electrical parameters, affects the original EM response of the high frequency circuit. By using these parameters, in Chapter 3 it was presented a general formulation for developing multiphysical surrogate models of high frequency structures in the frequency domain. The proposal was exemplified by developing a surrogate model for a microstrip line subject to changes in its temperature. Corresponding results show a very good match between the original and the surrogate model responses.

Finally, in Chapter 4, a space mapping design optimization technique exploiting polynomial functions was presented. The proposal was limited to linear polynomial functions and was compared with ASM, which exploits the Broyden algorithm to solve systems of nonlinear equations. Corresponding results showed a very similar performance for both techniques when the map between fine and coarse model designs is not too complex.

This thesis dissertation offers the possibility of a number of future research opportunities. One possible future research work consists of using higher order polynomials to better fit complex maps in space mapping problems. This could be done not only for the input mapping (at the level

of the design parameters), but also for the output mapping (at the level of the responses). Additionally, the use of polynomial-based surrogate models as coarse models could be explored to further speed up the space mapping optimization process.

Multiphysical simulation of more complex high frequency structures can also be implemented in future research works to study the capability of the PSM technique to properly represent the EM response of these structures subject to a multiphysical analysis.

The methodology proposed in this doctoral dissertation is no intrinsically limited to high frequency structures neither to the frequency domain. The same procedure could be applied to other research applications where the main problem focuses on solving computationally expensive designs (for instance, for the design of DC magnetic components).

Based on the applications and corresponding results showed in this doctoral dissertation, it is demonstrated that polynomial functions exploiting the multinomial theorem are very suitable for modeling and optimizing high frequency structures in the frequency domain, with the main advantage of being mathematically much less complex than other advanced surrogate modeling techniques.

Conclusiones Generales

En esta tesis doctoral fueron presentadas diferentes técnicas explotando funciones polinomiales para el modelado y optimización de estructuras de alta frecuencia, en el dominio de la frecuencia. Tales técnicas incluyen el modelado sustituto basado en polinomios y el mapeo espacial basado en polinomios.

En el Capítulo 1 se presentó la formulación general del modelado sustituto basado en polinomios (PSM), explotando el teorema multinomial, para representar las respuestas electromagnéticas de estructuras de alta frecuencia en el dominio de la frecuencia. El desempeño de la metodología PSM propuesta fue comparada contra cuatro bien establecidas técnicas de modelado sustituto: RSM, SVM, GRNN y Kriging. Los resultados correspondientes arrojaron un mejor desempeño para PSM cuando la región de interés es pequeña y se emplea una cantidad escasa de puntos base de aprendizaje.

En el Capítulo 2 se describieron los efectos sobre las respuestas electromagnéticas, para estructuras de alta frecuencia, causados por los cambios en la temperatura de la estructura. Estos efectos fueron ilustrados definiendo los parámetros electro-termo-mecánicos más importantes para materiales de alta frecuencia. Para ilustrar de manera simple y fundamental dichos efectos, se implementó una línea microcinta en COMSOL, mostrando como la estructura sufría deformaciones debido a los cambios en la temperatura y demostrando como dicha deformación, en conjunto con los cambios en sus parámetros eléctricos, afectaban la respuesta electromagnética original del circuito de alta frecuencia. Empleando estos parámetros, en el Capítulo 3 se presentó una formulación general para desarrollar modelos sustitutos multifísicos para estructuras de alta frecuencia, en el dominio de la frecuencia. Dicha propuesta fue ejemplificada mediante el desarrollo de un modelo sustituto para una línea microcinta sujeta a cambios en su temperatura. Los resultados correspondientes mostraron muy buen emparejamiento entre la respuesta del modelo original y del modelo sustituto.

Finalmente, en el Capítulo 4, se presentó una técnica de optimización de mapeo espacial explotando el uso de funciones polinomiales. La propuesta se limitó al uso de funciones polinomiales lineales y fue comparada con la técnica de mapeo espacial agresivo, la cual explota el algoritmo de Broyden para resolver sistemas de ecuaciones no lineales. Los resultados

correspondientes mostraron un desempeño muy similar para ambas técnicas cuando el mapa entre el modelo fino y burdo no es demasiado complejo.

Esta tesis doctoral abre la posibilidad a futuros trabajos de investigación. Uno de ellos consiste en el uso de funciones polinomiales de alto orden para mejorar el desempeño de mapas complejos en los problemas de mapeo espacial. Esta idea podría aplicarse no sólo al mapa de entrada (al nivel de los parámetros de diseño), sino también al mapa de salida (al nivel de las respuestas de ambos modelos). Adicionalmente, el uso de modelos sustitutos polinomiales como modelos burdos puede ser explorado para acelerar el proceso de optimización de mapeo espacial.

La simulación multifísica de estructuras de mayor complejidad también podría ser considerada en un trabajo futuro, para estudiar la capacidad de PSM para representar apropiadamente la respuesta electromagnética de estas estructuras sujetas a un análisis multifísico.

La metodología propuesta en esta tesis doctoral no se encuentra intrínsecamente limitada a estructuras de alta frecuencia ni al dominio de la frecuencia. El mismo procedimiento podría ser aplicado en principio a otras áreas de investigación donde el principal problema radique en resolver problemas de diseño computacionalmente costosos (por ejemplo, el diseño de componentes magnéticos en corriente directa).

Basados en las aplicaciones y los resultados globales mostrados en esta tesis doctoral, hemos demostrado que el uso de funciones polinomiales, explotando el teorema multinomial, son muy viables para el modelado y optimización de estructuras de alta frecuencia, en el dominio de la frecuencia, con la principal ventaja de ser matemáticamente mucho menos complejas que otras técnicas avanzadas de modelado sustituto.

Appendix

A. LIST OF INTERNAL RESEARCH REPORTS

1) J. L. Chávez-Hurtado, Z. Brito-Brito, and J. E. Rayas-Sánchez, "Coarse and fine models for a fifth order Chebyshev bandstop microstrip filter with L-shaped resonators using COMSOL and Sonnet," Internal Report *PhDEngScITESO-13-01-R* (*CAECAS-13-08-R*), ITESO, Tlaquepaque, Mexico, Dec. 2013.

2) J. L. Chávez-Hurtado and J. E. Rayas-Sánchez, "Four benchmark microstrip line models," Internal Report *PhDEngScITESO-14-03-R* (*CAECAS-14-04-R*), ITESO, Tlaquepaque, Mexico, Jul. 2014.

3) J. L. Chávez-Hurtado, J. E. Rayas-Sánchez, and Z. Brito-Brito, "COMSOL configuration for the EM simulation of a single-layer SIW interconnect with transitions to microstrip lines," Internal Report *PhDEngScITESO-14-07-R* (*CAECAS-14-07-R*), ITESO, Tlaquepaque, Mexico, Oct. 2014.

4) J. L. Chávez-Hurtado and J. E. Rayas-Sánchez, "Surrogate modeling using polynomials," Internal Report *PhDEngScITESO-15-05-R* (*CAECAS-15-08-R*), ITESO, Tlaquepaque, Mexico, Jun. 2015.

5) J. L. Chávez-Hurtado and J. E. Rayas-Sánchez, "Polynomial surrogate modeling based on the multinomial theorem," Internal Report *PhDEngScITESO-15-08-R* (*CAECAS-15-10-R*), ITESO, Tlaquepaque, Mexico, Aug. 2015.

6) J. L. Chávez-Hurtado and J. E. Rayas-Sánchez, "General formulation for polynomial-based surrogate modeling of microwave structures in frequency domain using the multinomial theorem," Internal Report *PhDEngScITESO-15-12-R* (*CAECAS-15-14-R*), ITESO, Tlaquepaque, Mexico, Nov. 2015.

7) J. L. Chávez-Hurtado and J. E. Rayas-Sánchez, "An initial temperature-dependent polynomial surrogate model of a microstrip bandpass filter using COMSOL multiphysics," Internal Report *PhDEngScITESO-16-03-R* (*CAECAS-16-04-R*), ITESO, Tlaquepaque, Mexico, Feb. 2016.

8) J. L. Chávez-Hurtado, Z. Brito-Brito, and J. E. Rayas-Sánchez, "Multiphysical characterization

of microwave structures in frequency domain," Internal Report *PhDEngScITESO-16-13-R* (*CAECAS-16-10-R*), ITESO, Tlaquepaque, Mexico, Nov. 2016.

9) J. L. Chávez-Hurtado, Z. Brito-Brito, and J. E. Rayas-Sánchez, "Multiphysics modeling of microwave structures in frequency domain using PSM," Internal Report *PhDEngScITESO-16-21-R* (*CAECAS-16-12-R*), ITESO, Tlaquepaque, Mexico, Dec. 2016.

10) J. L. Chávez-Hurtado and J. E. Rayas-Sánchez, "A formulation for solving linear and non-linear systems using linear approximations," Internal Report *PhDEngScITESO-17-10-R* (*CAECAS-17-07-R*), ITESO, Tlaquepaque, Mexico, May 2017.

11) J. L. Chávez-Hurtado and J. E. Rayas-Sánchez, "Space mapping technique exploiting linear approximations," Internal Report *PhDEngScITESO-17-21-R* (*CAECAS-17-10-R*), ITESO, Tlaquepaque, Mexico, Jun. 2017.

B. LIST OF PUBLICATIONS

B.1. CONFERENCE PAPERS

1) J. L. Chávez-Hurtado, J. E. Rayas-Sánchez, and Z. Brito-Brito, "Reliable full-wave EM simulation of a single-layer SIW interconnect with transitions to microstrip lines," in *COMSOL Conf.*, Boston, MA, Oct. 2014, pp. 1-5. (DOI: 10.13140/RG.2.1.2579.1445).

2) Z. Brito-Brito, J. E. Rayas-Sánchez, and J. L. Chávez-Hurtado, "Enhanced procedure to setup the simulation bounding box and the meshing scheme of a 3D finite element EM simulator for planar microwave structures," in *IEEE MTT-S Int. Microwave Symp. Dig.*, Phoenix, AZ, May 2015, pp. 1-3. (ISBN: 978-1-4799-8274-5; INSPEC: 15326132; DOI: 10.1109/MWSYM.2015.7166960).

3) J. E. Rayas-Sánchez, J. L. Chávez-Hurtado, and Z. Brito-Brito, "Enhanced formulation for polynomial-based surrogate modeling of microwave structures in frequency domain," in *IEEE MTT-S Int. Conf. Num. EM Mutiphysics Modeling Opt. RF, Microw., Terahertz App. (NEMO-2015)*, Ottawa, Canada, Aug. 2015, pp. 1-3. (ISBN: 978-1-4799-6811-4; e-ISBN: 978-1-4799-6810-7; INSPEC: 15805348; DOI: 10.1109/NEMO.2015.7415094).

4) J. L. Chávez-Hurtado and J. E. Rayas-Sánchez, "Polynomial-based surrogate modeling of microwave structures in frequency domain exploiting the multinomial theorem," in *IEEE MTT-S Int. Microwave Symp. Dig.*, San Francisco, CA, May 2016, pp. 1-3. (ISBN: 978-1-5090-0699-1; e-ISBN: 978-1-5090-0698-4; INSPEC: 16213637; DOI: 10.1109/MWSYM.2016.7540398).

5) J. L. Chávez-Hurtado, J. E. Rayas-Sánchez, and Z. Brito-Brito, "Multiphysics polynomial-based surrogate modeling of microwave structures in frequency domain," in *IEEE MTT-S Latin America Microwave Conf. (LAMC-2016)*, Puerto Vallarta, Mexico, Dec. 2016, pp. 1-3. (ISBN: 978-1-5090-4288-3; e-ISBN: 978-1-5090-4287-6; INSPEC: 16670760; DOI: 10.1109/LAMC.2016.7851279).

6) I. Duron-Rosales, F. Rangel-Patino, J. E. Rayas-Sánchez, J. L. Chávez-Hurtado, and N. Hakim,

"Reconfigurable FIR filter coefficient optimization in post-silicon validation to improve eye diagram for optical interconnects," in *Int. Caribbean Conf. Devices, Circuits, and Systems (ICCDCS-2017)*, Cozumel, Mexico, Jun. 2017, pp. 85-88. (e-ISSN: 2165-3550; p-ISBN: 978-1-5386-1963-6; e-ISBN: 978-1-5386-1962-9; INSPEC: 16996086; DOI: 10.1109/ICCDCS.2017.7959697).

7) F. Rangel-Patino, J. L. Chávez-Hurtado, A. Viveros-Wacher, J. E. Rayas-Sánchez, and N. Hakim, "Eye diagram system margining surrogate-based optimization in a server silicon validation platform," in *European Microwave Conf. (EuMC-2017)*, Nuremberg, Germany, Oct. 2017, pp. 540-543. (pending publication in IEEE Xplore).

B.2. JOURNAL PAPERS

1) J. E. Rayas-Sánchez, J. L. Chavez-Hurtado, and Z. Brito-Brito, "Design optimization of full-wave EM models by low-order low-dimension polynomial surrogate functionals," *Int. J. Numerical Modelling: Electron. Networks, Dev. Fields*., vol. 30, no. 3-4, pp. **-**, May-Aug. 2017. (ISSN: 0894-3370; Online ISSN: 1099-1204; published online: 13 Sep. 2015, DOI: 10.1002/jnm.2094) (regular publication pending).

2) J. C. Cervantes-González, J. E. Rayas-Sánchez, C. A. López, J. R. Camacho-Pérez, Z. Brito-Brito, and J. L. Chavez-Hurtado, "Space mapping optimization of handset antennas considering EM effects of mobile phone components and human body," *Int. J. RF and Microwave CAE*, vol. 26, no. 2, pp. 121-128, Feb. 2016. (ISSN: 1096-4290; Online ISSN: 1099-047X; published online: 21 Oct. 2015, DOI: 10.1002/mmce.20945).

3) J. L. Chavez-Hurtado and J. E. Rayas-Sánchez, "Polynomial-based surrogate modeling of RF and microwave circuits in frequency domain exploiting the multinomial theorem," *IEEE Trans. Microwave Theory Techn.*, vol. 64, no. 12, pp. 4371-4381, Dec. 2016. (p-ISSN: 0018-9480; e-ISSN: 1557-9670; published online: 17 Nov. 2016; DOI: 10.1109/TMTT.2016.2623902).

4) F. E. Rangel-Patiño, J. L. Chávez-Hurtado, A. Viveros-Wacher, J. E. Rayas-Sánchez, and N. Hakim, “System margining surrogate-based optimization in post-silicon validation,” *IEEE Trans. Microwave Theory Techn.*, vol. 65, no. 9, pp. 3109-3115, Sep. 2017. (p-ISSN: 0018-9480; e-ISSN: 1557-9670; published online: 29 May 2017; DOI: 10.1109/TMTT.2017.2701368).

Bibliography

[Angiulli-07] G. Angiulli, M. Cacciola, and M. Versaci, "Microwave devices and antennas modelling by support vector regression machines," *IEEE Trans. on Magnetics*, vol. 43, no. 4, pp. 1589-1592, 2007.

[Antia-12] H. M. Antia, *Numerical Methods for Scientists and Engineers*. India: Hindustan 2012.

[Bandler-94] J. W. Bandler, R. M. Biernacki, S. H. Chen, P. A. Grobelny, and R. H. Hemmers, "Space mapping technique for electromagnetic optimization," *IEEE Trans. Microwave Theory Tech.*, vol. 42, no. 12, pp. 2536-2544, Dec. 1994.

[Bandler-95] J. W. Bandler, R. M. Biernacki, S. H. Chen, R. H. Hemmers, and K. Madsen, "Electromagnetic optimization exploiting aggressive space mapping," *IEEE Trans. Microwave Theory Tech.*, vol. 43, no. 12, pp. 2874-2882, Dec. 1995.

[Bandler-04] J. W. Bandler, Q. S. Cheng, S. A. Dakroury, A. S. Mohamed, M. H. Bakr, K. Madsen, and J. Sondergaard, "Space mapping: the state of the art," *IEEE Trans. Microwave Theory Tech.*, vol. 52, no. 1, pp. 337-361, Jan. 2004.

[Barmuta-15] P. Barmuta, F. Ferranti, G. P. Gibiino, A. Lewandoski, and D. Schreurs, "Compact behavioral model of nonlinear active devices using response surface methodology," *IEEE Trans. Microwave Theory Tech.*, vol. 63, pp. 56-64, Jan. 2015.

[Binner-05] J. Binner, R. Bissoondeeal, and T. Elger, "A comparison of linear forecasting models and neural networks: an application to Euro inflation," *Applied Economics*, vol. 37, no. 6, pp. 665-680, 2005.

[Brito-Brito-13] Z. Brito-Brito, J. E. Rayas-Sánchez, J. C. Cervantes-González, and C. A. López, "Impact of 3D EM model configuration on the direct optimization of microstrip structures," in *COMSOL Conf.*, Boston, MA, Oct. 2013, pp. 1-5.

[Burford-14] N. M. Burford and M. El-Shenawee, "Multiphysics modeling of THz photoconductive antennas," in *Int. Conf. on Infrared, Millimiter, and Terahertz Waves (IRMMW-THz 2014)*, Tucson, AZ, Sept. 14-19, 2014, pp. 1-2.

[Ceperic-04] V. Ceperic and A. Baric, "Modeling of analog circuits by using support vector regression machines," in *IEEE Int. Conf. on Electronics, Circuits and Systems (ICECS 2004)*, Tel-Aviv, Israel, Dec. 2004, pp. 391-394.

[Cervantes-González-12] J. C. Cervantes-González, Z. Brito-Brito, C. A. López, and J. E. Rayas-Sánchez, "EM-thermo-mechanical simulation of a microstrip bandpass filter using COMSOL Multiphysics," Internal Report *CAECAS-12-12-R*, ITESO, Tlaquepaque, Mexico, Jun. 2012.

[Cervantes-González-13] J. C. Cervantes-González, C. A. López, J. E. Rayas-Sánchez, Z. Brito-Brito and G. Hernández-Sosa, "Return-loss minimization of package interconnects through input space mapping using FEM-based models," in *Proc. SBMO/IEEE MTT-S Int. Microwave Optoelectronics Conf. (IMOC-2013)*, Rio de Janeiro, Brazil, Aug. 2013, pp. 1-4.

[Cervantes-González-15] J. C. Cervantes-González, J. E. Rayas-Sánchez, C. A. López, J. R. Camacho-Pérez, Z. Brito-Brito, and J. L. Chávez-Hurtado, "Space mapping optimization of handset antennas

considering EM effects of mobile phone components and human body", *Int. Journal of RF and Microwave Computer-Aided Engineering*, vol. xx, no. xx, 2015 (accepted).

[Chávez-Hurtado-14a] J. L. Chavez-Hurtado and J. E. Rayas-Sánchez, "Four benchmark microstrip line moels," Internal Report *PhDEngScITESO-14-03-R* (*CAECAS-14-04-R*), ITESO, Tlaquepaque, Mexico, July, 2014.

[Chávez-Hurtado-14b] J. L. Chavez-Hurtado, J. E. Rayas-Sánchez, and Z. Brito-Brito, "Reliable full-wave EM simulation of a single-layer SIW interconnect with transitions to microstrip lines," in *COMSOL Conf.*, Boston, MA, Oct. 2014, pp. 1-5.

[Chávez-Hurtado-15] J. L. Chávez-Hurtado and J. E. Rayas-Sánchez, "General formulation for polynomial-based surrogate modeling of microwave structures in frequency domain using the multinomial theorem," Internal Report *PhDEngScITESO-15-12-R* (*CAECAS-15-14-R*), ITESO, Tlaquepaque, Mexico, Nov. 2015.

[Chávez-Hurtado-16a] J. L. Chávez-Hurtado, Z. Brito-Brito, and J. E. Rayas-Sánchez, "Multiphysical characterization of microwave structures in frequency domain," Internal Report *PhDEngScITESO-16-13-R* (*CAECAS-16-10-R*), ITESO, Tlaquepaque, Mexico, Nov. 2016.

[Chávez-Hurtado-16b] J. L. Chávez-Hurtado, J. E. Rayas-Sánchez, and Z. Brito-Brito, "Multiphysics polynomial-based surrogate modeling of microwave structures in frequency domain," in *IEEE MTT-S Latin America Microwave Conf. (LAMC-2016)*, Puerto Vallarta, Mexico, Dec. 2016, pp. 1-3.

[Chávez-Hurtado-16c] J. L. Chavez-Hurtado and J. E. Rayas-Sanchez, "Polynomial-based surrogate modeling of RF and microwave structures in frequency domain exploiting the multinomial theorem," *IEEE Trans. Microwave Theory Tech.*, vol. 64, no. 12, pp. 4371-4381, Dec. 2016.

[Chávez-Hurtado-17] J. L. Chávez-Hurtado and J. E. Rayas-Sánchez, "A formulation for solving linear and non-linear systems using linear approximations," Internal Report *PhDEngScITESO-17-10-R* (*CAECAS-17-07-R*), ITESO, Tlaquepaque, Mexico, May 2017.

[Couckuyt-11] I. Couckuyt, S. Koziel, and T. Dhane, "Kriging, co-kriging and space mapping for microwave circuit modeling," in *European Microwave Conference (EuMC 2011)*, Manchester, UK, Oct. 2011, pp. 444-447.

[Demirel-13] S. Demirel, F. Günes, and A. K. Keskin, "Design of an ultrawide band low noise microstrip amplifier using 3D Sonnet-based SVRM with particle swarm optimization for space applications," in *IEEE Int. Conf. on Recent Advances in Space Technologies (RAST)*, Istanbul, Turkey, Jun. 2013, pp. 445-450.

[Deuflhard-11] P. Deuflhard, *Newton Methods for Nonlinear Problems*. Germany: Springer 2011.

[Encyc. Britannica-15] Encyclopedia Britannica Online. (2015). *Multinomial Theorem (rev. May 17)* [Online]. Available: http://www.britannica.com/EBchecked/topic/1559457-/multinomial-theorem.

[Fu-14] M. C. Fu, *Handbook of Simulation Optimization*. New York, NY: Springer, 2014.

[García-Guzmán-15] J. García-Guzmán, A. Mendoza-Gutiérrez, J. A. Vélez-Enríquez, A. Ramírez-Ramírez, and F. H. Villa-López, "Multiphysics modelling of a resistive polymeric sensor for VOC," in *Int. Conf. on Industrial Technology (ICIT 2015)*, Seville, Spain, Mar. 17-19, 2015, pp. 3361-3364.

[Hawe-07] G. Hawe and J. Sykulski, "Considerations of accuracy and uncertainty with kriging surrogate models in single-objective electromagnetic design optimization," *IET Science, Measurement and Technology*, vol. 1, no. 1, pp 37-47, Jan. 2007.

[Hammadi-99] S. Hammadi, R. O. Grondin, S. El-Ghazaly, and S. Goodnick, "Full-wave electromagnetic simulation of millimeter-wave active devices and circuits," *Annales Des Télécommunications*, vol. 54, no. 1-2, pp. 30-42, Jan. 1999.

[Haykin-99] S. Haykin, *Neural Networks. A Comprehensive Foundation*. USA: Prentice Hall, 1999.

[Jacobs-12] J. P. Jacobs, "Bayesian support vector regression with automatic relevance determination kernel for modeling of antenna input characteristics," *IEEE Trans. on Antennas and Propagation*, vol. 60, no. 4, pp. 2114-2118, 2012.

[Koziel-09] S. Koziel, "Surrogate-based optimization of microwave structures using space mapping and kriging," in *European Microwave Conference (EuMC 2009)*, Rome, Italy, Sept. 2009, pp. 1062-1065.

[Koziel-11] S. Koziel and X. S. Yang, *Computational Optimization, Methods and Algorithms*. Berlin, BE: Springer, 2011.

[Koziel-13] S. Koziel and L. Leifsson, Ed., *Surrogate-Based Modeling and Optimization: Applications in Engineering*. New York, NY: Springer, 2013.

[Koziel-14] S. Koziel, L. Leifsson, and X. S. Yang, *Solving Computationally Expensive Engineering Problems*. Sqitzerland, CH: Springer, 2014.

[Leng-13] Z. Leng, J. Gao, Y. Qin, X, Liu, and J. Yin, "Short-term forecasting model of traffic flow based on GRNN," in *Chinese Control and Decision Conference (CCDC 2013)*, China, May 2013, pp. 3816-3820.

[Li-15] D. Li, M. Packwood, F. Qi, Y. Wu, Y. Wang, S. Jones, X. Dai, and G. Liu, "3D Multiphysics modelling of high voltage IGBT module packaging," in *Int. Conf. on Electronic Packaging Technology (ICEPT 2015)*, Changsha, China, Aug. 11-14, 2015, pp. 598-602.

[Li-Na-11] H. Li-Na and N. Jing-Chang, "Researches on GRNN neural network in RF nonlinear systems modeling," in *IEEE Int. Conf. on Computational Problem-Solving (ICCP 2011)*, Romania, Aug. 2011, pp. 1-4.

[Mahouti-14] P. Mahouti, F. Günes, S. Demirel, A. Uluslu, and M. A. Belen, "Efficient scattering parameter modeling of a microwave transistor using generalized regression neural network," in *IEEE Int. Conf. on Microwaves, Radar, and Wireless Communication (MIKON 2014)*, Poland, Jun. 2014, pp. 1-4.

[Mandic-13] T. Mandic, R. Gillon, and A. Baric, "IC-Stripline design optimization using response surface methodology," in *Int. Workshop on Electromagnetic Compatibility of Integrated Circuits (EMC Compo 2013)*, Nara, Japan, Dec. 2013, pp. 69-73.

[Mussetta-09] M. Mussetta, D. Caputo, A. Pirisi, F. Grimaccia, L. Valbonesi, and R. E. Zich, "Neural networks and evolutionary algorithm application to complex EM structures modeling," in *Int. Conf. on Electromagnetics in Advanced Applications (ICEAA 2009)*, Sept. 2009, pp. 1020-1023.

[Ogurtsov-10] S. Ogurtsov, S. Koziel and J. E. Rayas-Sánchez, "Design optimization of a broadband microstrip-to-SIW transition using surrogate modeling and adaptive design specifications,"

in *Int. Review of Progress in Applied Computational Electromagnetics (ACES 2010)*, Tampere, Finland, Apr. 2010, pp. 878-883.

[Osborne-97] D. M. Osborne, R. L. Armacost, and J. Pet-Edwards, "State of the art in multiple response surface methodology," in *IEEE Int. Conf. on Systems, Man, and Cybernetics*, Florida, USA, Oct. 12 – 15, 1997, pp. 3833-3838.

[Panda-14] B. N. Panda, M. V. A. R. Bahubalendruni, and B. B. Biswal, "Optimization of resistance spot welding parameters using differential evolution algorithm and GRNN," in *IEEE Int. Conf. on Intelligent Systems and Control (ISCO 2014)*, vol. 2, no. 6, India, Jan. 2014, pp. 50-55.

[Parkhurst-06] D. F. Parkhurst, *Introduction to Applied Mathematics for Environmental Science*. USA: Springer 2006.

[Parry-00] J. Parry, F. Ferranti, C. Bailey, and C. Aldham, "Multiphysics modelling for electronics design," in *Intersociety Conf. on Thermal and Thermomechanical Phenomena in Electronic Systems (ITHERM 2000)*, Las Vegas, NV, May 23-26, 2000, pp. 86-93.

[Pozar-98] D. M. Pozar, *Microwave Engineering. Amherst*. MA: Wiley, 1998.

[Raida-02] Z. Raida, "Modeling EM structures in the neural network toolbox of MATLAB," *IEEE Antennas and Propagation Magazine*, vol. 44, no. 6, pp. 46-67, Dec. 2002.

[Rayas-Sánchez-04] J. E. Rayas-Sánchez, "EM-based optimization of microwave circuits using artificial neural networks: the state-of-the-art," *IEEE Transactions on Microwave Theory and Techniques*, vol. 52, no. 1, pp. 420-435, Jan. 2004.

[Rayas-Sánchez-05] J. E. Rayas-Sánchez, F. Lara-Rojo and E. Martínez-Guerrero, "A linear inverse space mapping (LISM) algorithm to design linear and nonlinear RF and microwave circuits," *IEEE Trans. Microwave Theory Tech.*, vol. 53, pp. 960-968, Mar. 2005.

[Rayas-Sánchez-06] J. E. Rayas-Sánchez and V. Gutiérrez-Ayala, "EM-based Monte Carlo analysis and yield prediction of microwave circuits using linear-input neural-output space mapping," *IEEE Trans. Microwave Theory Techn.*, vol. 54, no. 12, pp. 4528-4537, Dec. 2006.

[Rayas-Sánchez-10] J. E. Rayas-Sánchez, J. Aguilar-Torrentera, and J. A. Jasso-Urzúa, "Surrogate modeling of microwave circuits using polynomial functional interpolants," in *IEEE MTT-S Int. Microwave Symp. Dig.*, Anaheim, CA, May 2010, pp. 197-200.

[Rayas-Sánchez-15a] J. E. Rayas-Sánchez, J. L. Chávez-Hurtado, and Z. Brito-Brito, "Enhanced formulation for polynomial-based surrogate modeling of microwave structures in frequency domain," in *IEEE MTT-S Int. Conf. Num. EM Mutiphysics Modeling Opt. RF, Microw., Terahertz App. (NEMO-2015)*, Ottawa, ON, Aug. 2015, pp. 1-3

[Rayas-Sánchez-15b] J. E. Rayas-Sánchez, J. L. Chavez-Hurtado, and Z. Brito-Brito, "Design optimization of full-wave EM models by low-order low-dimension polynomial surrogate functionals," *Int. J. Numerical Modelling: Electron. Networks*, Dev. Fields., vol. xx, pp. xx-xx, Oct. 2015 (accepted).

[Rayas-Sánchez-16] J. E. Rayas-Sanchez, "Power in simplicity with ASM," *IEEE Microwave Magazine*, vol. 17, no. 4, pp. 64-76, Apr. 2016.

[Redhe-04] M. Redhe and L. Nilsson, "Optimization of the new Saab 9-3 exposed to impact load using a space mapping technique," *Structural and Multidisciplinary Optimization*, vol. 27, pp. 411-420, Jul. 2004.

[Ren-07] X. Ren and T. Kazmierski, "Performance modelling and optimization of RF circuits using support vector machines," in *Int. Conf. on Mixed Design (MIXDES 2007)*, Poland, Jun. 2007, pp. 317-321.

[Sánchez-Soriano-14] M. A Sánchez-Soriano, M. Edwards, Y. Quére, D. Andersson, S. Cadiou, and C. Quendo, "Multiphysics study of RF/microwave planar devices: effect on the input signal power," in *Int. Conf. on Thermal, Mechanical and Multi-Physics Simulation and Experiments in Microelectronics and Microsystems (EuroSimE 2014)*, Ghent, Belgium, Apr. 7-9, 2014, pp. 1-7.

[Specht-91] D. F. Specht, "A general regression neural network," *IEEE Trans. on Neural Networks*, vol. 2, no. 6, pp. 568-576, 1991.

[Tokan-08] N. T. Tokan and F. Günes, "Analysis and synthesis of the microstrip lines based on support vector regression," in *IEEE European Microwave Conf. (EuMC 2008)*, Amsterdam, Netherlands, Oct. 2008, pp. 1473-1476.

[Tokan-09] N. T. Tokan and F. Günes, "Knowledge-based support vector synthesis of the microstrip lines," *Progress in Electromagnetics Research*, vol. 92, pp. 65-77, 2009.

[Vai-99] M. Vai and S. Prasad, "Neural networks in microwave circuit design – beyond black-box models," *Int. Journal of RF and Microwave Computer-Aided Engineering*, vol. 9, no. 3, pp. 187-197, May 1999.

[Van Beers-04] W. C. M. Van Beers and J. P. C. Keijnen, "Kriging interpolation in simulation: a survey," in *Simulation Conference, 2004. Proceedings of the 2004 Winter*, Dec. 2004, pp. 5-8.

[Van Beers-05] W. C. M. Van Beers, "Kriging metamodeling in discrete-event simulation: an overview," in *Simulation Conference, 2005. Proceedings of the 2005 Winter*, Dec. 2005, pp. 4-7.

[Xia-06] L. Xia, J. Meng, R. Xu, B. Yan, and Y. Guo, "Modeling of 3-D vertical interconnect using support vector machine regression," *IEEE Microwave and Wireless Components Letters*, vol. 16, no. 12, pp. 639-641, 2006.

[Xia-14] B. Xia, Z. Ren, and C. S. Koh, "Selecting proper kriging surrogate model for optimal design of electromagnetic problem," in *IET Int. Conf. on Computation in Electromagnetics*, London, UK, Mar., 2014, pp. 1-4.

[Zhang-00] Q. J. Zhang and K. C. Gupta, *Neural Networks for RF and Microwave Design*. Norwood, MA: Artech House, 2000.

[Zhang-08] Y. Zhang, Q. Cheng, S. S. Yoon, P. S. Shin, and C. S. Koh, "A robust and computationally efficient optimal design algorithm of electromagnetic devices using adaptive response surface method," *Journal of Electrical Engineering and Technology*, vol. 3, no. 2, pp. 207-212, 2008.

[Zhang-13] J. Zhang and D. Zhang, "Study of response surface methodology in thermal optimization design of multichip modules," *Trans. on Components, Packaging and Manufacturing Technology*, vol. 3, pp. 2075-2080, Dec. 2013.

Author Index

Subject Index